THE FUNCTION OF MAMMALIAN COPII COMPONENTS *Sec23a* AND *Sec23b*

by

Matthew Paul Vasievich

A dissertation submitted in partial fulfillment
of the requirements for the degree of
Doctor of Philosophy
(Human Genetics)
in The University of Michigan
2011

Doctoral Committee:

Professor David Ginsburg, Chair
Professor Randal J. Kaufman
Professor Miriam H. Meisler
Professor John V. Moran
Associate Professor David C. Kohrman

DEDICATION

For Louise

ACKNOWLEDGEMENTS

In working on this PhD I have many people in my life to thank; starting with my family who has been there for me every step of the way. My beautiful wife Louise who, being a professor's daughter, I think understands graduate school better than I do most days. Thank you also to our son Anthony who was born between chapters 2 and 3.

Thank you also to my parents – my mom and dad for providing such support and encouragement over the years. Thank you to my sisters Beth and Teresa for their love and support and phone calls and lending a listening ear. Many thanks as well to Joe, Barbara, Sean and Kathleen my family-in-law. Thanks to Joe for letting me invade his dining room table/math research space to write my dissertation when my desk at home was converted to the changing table. Thanks to Barbara for being the couch warrior covering the night shift with Anthony and Louise so I could write. Thank you to all the folks at St. Thomas the Apostle Church from Generation Christ and our newlyweds group; for your prayers, support and friendships.

Thanks to David for letting me join the lab. He is perhaps one of the most patient and generous people I've met. Thanks also to all the lab members past and present for your help and teaching me how to do things like run a mouse colony and pour gels and also for putting up with my jokes.

Thanks to the UM MSTP – to Ron, Ellen (and Penny before her), Laurie and Hilkka. You're always there for us students with a smile and willing to chat to take our minds off the daily stresses of being a grad student. Thanks to my department, Human Genetics for their support and my thesis committee for all their helpful suggestions and comments.

TABLE OF CONTENTS

LIST OF FIGURES

LIST OF TABLES

ABSTRACT

The Function of Mammalian COPII Components *Sec23a* and *Sec23b*

by

Matthew Paul Vasievich

Chair: David Ginsburg

In all eukaryotic cells, cargo proteins are transported from the endoplasmic reticulum (ER) to the Golgi apparatus in COPII-coated vesicles. Human diseases have recently been described that result from inherited mutations in the paralagous genes *SEC23A* and *SEC23B*, which encode a key component of the COPII vesicle coat. In this thesis, I explore the phenotypes of gene targeted mice deficient for the mouse SEC23 orthologs *Sec23a* and *Sec23b*.

Congenital dyserythropoietic anemia type II (CDAII) is an autosomal recessive disorder characterized by mild to severe anemia, and recently reported to be due to mutations in the *SEC23B* gene. Mice homozygous for a gene trap insertion in the last intron of the mouse *Sec23b* gene (*Sec23b gt/gt*) were demonstrated to exhibit massive pancreatic degeneration and die within a day of birth, with no evidence of anemia on blood analysis. Chimeric mice generated by transplantation of *Sec23b gt/gt* hematopoietic precursor cells into wild type mice demonstrated full reconstitution of erythropoiesis, as well as other blood cell lineages. Mass spectrometry analysis of *Sec23b gt/gt* RBC ghosts prepared from chimeric mice using a comparative SILAC

approach detected no proteins that were quantitatively decreased compared to control RBC ghosts. These results suggest divergence in tissue-specific SEC23B function between mice and humans.

Humans with mutations in *SEC23A* are affected with Cranio-Lenticulo-Sutural Dysplasia (CLSD), which is characterized by late closure of the cranial fontanelles and mild mental retardation. Mice with a gene trap insertion in the second intron of the *Sec23a* gene die between day 10.5 and 11.5 of embryogenesis. Mice heterozygous for both the *Sec23a gt* and *Sec23b gt* alleles (*Sec23a+/gt Sec23b+/gt*) are viable and fertile with no apparent pathologic phenotype. However, *Sec23a gt/gt Sec23b+/gt* mice die at an earlier time point in embryogenesis than *Sec23a gt/gt* mice, suggesting functional overlap between SEC23A and SEC23B. These studies have shown that humans and mice with mutations in *Sec23a* and *Sec23b* have disparate but tissue specific phenotypes. This demonstrates the importance of the COPII pathway in human disease and could suggest functional divergence of these isoforms over evolutionary time between human and mouse.

CHAPTER I:
Introduction

Abstract

The Endoplasmic Reticulum (ER) is an important organelle for protein synthesis and is an early step in the secretory pathway of all eukaryotic cells. In the ER, proteins undergo folding and a subset destined for secretion is transported to the Golgi apparatus for further post-translational modification. In this process, soluble proteins in the ER lumen that are destined for the Golgi apparatus are recruited to the membrane of the ER where they bind either transmembrane proteins or other soluble protein adaptors that bind to transmembrane proteins. These transmembrane proteins are then bound by a five protein coat complex called the Coat Protein complex II (COPII) that deforms the ER membrane into a transport vesicle containing cargo proteins that is trafficked to the Golgi apparatus. Two hematologic diseases have been discovered that are caused by mutations in proteins in this pathway: combined deficiency of coagulation factors V and VIII (F5F8D) and Congenital Dyserythropoietic Anemia type II (CDAII). F5F8D is characterized by decrease in FV and FVIII to 5-30% their normal levels. CDAII is a mild anemia associated with >10% bi-or multi- nucleate erythroblasts in their bone marrow. F5F8D is due to mutation in the genes encoding LMAN1 and MCFD2, an ER transmembrane protein and soluble cargo adaptor, respectively, which form a specific cargo receptor for FV and FVIII. Mutations in the gene encoding the COPII coat protein SEC23B cause CDAII. In this chapter we will discuss what is known about the mutations underlying these two diseases and the surprising discovery that mutations interrupting such a fundamental cellular process as ER to Golgi transport can give rise to specific and limited phenotypes.

ER to Golgi transport is a fundamental process to all eukaryotic cells and has been studied at the genetic and cellular levels in the yeast S*accharomyces cerevisiae.* In eukaryotic cells, proteins are translated by mRNAs on ribosomes on the membrane of the ER and co-translationally translocated into the ER lumen. Once in the ER the proteins fold into their native conformation. A fraction of the proteins remain in the ER as resident ER proteins but others are transported to the Golgi apparatus for further post-translational modifications[1,2]. Once folding has occurred, the proteins that are to be transported out of the ER are routed to ER exit sites where they are packaged into COPII coated vesicles[3-5]. CDAII and F5F8D are two hematologic diseases that will be discussed in this review that result from mutations in this pathway. CDAII is caused by mutations in the COPII coat protein *SEC23B* while F5F8D can be caused by mutations in either of two genes: *LMAN1* or *MCFD2*[6,7]. The phenotype of patients with CDAII appears to be limited to the erythroid lineage in the bone marrow, while the phenotype of patients with F5F8D is a reduction of clotting factors V and VIII. The genetics and pathogenesis of these diseases will be the focus of this review.

COPII transport

Overview of the COPII coat. An *in silico* analysis of known transmembrane proteins or proteins with an ER signal peptide estimated that approximately 1/3 of known open reading frames (ORFs) are transported into the ER during translation[8]. Transport of newly synthesized proteins from the ER to Golgi occurs in a COPII coated vesicle. The COPII coat was initially described in yeast[9-11] and consists of 5 components that form a complex on the surface of the budding ER: Sar1p, Sec23p, Sec24p, Sec13p and Sec31p. Assembly of the COPII coat on the surface of the ER begins with the cytoplasmic protein Sar1p exchanging its bound GDP for GTP by the GTP-exchange-protein (GEF) Sec12p, which is a protein bound to the cytoplasmic surface of the ER. GTP-bound Sar1p is tethered by insertion of a specific alpha-helix into the ER membrane followed by recruitment of a Sec23p-Sec24p heterodimer from the cytoplasm through direct binding of Sec23p to Sar1p. The Sar1p-Sec23p-Sec24p complex assembled on the cytoplasmic surface of the ER membrane binds ER luminal transmembrane proteins primarily through

interaction of the cytoplasmic tails of these proteins with Sec24p. After the binding of Sec23p-Sec24p heterodimers to Sar1p and membrane proteins, the outer COPII coat begins to form. This process involves recruitment from the yeast cytosol of heterotetramers of the proteins Sec13p and Sec31p. This outer coat of the vesicle binds to the inner complex and facilitates budding off the surface of the ER. The outer COPII coat along with Sec23p also facilitates the hydrolysis of the GTP bound to Sar1p to GDP which allows membrane deformation, budding and scission to occur[1,2,12,13] (Figure 1-1). The protein Sec16 also helps facilitate COPII budding and scission and marks the ER exit sites which are the sites on the ER from which the COPII vesicles bud[3,4,14]. Shortly after the vesicle buds from the ER, the COPII components un-coat and are dispersed back into the cytoplasm while the COPII vesicle is transported to the Golgi along microtubules[5,15]. Formation of a COPII coat in a mammalian cell works much the same way as in yeast; however, for many of the COPII coat proteins in mammals and other organisms there are additional isoforms encoded by parologous genes.

Isoforms of COPII coat proteins. In mammals, there are the same five classes of proteins that make up a COPII vesicle; however, most classes are encoded by paralogous genes. There are two Sar1 genes named *Sar1a* and *Sar1b*, two Sec23 genes – *Sec23a* and *Sec23b*, four Sec24 genes – *Sec24a*, *b, c* and *d* and two Sec31 genes – *Sec31a* and *Sec31b*. There remains one *Sec13* gene in mammals. Yeast also have two additional paralogs of Sec24p[16-18]. The precise function of these proteins is not known, but some insight can be derived from mouse and human studies to date.

Cargo mediated transport. The current paradigm in COPII transport suggests concentration of cargo is necessary for efficient transport to occur[16,19-24]. This is thought to occur by transmembrane proteins in the ER binding to Sec24p that are either themselves cargo or serve as an adaptor to concentrate a soluble protein in the ER lumen. One example in yeast is the transmembrane protein Erv29p, which serves as a cargo adaptor for the glycosylated soluble protein pro-alpha factor[25]. In mammals, cargo-mediated transport has been shown to play a role in a diverse array of cellular processes in both normal physiology and disease states. In humans the LMAN1-MCFD2 complex is responsible for transporting coagulation factors V and VIII[6,7]. In addition to

transporting these two clotting proteins, LMAN1 has also been reported to act as a cargo receptor for two lysosomal proteins - Cathepsin C (CatC) and Cathepsin Z (CatZ), as well as the serum protein alpha-1-antitrypsin[26-28].

COPII in disease. Several recent reports have demonstrated in humans and mice seemingly tissue specific mutant phenotypes for what appear to be processes ubiquitous to all cells (Table 1-1). The first of these reports was a mutation in the human gene *SAR1B*. People with recessive mutations in *SAR1B* are affected with Anderson's disease or Chylomicron Retention Disorder (CMRD)[29]. The phenotype of this disorder is accumulation of chylomicrons in gut endothelial cells and malabsorption of lipids from the diet. Mice homozygous for a nonsense mutation in *Sec24b* have a completely open neural tube. The data also suggested that SEC24B transports Vangl2, a protein previously implicated in nervous system development[30]. Humans homozygous for an F382L missense mutation in the trunk domain of *SEC23A* are affected with Cranio-Lenticulo-Sutural-Dysplasia (CLSD)[31]. In this disease, patients are born with Y-shaped cataracts, late closure of their cranial fontanelles, and mild mental retardation. The F382L mutation caused decreased vesicle forming ability due to decreased interaction with the Sec13/31 outer coat[32]. However, this defect in vesicle formation was only observed when the F382L mutant was bound to SAR1B, but when SAR1A was used in the assays the mutant had similar activity to the wild type protein. There has also been a Sec23a zebrafish mutant described with a defect in cartilage development[33]. Patients with mutations in *SEC23B* are affected with CDAII and patients with mutations in either LMAN1 or MCFD2 have F5F8D, both of which are described in more detail below.

Combined Factor V and Factor VIII deficiency

LMAN1. One of the two causative genes for F5F8D was identified to be Lectin Mannose binding protein 1 (*LMAN1*). *LMAN1* is a type I transmembrane protein spanning between the lumen of the endoplasmic reticulum and the cytosol[34,35]. The protein name for the gene *LMAN1* is ERGIC-53, as the protein was initially used as a marker for the ER-Golgi Intermediate Compartment (ERGIC). ERGIC-53 exists in a hexameric complex that cycles between the ER and the ERGIC via a di-phenylalanine

export signal at its C-terminal cytoplasmic tail an and adjacent di-lysine retrieval signal that causes the protein to recycle to the ER[36]. Surprisingly, ERGIC-53 was implicated in transport of coagulation factors V and VIII from the ER to the Golgi apparatus[6,37] as these clotting factors are reduced to 5-30% their normal levels in patients with F5F8D. Factor V is made in the hepatocyte in humans and the megakaryocyte in mice[38-40]. The biosynthetic origin of Factor VIII is still a question of some debate, though the prevailing view is the hepatic endothelial cell[41,42]. While patients with mutations in *LMAN1* have a defect in FV and FVIII, it is likely that *LMAN1* is important for transporting other cargoes out of the ER as well. First, orthologs of *LMAN1* are present in species that do not have a FV or FVIII ortholog such as *D. melanogaster* and *C. elegans.* Further, the lysosomal proteins cathepsin C and cathepsin Z as well as α-1-anti-trypsin have been reported as cargoes for *LMAN1*[26,27] (Figure 1-2).

ERGIC-53 is a 510 amino acid protein that consists of several distinct domains. The first 31 amino acids form a signal sequence that targets ERGIC-53 to the ER. The Carbohydrate Recognition Domain (CRD) is important for cargo binding[43]. Following the CRD is a coiled-coil domain, which has two cysteines that allow for the oligomerization of ERGIC-53, either as a homohexamer or as three dimers[44]. The N-terminal side of the ERGIC-53 protein exists on the luminal side of the ER while only the C-terminal 12 amino acids of the are on the cytoplasmic side of the membrane[36]. The C-terminal four amino acids are KKFF; the di-phenylalanine residues acts to transport the ERGIC-53 hexamers out of the ER while the di-lysine residues allow for retrieval back to the ER[45].

MCFD2. MCFD2 is a soluble protein in the ER lumen that binds to ERGIC-53 in a calcium-dependent manner and mutations in this protein also cause F5F8D[6]. *MCFD2* and *LMAN1* bind with a 1:1 stoichiometry. In the absence of ERGIC-53, MCFD2 is not recycled back to the ER but secreted out of the cell[37]. *MCFD2* is a four exon gene with a 145 bp open reading frame that translates to a 16 kDa protein. MCFD2 contains a signal sequence and two EF-hand domains, which are important for binding calcium in the ER[46].

The EF-hand domains of MCFD2 are critical for ERGIC-53 binding. MCFD2 disease-associated proteins resulting from missense mutations interact with FV or FVIII although they disrupt binding of MCFD2 to ERGIC-53[47]. However, FVIII can bind LMAN1 independently of MCFD2. Deleting the EF hand domain in MCFD2 also markedly decreases its interaction with FV and FVIII. Recently, the carbohydrate recognition domain (CRD) on ERGIC-53 was shown to be responsible for binding MCFD2. This was also confirmed by two reports of the crystal structure of the CRD-MCFD2 complex[48,49]. Oligomerization of ERGIC-53 into homohexamers is also necessary for MCFD2 binding; monomeric ERGIC-53 cannot exit the ER. Experiments *in vitro* have shown the interaction among ERGIC-53, MCFD2, FV and FVIII to be transient as chemical crosslinking is required to detect interaction between these proteins[37]. These data, when taken together with the other cargoes for ERGIC-53, suggest that transmembrane cargo receptors could transport other cargoes by using soluble protein adaptors in the ER.

MCFD2 mutations identified in patients with F5F8D include three frameshift and two splice site mutations[6]. Genotype-phenotype correlation identified slightly lower levels of FV and FVIII in patients with MCFD2 mutations compared to those with *LMAN1* mutations[50] .

Congenital Dyserythropoietic Anemia type II

Clinical features of CDAII. CDAII is an autosomal recessive disease characterized by mild to severe anemia, with median hemoglobin of 9-10 g/dL[51]. Other clinical findings include jaundice and >10% bi- or multi-nucleate bone marrow erythroblasts. An increased migration or shift of the red blood cell membrane protein band 3 by SDS-PAGE is also seen in CDAII patients. This shift is caused by truncated sugar structures on the surface of the band 3 protein[52]. Late erythroblasts and red blood cells in CDAII have an internal double plasma membrane which can be appreciated by transmission electron microscopy. Further studies of the membrane fraction of RBCs by western blot analysis and immunogold staining demonstrated the double membrane to be residual endoplasmic reticulum in the cells[53] (Figure 1-3). The RBCs of patients affected

by CDAII can be lysed in acidified normal serum which led to the name, "Hereditary Erythroblastic Multi-nuclearity associated with a Positive Acidified-Serum test (HEMPAS)" when CDAII was first described.[54] Approximately 50-60% of patients also have an enlarged spleen[55] and peripheral blood smears from these patients are mostly normocytic with anisocytosis and poikilocytosis[56]; patients can also have iron overload[55]. Patients are typically treated with blood transfusions and iron chelation therapy[51].

It is not yet known if the multi-nucleate red cell precursors in CDAII are caused by a "cell autonomous" defect in the erythroblast. A cell autonomous defect is one in which the disease is caused by a defect intrinsic to the cellular machinery of the red cell lineage. However there have been several recent case reports showing that bone marrow transplant is curative for CDAII[57-59]. In one of these reports, the patient became chimeric for host and donor cells in every lineage except the erythroid lineage which were entirely donor derived[59]. These data could indicate an erythroid cell autonomous defect being causative for CDAII.

Mutations in SEC23B cause CDAII. Recently, the molecular basis for CDAII has been discovered as recessive mutations in the COPII coat protein SEC23B. To date, 53 mutations have been described in 99 different patients, including missense, frameshift, nonsense and splice site mutations[60-62] (Figure 1-4). Patients have been identified as either homozygotes for the same mutation or compound heterozygotes for different mutations in *SEC23B*. The mutations in *SEC23B* are distributed throughout the gene and affect every domain of the protein[60]. No patient has yet been reported with two nonsense mutations in *SEC23B* which could mean that total SEC23B deficiency is not compatible with life. There is no clear genotype-phenotype correlation in CDAII[63] and the molecular and mechanistic underpinnings of the disease also have yet to be determined.

There have been animal models proposed for CDAII both in mice and zebrafish. Knockout mice for alpha-mannosidase-II show anemia, splenomegaly and an increase in erythroblasts in the mouse bone marrow[64]. Zebrafish with a mutation in the gene encoding the band 3 protein have bi-nucleate erythrocytes and decreased staining for hemoglobinized cells[65]. Although these animal models have many similar features of the

human disease, now that *SEC23B* has been identified as the gene responsible for CDAII, the phenotypes of mice and zebrafish with mutations in *Sec23b* will be of particular interest. A summary of the *Sec23a* and *Sec23b* mutant mice described in this thesis are listed in Table 1-2.

Conclusions

A common theme in biology is the manifestation of genetic diseases in specific cell types from mutations in genes expressed in a wide variety of tissues. This observation holds true for CDAII, F5F8D and other hematologic diseases as well. Diamond-Blackfan anemia, which is characterized by erythroid aplasia, is caused by mutations in distinct ribosomal protein genes[66,67]. In the COPII pathway, the paralog to SEC23B – SEC23A appears to overlap SEC23B in expression pattern and function[32], yet it is not yet clear why mutations in *SEC23A* cause defects in cranial cartilage and cataracts, while mutations in *SEC23B* cause anemia.

Since SEC23B, LMAN1 and MCFD2 all function in the COPII pathway the question of what other cargoes might traffic with these proteins remains an important one for the field. While there is evidence for other cargoes trafficking with LMAN1, there is no evidence for any other clinical manifestation besides bleeding symptoms. Perhaps other cargoes for LMAN1 or MCFD2 may be more subtly affected in F5F8D, below what might present clinically. In CDAII, there could be some critical cargo involved in erythroid differentiation or mitosis which could lead to a bi-nucleate phenotype. In regards to the presence of residual ER in the cells, a defect in COPII trafficking could result in failure to secrete this organelle during red cell maturation. Discoveries of the genes responsible for rare hematologic diseases have led to insight into the biology of the early secretory pathway. Using blood diseases as a model for protein trafficking may yield further insight into this fundamental process in other cell types.

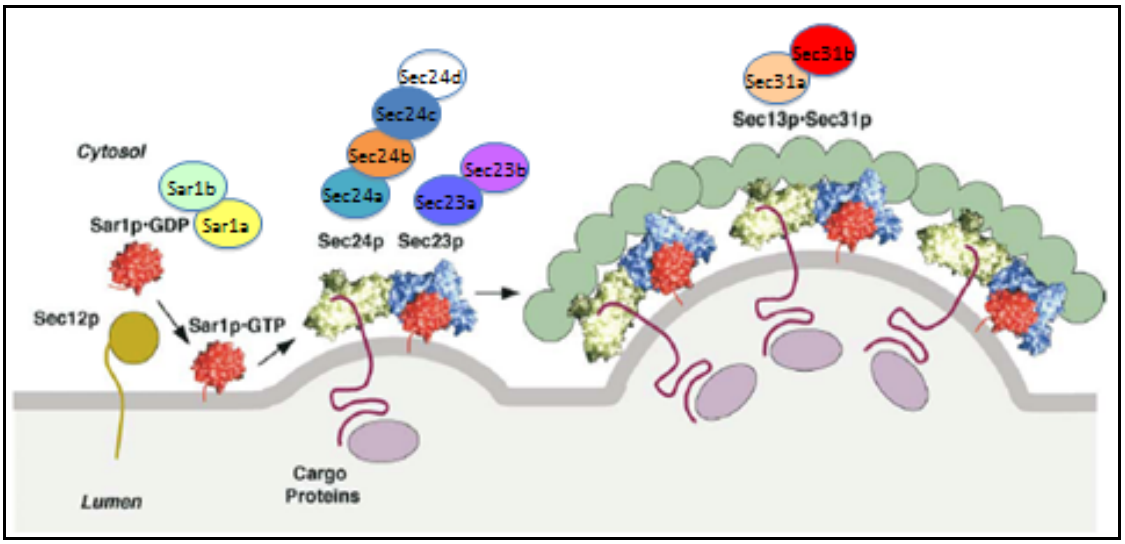

Figure 1- 1: Formation of the COPII coat on the surface of the endoplasmic reticulum

Sar1p changes from the GDP bound state to the GTP bound state by the exchange factor Sec12p. GTP bound Sar1p is then bound by the Sec23p-Sec24p heterodimer. Sec24p also binds transmembrane proteins in the ER membrane that are cargo themselves or bind other soluble cargo. Lastly the outer coat consisting of Sec13p and Sec31p binds and the vesicle buds and separates from the ER membrane. Mammalian COPII paralogs are depicted as colored ovals. (Adapted with permission from Bonifacino and Glick 2004)

Table 1- 1: Mutations reported in COPII component paralogs in humans and mice.

COPII paralog	Human disease or mouse phenotype (all are recessive)	Mutation	Description	Reference
Sar1b	Anderson's disease (Human)	Missense, Nonsense, Frameshift	Gut malabsorption of lipids and accumulation of chylomicrons in intestinal cells	29
Sec23a	Cranio-Lenticulo-Sutural Dysplasia (CLSD) (Human)	Missense	Open cranial fontanelles, Y-shaped cataracts, mental retardation	31
Sec23b	Congenital Dyserythropoietic Anemia type II (CDAII) (Human)	Missense, nonsense and splice site	Anemia, multi-nucleate erythroblasts, enlarged spleen	61,62
Sec24b	Neural tube defect in mice (Mouse)	Nonsense	Mice develop to term with completely open neural tube	30

Table 1- 2: Summary of mouse mutants described in this thesis.

Gene	Mutation	Mouse phenotype
Sec23a	Gene trap insertion intron 2	Embryonic lethal
Sec23b	Gene trap insertion intron 19	Pancreatic degradation No erythroid phenotype
Sec23b	Gene trap insertion intron 4	Pancreatic degradation

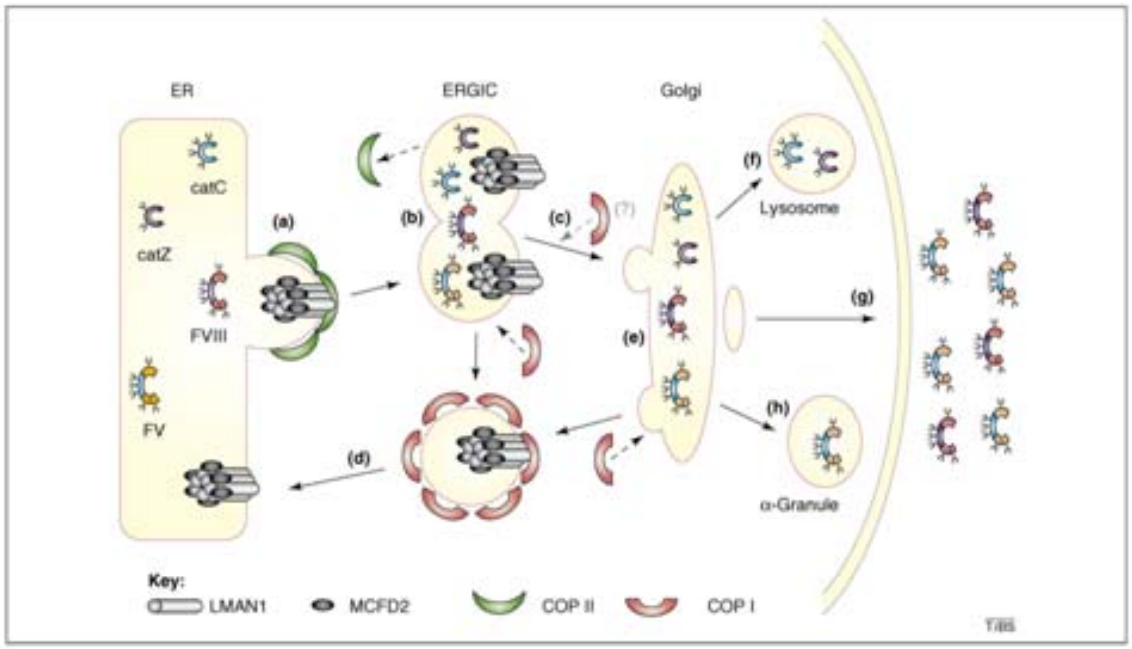

Figure 1- 2: Transport of cargo by the LMAN1-MCFD2 complex

A) Coagulation factors V and VIII, cathepsin C (catC) and cathepsin Z (catZ) are transported with the LMAN1-MCFD2 complex in a COPII coated vesicle. B) COPII coats fuse into the ER-Golgi Intermediate Compartment. C) Proteins are transported forward to the Golgi apparatus. D) The LMAN1-MCFD2 complex is recycled back to the ER. E) The cargo proteins are further modified in the Golgi apparatus. F) CatC and catZ are transported to the lysosome while FV and FVIII are secreted from the cell. H) Factor V can also be stored in α-granule in megakaryocytes that will eventually form platelets. (Reprinted with permission from Baines and Zhang 2007)

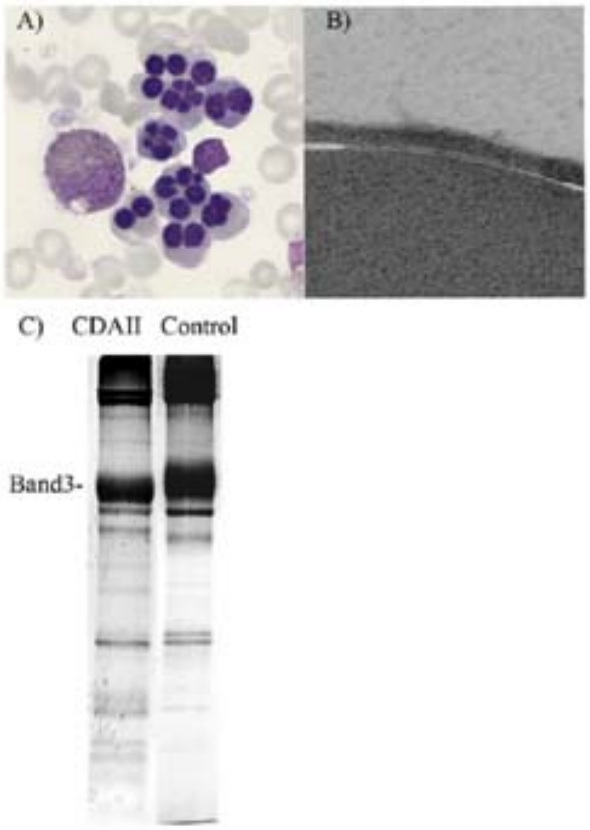

Figure 1- 3: Abnormal findings in CDAII.

A) Multi-nucleate erythroblasts in patients with CDAII. B) Transmission electron microscopy showing double internal plasma membrane in red blood cells and erythroblasts. C) Shift of Band 3 protein by SDS-PAGE (Reprinted with permission from Denecke and Marqardt 2009).

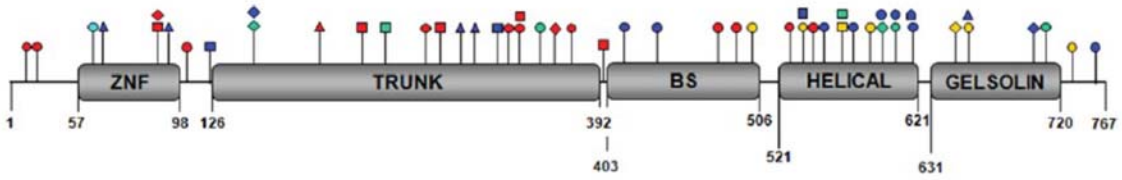

Figure 1- 4: Distribution of *SEC23B* mutations identified in CDAII patients.

Mutations that cause CDAII have been identified in every domain of the SEC23B protein. ZNF=Zinc finger domain, BS=β-sheet. Circles represent missense mutations, squares represent nonsense mutations, diamonds are splice site mutations, triangles are frameshift mutations and pentagons are amino acid deletions. (Reprinted with permission from Russo et al. 2010).

Note: Chapter 1 will be submitted to the journal Blood as an invited review titled "The importance of the COPII pathway in hematologic disease" by Matthew Vasievich and David Ginsburg.

CHAPTER II:

Sec23b Deficiency in Mice Results in Pancreatic Destruction but No Apparent Defect in Hematopoiesis

Abstract

Human mutations in *SEC23B* cause Congenital Dyserythropoietic Anemia type II (CDAII). Here we study the effects of SEC23B deficiency on mouse hematopoiesis. *Sec23b* mutant mice were generated by integration of a gene trap cassette into the last intron of the *Sec23b* gene (*Sec23b gt)*. *Sec23b gt/gt* mice die at birth due to severe disruption of the exocrine pancreas. Complete blood counts (CBC) showed no significant differences in hemoglobin or hematocrit in *Sec23b gt/gt* neonates compared to littermate controls. To study the role of *Sec23b* in adult murine hematopoiesis, bone marrow of irradiated adult wild-type mice was reconstituted by transplantation of *Sec23b gt*/*gt* or wild-type fetal liver cells. No significant differences in hemoglobin or hematocrit were observed up to 25 weeks following transplant of *Sec23b gt/gt*, or wild-type fetal liver cells. Competitive transplants using *Sec23b gt/gt* or control fetal liver cells mixed with competitor cells, showed no significant difference in contribution to peripheral blood Red Blood Cells (RBCs), neutrophils, B- or T-cells, or hematopoietic stem cells. Transplantation of bone marrow obtained from primary competitive transplant recipients into a second wild-type recipient also showed no significant difference in reconstitution of peripheral blood lineages by *Sec23b gt/gt* or control cells. These data suggest disparate functions in hematopoiesis between human and mouse, though a contribution from residual hypomorphic SEC23B function in the *Sec23b gt* allele cannot be excluded.

Introduction

The congenital dyserythropoietic anemias (CDAs) were first reported in the 1960s and are divided into three distinct syndromes, distinguished by specific morphologic changes in the bone marrow and biochemical findings in peripheral blood [68]. CDAII is an autosomal recessive disease that is the most common of the CDAs, with over 300 cases reported [51]. Patients with CDAII are anemic (mean hemoglobin concentration 9.1-9.8 g/dl) and frequently develop jaundice, splenomegaly [51], gallstones, and iron overload [69]. Bone marrow from patients typically exhibit a markedly hypercellular appearance, comprised of 45-90% erythroid precursors, with 10-45% of mature erythroblasts bi- or multinucleated [68,70]. Erythrocytes isolated from peripheral blood show a double plasma membrane on electron micrograph, which has been shown to be comprised of residual endoplasmic reticulum (ER) [53,71,72]. Red blood cell ghosts from CDAII patients analyzed by SDS-PAGE show faster migration of Band 3[73,74], which is thought to result from hypoglycosylation of the protein. Treatment of CDAII typically consists of transfusions, as needed, as well as splenectomy and/or cholecystectomy in some patients [51]. Iron overload is a common complication, treated by judicious phlebotomy or iron chelation [75].

Mice deficient in alpha-mannosidase-II exhibit dyserythropoiesis, splenomegaly, increased reticulocytes, and a decrease in myeloid:erythroid ratio in the bone marrow, suggesting a role for the corresponding gene in human CDAII [64]. Similarly, mutations in the zebrafish gene encoding Band 3 result in a phenotype resembling CDAII, with severe anemia, bi-nucleate circulating erythroblasts and a double membrane on transmission electron microscopy [65]. Despite these earlier clues from animal models, recent reports demonstrate that most cases of CDAII in humans are due to mutations in *SEC23B*, which encodes a key component of the COPII vesicle coat, mediating transport of proteins between the ER and Golgi [61,62]. Of note, although these reports describe a range of defects in *SEC23B*, including nonsense mutations and deletions, no patient has yet been described homozygous or compound heterozygous for a clearly null mutation, suggesting that complete SEC23B deficiency may be lethal.

We now describe the characterization of mice homozygous for integration of a gene trap cassette into the last intron of the murine *Sec23b* gene, resulting in loss of SEC23B function. The gene trap consists of a strong splice acceptor upstream of a β-galactosidase reporter. The gene trap will intercept splicing to any downstream exons and result in a fusion protein of the amino acids encoded in the exons upstream of the gene trap and the β-galactosidase reporter. SEC23B-deficient mice die within a day of birth with severe disruption of the pancreas (Bin Zhang, unpublished observations). Fetal liver cell transplants to generate adult mice with SEC23B-deficient hematopoiesis fail to recapitulate the CDAII phenotype. These findings sugges that SEC23B, and potentially other COPII coat protein paralogs, may have disparate functions in mice and humans.

Materials and Methods

Mice. The *Sec23b* embryonic cell gene trap line AD0407 was obtained from Bay Genomics (http://www.genetrap.org/) and injected into C57BL/6J blastocysts in the University of Michigan Transgenic Animal Core as previously described [76]. Germline transmission was achieved and *Sec23b +/gt* mice were subsequently backcrossed >10 generations onto C57BL/6J. Mice were housed at the University of Michigan in accordance with the regulations of the University Animal Care and Use Committee (UCUCA). A second mutant *Sec23b* allele was obtained as a gift from Bin Zhang which was generated from the European Conditional Mutant Mutagenesis program (EUCOMM). In order to remove the gene trap cassette and delete the exons flanked by the LoxP sites, these mice were then crossed to mice expressing *Flp* under the control of the human β-actin promoter (stock #005703) and subsequently mice expressing cre recombinase under the control of the adenovirus EIIa promoter (stock #003724) both were obtained from the Jackson Laboratory.

PCR and genotyping. DNA was prepared from a tail biopsy using standard methods [77] and genotyping was performed by PCR on the *Sec23b* gene trap line with one primer in intron 19 of *Sec23b,* upstream of the gene trap insertion (primer F, 5'-GTGATCACATTCCAGCTCCA-3'), a second primer within the gene trap vector (primer V, 5'-GGCCTCTTCGCTATTACGC-3') and a third primer downstream of the

gene trap insertion in intron 19 (primer R, 5'-AGGAGCAACCAGTGCTCTTCA-3') (Figure 2-1). Fractionation of PCR products by gel electrophoresis yields generates a 325 bp band from the gene trap allele and 275 bp band from the wild-type allele (Figure 2-1). The *Sec23b* mutant line from EUCOMM was genotyped with one primer upstream of the LoxP sites (primer F1, 5'- ATAGACCAGGCTGGCCTCAGTC-3') and two primers flanking one of the LoxP sites (primer F2, 5'-AACAGCCCAGGTGACTAGGA-3') and (primer R1, 5'-CAAGTGAGTGCCTCCTCACA-3'). The wildtype allele yields a 235 bp band, deleting the LoxP sites yields a 336 bp band and the floxed allele yields a 269 bp band.

Fetal liver cell transplant. Fetal liver cell transplant was performed as previously described [40]. Briefly, pregnant female mice from heterozygous *Sec23b+/gt* intercrosses were sacrificed at 17.5 days post coitus and fetal livers of pups disrupted and suspended in 65% RPMI 1640 medium, 25% Fetal Bovine Serum (FBS) and 10% DMSO. Fetal liver cells were frozen at -80ºC overnight and stored in vapor phase liquid nitrogen at -186ºC. DNA was prepared and genotype was determined by PCR as described above. 6-12 week old C57BL/6J mice (Jackson Laboratory, Bar Harbor, ME) were administered two doses of 550 rads (spaced by 3 hours) in a Cs Gammacell 40 Exactor irradiator (MDS Nordion). Frozen wildtype (WT) and *Sec23b gt/gt* fetal liver cells were incubated until thawed in a 37ºC water bath and 106 cells in a total volume of 300 µL RPMI 1640 with 2% FBS were injected into the retro-orbital venous sinus of irradiated recipient mice. Treated mice were administered acidified tap water (pH=2.35) for 3 weeks post transplant.

Blood and bone marrow studies. Approximately 20 µL of peripheral blood was drawn from the retro-orbital plexus of transplanted mice and diluted 1:10 in 5% Bovine Serum Albumin (BSA) in Phosphate Buffered Saline (PBS) pH 7.4 (Gibco). Complete blood counts were obtained using an Advia120 blood analyzer (Bayer). Mice were anesthetized using pentobarbital and blood was drawn via cardiac puncture and diluted 1:9 with sodium citrate (Sigma). Bone marrow was flushed from femurs and tibias using Hank's Balanced Salt Solution (HBSS, Gibco) supplemented with 5% FBS. Bone marrow cells were diluted to 800,000 cells/mL, collected by centrifugation in a Cytospin

4 (Thermo Scientific), and stained with the HEMA 3 kit (Fisher). Red blood cells (RBCs) were submitted to the University of Michigan Microscopy and Imaging core for processing and analyzed on a CM-100 Transmission Electron microscope (Philips). To prepare RBC ghosts, whole blood was subjected to centrifugation at 2300g, the RBC pellet washed twice with PBS, pH 7.4 and then lysed by suspension in ghost lysis buffer (5mM Na2PO4, 1.3 mM EDTA, pH=7.6) with 1 protease inhibitor tablet (Roche, stock#11873580001) per 50 mL buffer. Lysate was spun at 16,000g and the supernatant containing the RBC membrane fraction was removed following centrifugation at 16,000g for 15 minutes and washed 4-6 more times in ghost lysis buffer. RBC ghosts were stored at -80ºC in lysis buffer.

Flow cytometry. Staining for flow cytometry was carried out using antibodies from eBioscience, BD Biosciences or BioLegend: Ter119, Gr1 (RB6-8C5), Mac1 (M1/70), CD3 (145-2C11), CD16/CD32 (2.4G2), CD45R/B220 (RA3-6B2), CD150 (TC15-12F12.2), Sca1 (D7), CD117 (2B8), CD48 (BCM1), CD19 (6D5), TCRβ (H57-597), CD8 (53-6.7), CD11c (N418), CD4 (RM4-4), NK1.1 (PK136), and TCRγ/δ (GL3). Samples were run on either a Canto or Aria flow cytometer (Becton Dickinson). Flow cytometry data was analyzed with the FlowJo software package (Treestar).

Competitive fetal liver cell transplant. UBC-GFP mice that express a *GFP* transgene under control of the human ubiquitin C promoter were obtained from the Jackson laboratory (stock #004353). These mice express high levels of GFP in hematopoietic cells [78]. Male mice homozygous for the *UBC-GFP* transgene (*UBC-GFPTg+/+*) were used in timed matings to C57BL/6J females and fetal livers were harvested at 17.5 days post coitus (dpc) from progeny of a *UBC-GFPTg+/+* X C57BL6/J cross (all of whom should be hemizygous (GFP+/0) for the GFP transgene). Fetal livers were frozen in freezing medium as described above. Transplants into C57BL6/J recipients (Jackson Lab) were performed as described above, using as donor GFP+/0 fetal liver cells mixed 1:1 with either C57BL6/J or *Sec23b gt/gt* fetal liver cells. For secondary transplants, whole bone marrow cells from GFP:WT and GFP:*Sec23b gt/gt* recipients were pooled for each genotype. Lethally irradiated C57BL/6J males were injected with 2x106 cells from either the GFP:WT or GFP:*Sec23b gt/gt* pool.

Analysis of Murine Embryonic Fibroblasts. At 12.5 dpc, embryos were harvested from a *Sec23b+/gt* X *Sec23b+/gt* cross to generate primary murine embryonic fibroblast (MEF) cells. Briefly, embryos were disrupted using 0.05% trypsin and grown in Dulbecco's Modified Eagle Medium (DMEM) supplemented with 10% FBS and 1x penicillin/streptomycin. A portion of the cells were taken for genotyping using the protocol described above. The remaining MEF cells were frozen in Freezing Medium (Gibco, stock#12648-10) at -80ºC overnight and then transferred to vapor phase liquid nitrogen at -186ºC. Cells were subsequently thawed and expanded in DMEM medium as described above. MEF cells were grown to approximately 80% confluence and lysed in lysis buffer (100mM Tris pH 7.5, 1% N P-40, 10% Glycerol, 25mM sodium β-glycerolphosphate, 130mM NaCl, 10mM NaF, 1mM Na3VO4, 1mM EDTA, 5mM MgCl). Immunoprecipitation was performed as previously described [37] using a rabbit anti-SEC24A antibody made at Pacific Immunology by injecting a rabbit with the mouse Sec24a peptide NTYDEIEGGGFLATPQL. Western blots were carried out as previously described [37] using a rabbit antibody generated against the murine SEC23B peptide: LTKSAMPVQQARPAQPQEQP (Proteintech Group Inc, Chicago, IL). Protein A/G beads were purchased from Santa Cruz Biotechnology (stock#sc-2003).

Statistics. All data from transplant studies were analyzed by t test.

Results

Immunoprecipitation of the gene trap fusion protein

To examine any residual SEC23B expression from the *SEC23B*-gene trap allele was a null allele, timed matings were carried out by intercrossing *Sec23b*+/gt mice to generate murine embryonic fibroblasts (MEFs). WT, *Sec23b+/*gt and *Sec23b gt/gt* MEFs were subsequently grown in culture, lysed and SEC24A, the binding partner of SEC23B was immunoprecipitated. A western blot for SEC23B shows no detectable SEC23B protein at the expected size in *Sec23b gt/gt* MEFs, but the presence of a higher molecular weight band at the expected size of a SEC23B-β-gal fusion protein (Figure 2-2).

Fetal liver cell transplant

Sec23b gt/gt mice die perinatally with massive pancreatic degeneration. CBC analysis (Figure 2-3A) shows no evidence of anemia (Bin Zhang, personal communication). In order to study the effect of *Sec23b* deficiency on adult hematopoiesis, lethally irradiated 6-12 week old C57BL/6J mice were transplanted with E17.5 fetal liver cells from either WT or *Sec23b gt/gt* mice. The results of CBC analyses at 6, 8, 12 and 25 weeks post-transplant are shown in Figure 2-3B-C. No significant difference in either hemoglobin or hematocrit was found between WT and *Sec23b gt/gt* transplant recipients at any of the time points studied. No significant difference in spleen mass was observed between WT and *Sec23b gt/gt* transplant recipients at 20 weeks post-transplant (Figure 2-4C). Examination of the bone marrow revealed no significant difference in percent bi-nucleate erythroblasts between WT and *Sec23b gt/gt* animals (Figure 2-4A). Determination of myeloid:erythroid ratio also revealed no significant difference between WT and *Sec23b gt/gt* transplant recipients (Figure 2-4B). No shift the mobility of Band 3 was observed on polyacrylamide gel electrophoresis (Figure 2-5). Whole red blood cells were analyzed by transmission electron microscopy for the characteristic double membrane seen in CDAII patients. No double membrane was observed at any magnification in RBCs from mice receiving *Sec23b gt/gt* fetal liver cells (Figure 2-6).

Long Term Hematopoietic Stem Cells (LT-HSCs)

No significant difference in the number of LT-HSCs (ckit+Sca-1+CD150+CD48-(lineage-)) was seen between WT and *Sec23b gt/gt* fetal livers (Figure 2-8).

Competitive fetal liver transplant

The competitive fetal liver cell transplant procedure is illustrated in Figure 2-7. Over the 18 week course of the transplant, persistence of GFP- cells were observed in recipients of both GFP:*Sec23b gt/gt* and GFP:WT fetal liver cells including Ter119+ red blood cells, CD3+ T cells, B220+ B cells and Mac1+Gr1+ myeloid cells (Figure 2-9 to 2-

11). Of note, a lower percentage GFP- *Sec23b gt/gt* cells was consistently observed in all lineages over the course of the transplant.

Long term reconstituted GFP:WT and GFP:*Sec23b gt/gt* transplant recipient mice were sacrificed 18 weeks post-transplant. Persistence of GFP- cells was observed in all cell populations analyzed in both the bone marrow and thymus (Figures 2-12 to 2-16). No significant difference in GFP- cells was observed in the LT-HSC compartment, however, statistical trends were observed showing fewer GFP- *Sec23b gt/gt* cells among Mac1+Gr1+ myeloid cells, all thymocyte lineages, and Ter119+CD71loFSClo erythroid cells. There was also a statistically significant decrease in GFP- *Sec23b gt/gt* CD19+B220+ bone marrow B cells. However, in all of the lineages showing a trend or significant decrease in GFP- *Sec23b gt/gt* cells, no significant difference was found in the corresponding peripheral blood lineages in the secondary transplant and was not investigated further. To exclude the possibility that the observed populations of GFP- cells were derived from host reconstitution, Mac1+Gr1+ mature myeloid cells from the bone marrow were sorted from recipient mice. PCR of genomic DNA from these cells for the *Sec23b gt* allele detected no residual WT allele in any of the mice receiving GFP:*Sec23b gt/gt* fetal liver cells (Figure 2-14).

Secondary transplant

These data demonstrate that *Sec23b gt/gt* cells can stably engraft in a primary competitive transplant and support hematopoiesis in all compartments for up to 18 weeks. As a more stringent assay of hematopoietic function, secondary competitive transplants were performed using bone marrow cells from primary transplant recipients in a second round of transplantation. Stable persistence of GFP- cells was again observed over the 18 week course of the transplant (Figures 2-17). A subset of secondary transplant recipients was sacrificed 26 weeks post-transplant and bone marrow was taken for analysis of erythroid lineage cells and LT-HSCs. Persistence of GFP- cells was observed for both GFP:WT and GFP:*Sec23b gt/gt* recipients. No differences were observed in the total number of GFP- mature myeloid cells, erythroid progenitors or LT-HSCs (Figures 2-18 to 2-20).

Generation of a floxed allele for Sec23b

To exclude a contribution to the observed phenotype of *Sec23b* deficiency in hematopoiesis from any potential residual function from the *Sec23b gt* allele, a second allele was generated from a mouse embryonic stem cell line from the European Conditional Mouse Mutagenesis program (EUCOMM) (Figure 2-21). This allele has a gene trap in intron 4 of Sec23b flanked by FRT sites and downstream of that, exons 5 and 6 are flanked by LoxP sites. The gene trap was excised by crossing mice heterozygous for the mutant allele to mice expressing an FLP transgene under the control of the human β-actin promoter. Then, the mice were crossed to a transgenic mouse expressing Cre recombinase under the control of the adenovirus EIIa promoter. The deleted exons cause a frameshift resulting in a stop codon in exon 7. Genotypes of mice resulting from this Cre mating are shown in Figure 2-22. Preliminary analysis of mice homozygous for the EUCOMM Sec23b allele demonstrate a pancreas phenotype very similar to that seen with the initial *Sec23b gt* allele (Bin Zhang, personal communication). These findings support the data using the intron 19 gene trap allele.

Discussion

In this chapter, we studied the role of Sec23b in mouse hematopoiesis. Mice that are homozygous for a gene trap insertion in the last intron of the *Sec23b* gene die at birth with severe pancreatic degeneration. Humans with mutations in *SEC23B* are affected with CDAII [61,62]. Our data here suggest that SEC23B has disparate roles in mice and humans. CDAII is characterized by mild to severe anemia that can present anytime from the neonatal period to late in life. *Sec23b gt/gt* mice are not significantly anemic at birth, and adult chimeric mice with hematopoiesis derived from transplanted *Sec23b gt/gt* fetal liver cells also exhibit normal development of the erythroid as well as myeloid and lymphoid lineages up to 25 weeks post-transplant. In addition, other cellular and biochemical findings associated with human CDAII, such as a mobility shift of Band 3 on SDS-PAGE, increased myeloid:erythroid ratio in the bone marrow and double internal membrane in RBCs were also absent in *Sec23b gt/gt* transplant recipient mice. Severe CDAII has been successfully treated with allogeneic bone marrow transplant [58,59,79],

suggesting that the CDAII defect is cell autonomous and intrinsic to bone marrow derived cells. In one human transplant case, chimerism for donor and host blood cells was documented in every lineage except the erythroid which was entirely donor derived, suggesting a competitive disadvantage for SEC23B null precursors in engraftment of the erythroid lineage[59]. These data suggested that being deficient for SEC23B may cause a competitive disadvantage in engraftment of the erythroid lineage. However, no such deficiency in erythroid engraftment was observed for *Sec23b* deficient precursors in murine transplant, with long term persistence of *Sec23b gt/gt* cells observed in all blood lineages, even after a second round of transplantation into new recipients. It is worth noting that after the first round of competitive transplant, the GFP- *Sec23b gt/gt* cells were present at a lower percentage than GFP- WT cells, however this is likely due to mixing error in preparing the cell suspensions for the transplant.

The intron 19 location of the *Sec23b* gene trap allele studied here may have some residual function as evidenced by the presence of a higher molecular weight fusion protein that immunoprecipitates with SEC24A. Therefore, we cannot exclude a contribution of this hypomorphic allele to the observed phenotype. However, the severe pancreatic degeneration and death of mice homozygous for the gene trap allele is not likely a dominant negative phenotype resulting from the presence of this fusion protein since the pancreas of *Sec23b+/gt* mice remains intact. Mice with a gene trap insertion in intron 4 of *Sec23b* show recapitulation of the pancreas phenotype suggesting that this is the true result of *Sec23b* deficiency in the mouse. Patients with CDAII also show no evidence of any pancreatic defect. We cannot rule out that a species difference may exist in producing a phenotype in the pancreas but none in the blood in mice.

In erythroid development, there are known species differences in trying to model human globin switching in the mouse. In normal human erythropoiesis, the temporal sequence of gene activation at the β-globin locus begins with the embryonic globin gene (ε globin), followed by fetal hemoglobin (γ globin) and lastly adult β-globin. In transgenic mice with a yeast artificial chromosome (YAC) for the human β-globin locus and locus control region, the human fetal globin gene is the first to be activated followed by early activation of adult β-globin[80]. These differences were shown to be due to

differences in the expression and target genes of the transcriptional repressor *BCL11A* in humans and mice.

The *SEC23B* paralog *SEC23A* also forms a heterodimer with SEC24 in the formation of the COPII inner coat. These two proteins have an 85% identical amino acid sequence to each other and mutations in humans yield markedly different phenotypes[31,61,62]. As mentioned above, people with mutations in *SEC23B* get CDAII, however people with mutations in *SEC23A* are diagnosed with a disease called cranio-lenticulo-sutural dysplasia (CLSD) [31]. CLSD is an autosomal recessive disorder characterized by Y-shaped cataracts in the eyes, late closure of the cranial fontanelles after birth and mild mental retardation. The extent to which these two proteins overlap in function and tissue expression has not been clearly established in the mouse and human. It is possible that in mice, SEC23B and SEC23A have sufficient overlap in function that SEC23A in hematopoietic cells could rescue deficiency of SEC23B. While there are data showing that SEC23A and SEC23B are expressed in the same tissues [32], these two isoforms could be expressed in different cell types in the same organ, or be co-expressed in the same cells where one isoform is preferentially used.

Further it is not yet know if *SEC23B* deficiency in humans causes a cell autonomous defect in the erythroid lineage or if the disease is caused by lack of secretion of a trans-acting factor that is necessary for erythroid development. The data from the human transplant studies suggest that the defect is cell autonomous; however we cannot exclude a role for residual host bone marrow stromal cells or secretion of factors that promote red cell development from other sources outside the bone marrow. Further, since the gene trap allele is hypomorphic by both binding to SEC24 and also the possibility of residual normal splicing around the gene trap, there could be sufficient SEC23B activity to rescue any blood phenotype but not the pancreatic phenotype. Therefore, a null allele will be useful in addressing this point.

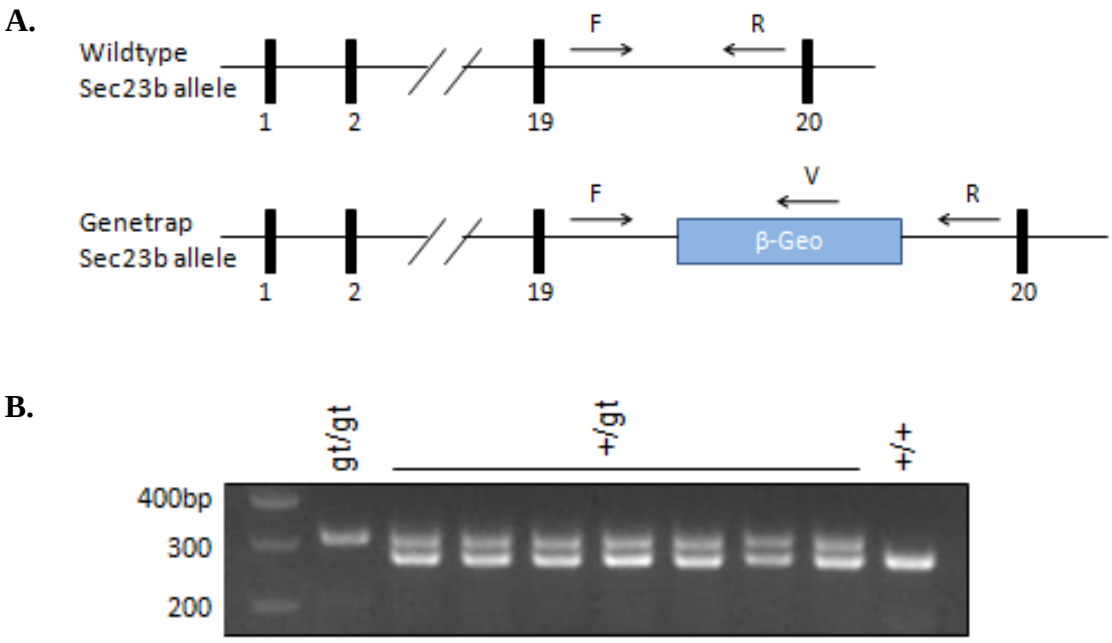

Figure 2- 1: *Sec23b* gene trap allele (*Sec23b gt*) and genotyping assay.

The *Sec23b* gene trap allele consists of a gene trap inserted into the last intron of the *Sec23b* gene. A) Genotyping was performed using a 3 primer assay, with primers upstream (F) and downstream (R) of the gene trap and a 3rd primer within the gene trap itself (V). This reaction yields a 275 bp band for the WT allele and a 325 bp band for the gene trap allele. B) Genotypes of DNA prepared from E17.5 fetal mice.

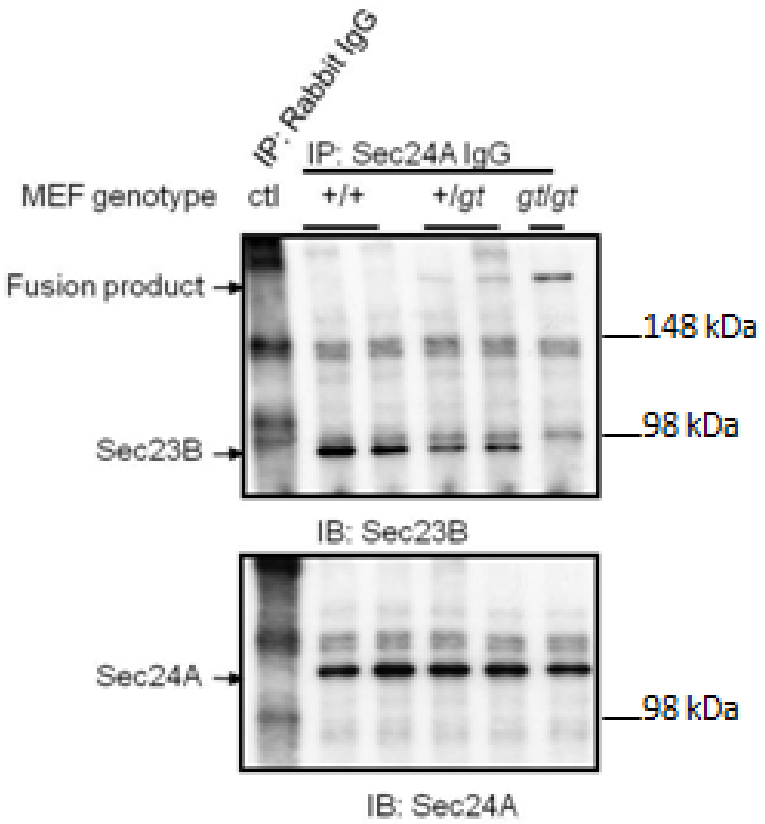

Figure 2- 2: Immunoprecipitation of Sec23b-gene trap fusion protein

WT, *Sec23b +/gt* and *Sec23b gt/gt* MEFs were lysed and immunoprecipitation performed with an antibody against SEC24A. IP lysates were analyzed by SDS-PAGE and reacted with an antibody against SEC23B. An 85 kDa band corresponding to SEC23B was observed in the WT and *Sec23b +/gt* lanes but not in the *Sec23b gt/gt* lane. A higher molecular weight band at the predicted mass of a SEC23B-gene trap fusion protein was also observed to bind to SEC24A in the *Sec23b +/gt* and *Sec23b gt/gt* lane but not the WT lane. The lower panel shows immunoprecipitation of SEC24A from all cell lysates except where rabbit IgG was used as a control.

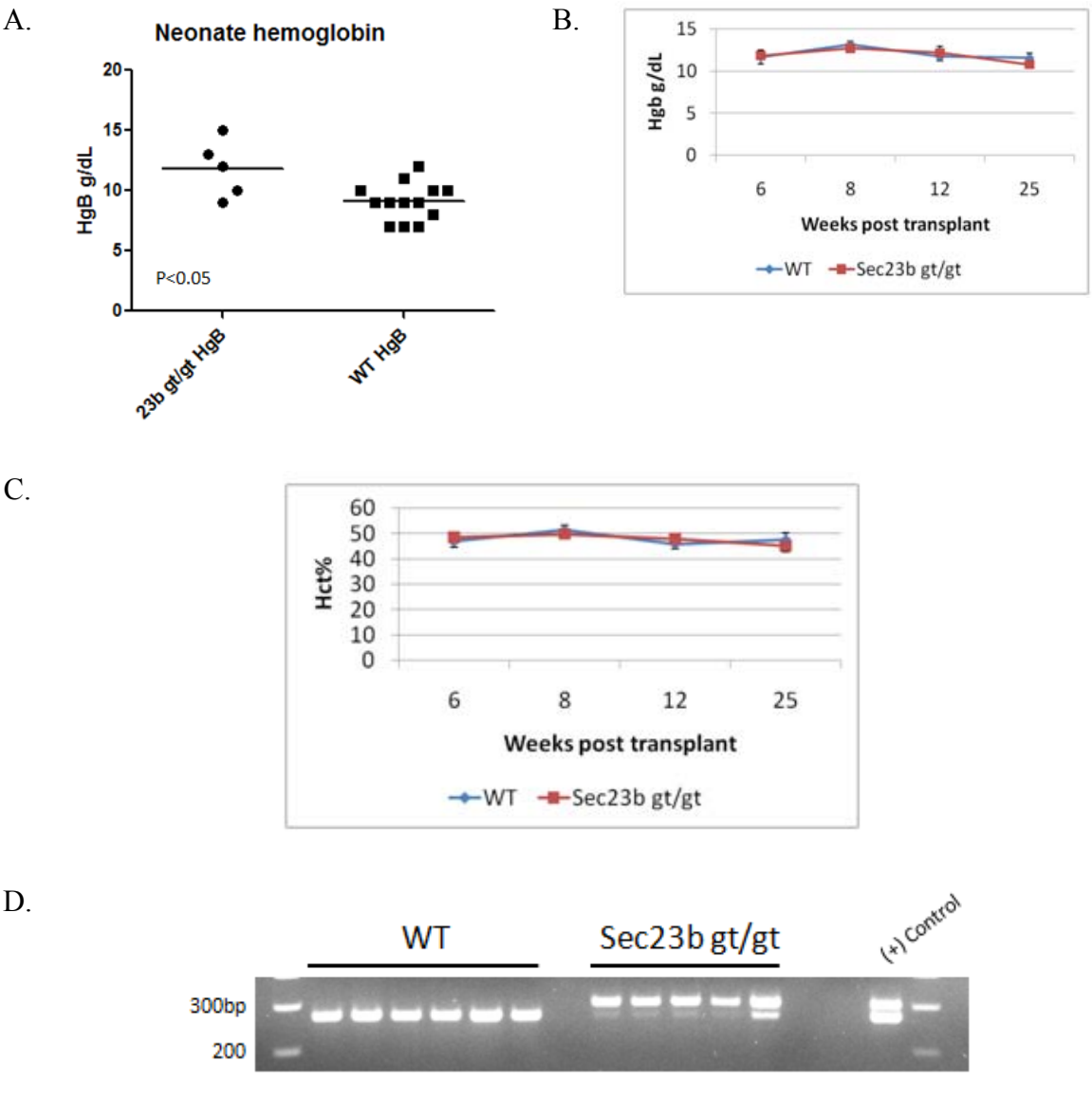

Figure 2- 3: Mean Hgb and Hct levels indistiguishable between *Sec23b gt/gt* and control neonates and transplant recipients.

A) Mean hemoglobin in neonate WT and *Sec23b gt/gt* mice (Bin Zhang, personal communication). B, C) Mean hemoglobin (B) and mean hematocrit (C) in WT and *Sec23b gt/gt* transplant recipients. N=5-7 mice per group, error bars represent standard deviation. No significant decrease in Hgb or Hct was observed between WT and *Sec23b gt/gt* recipients ($p>0.05$ for all timepoints). D) *Sec23b* genotypes from peripheral blood from WT and *Sec23b gt/gt* single transplant recipients. (+) control is a PCR from a *Sec23b+/gt* tail snip. Residual WT band in *Sec23b gt/gt* lanes is likely due to the presence of long-lived endogenous lymphocytes.

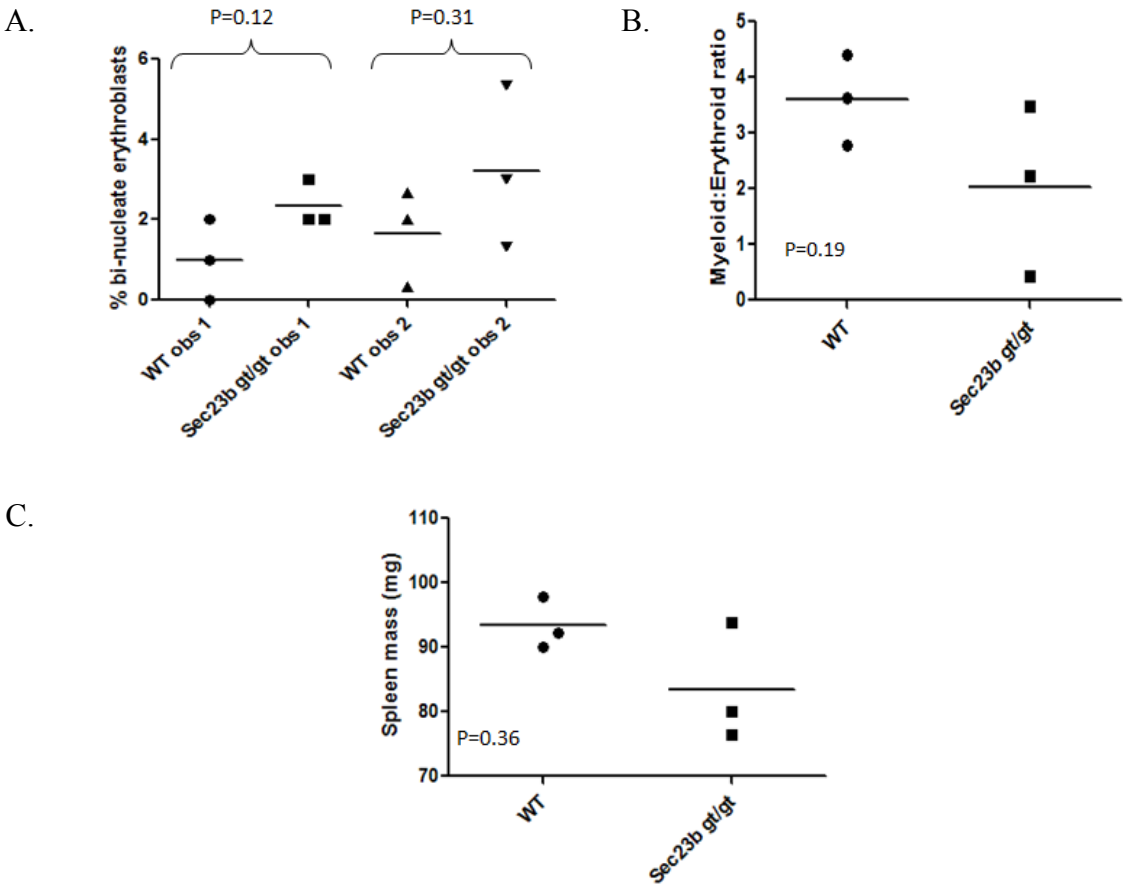

Figure 2- 4: No significant difference observed between *Sec23b gt/gt* transplant recipients and controls for percent bi-nucleate erythroblasts, myeloid:erythroid ratio and spleen mass.

Percent bi-nucleate erythroblasts in bone marrow were scored independently by two observers blinded to sample genotype. No significant difference in % bi-nucleate erythroblasts was observed between WT and Sec23b gt/gt transplant recipients. B) Myeloid:erythroid ratio was scored by an observer blinded to genotype. No significant difference was observed between groups. C) No difference in spleen mass was observed between WT and Sec23b gt/gt recipients. Each point represents one mouse and lines represent means for each group. P-values are the result of a t-test comparing each group.

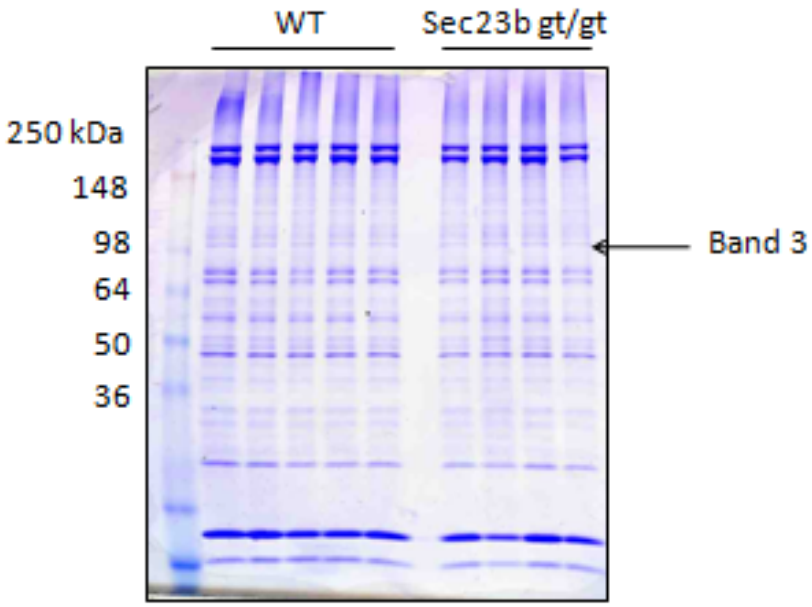

Figure 2- 5: No shift of band 3 was observed on Coomassie stain of RBC membrane fractions from Sec23b gt/gt transplant recipients.

The membrane fractions from red blood cells (RBC ghosts) were harvested from mice receiving WT and *Sec23b gt/gt* fetal liver cells, fractionated by electrophoresis on a 4-20% polyacrylamide gel, and stained with coomassie blue. No differences are apparent between the patterns in the two groups of recipients.

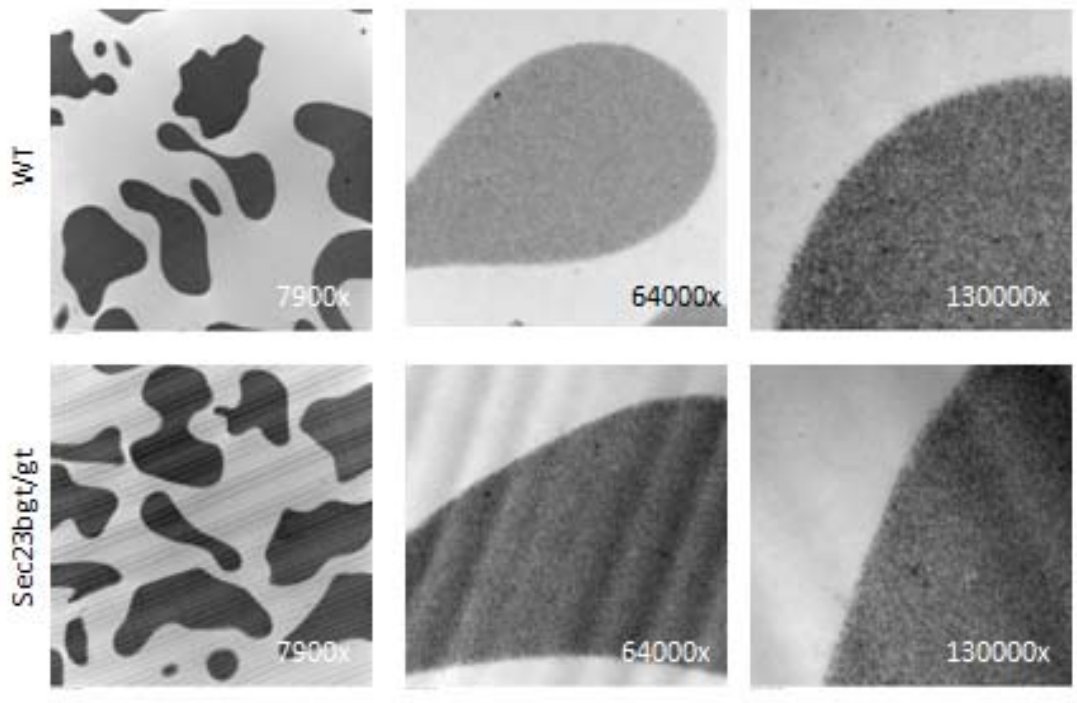

Figure 2- 6: Transmission electron micrograph of RBCs showing no double internal membrane for *Sec23b gt/gt* transplant recipients.

Red blood cells from lethally irradiated mice receiving WT or *Sec23b gt/gt* fetal liver cells were analyzed by transmission electron microscopy (TEM). The top panel shows red blood cells from a mouse receiving WT fetal liver cells and the bottom panel shows red blood cells from a mouse receiving *Sec23b gt/gt* fetal liver cells. Magnification of the images is in the lower right hand corner. No double internal membrane was observed at any magnification in mice receiving *Sec23b gt/gt* cells.

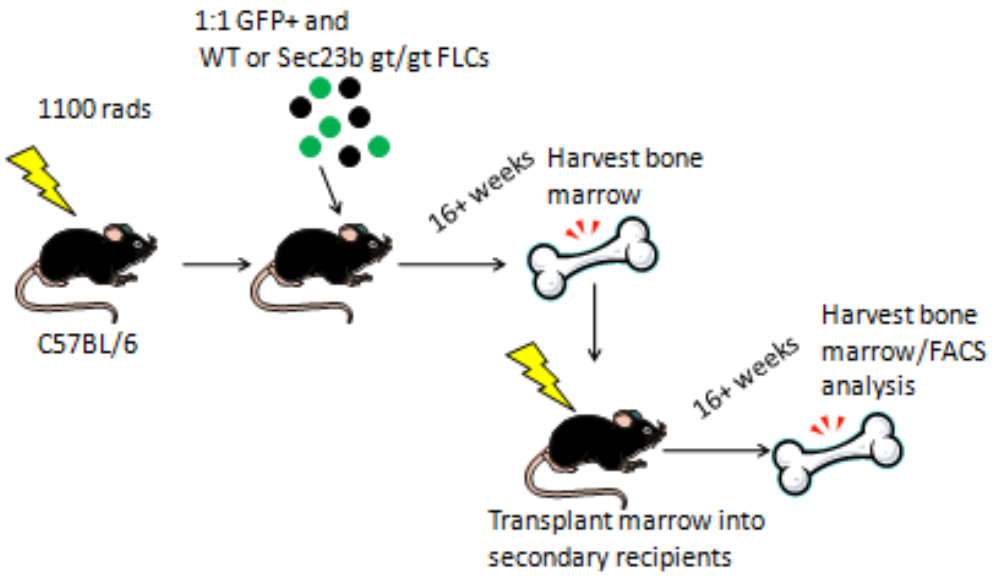

Figure 2- 7: Competitive fetal liver cell transplant

The competitive fetal liver cell transplant strategy is illustrated here. Lethally irradiated mice are transplanted 1:1 with a competitor cell population expressing GFP (green dots) and a tester cell population (black dots) – either WT control or *Sec23b gt/gt*. If the tester cells persist after a primary transplant, a secondary transplant can be used to further stress the bone marrow by re-transplanting the cells into a second set of recipients.

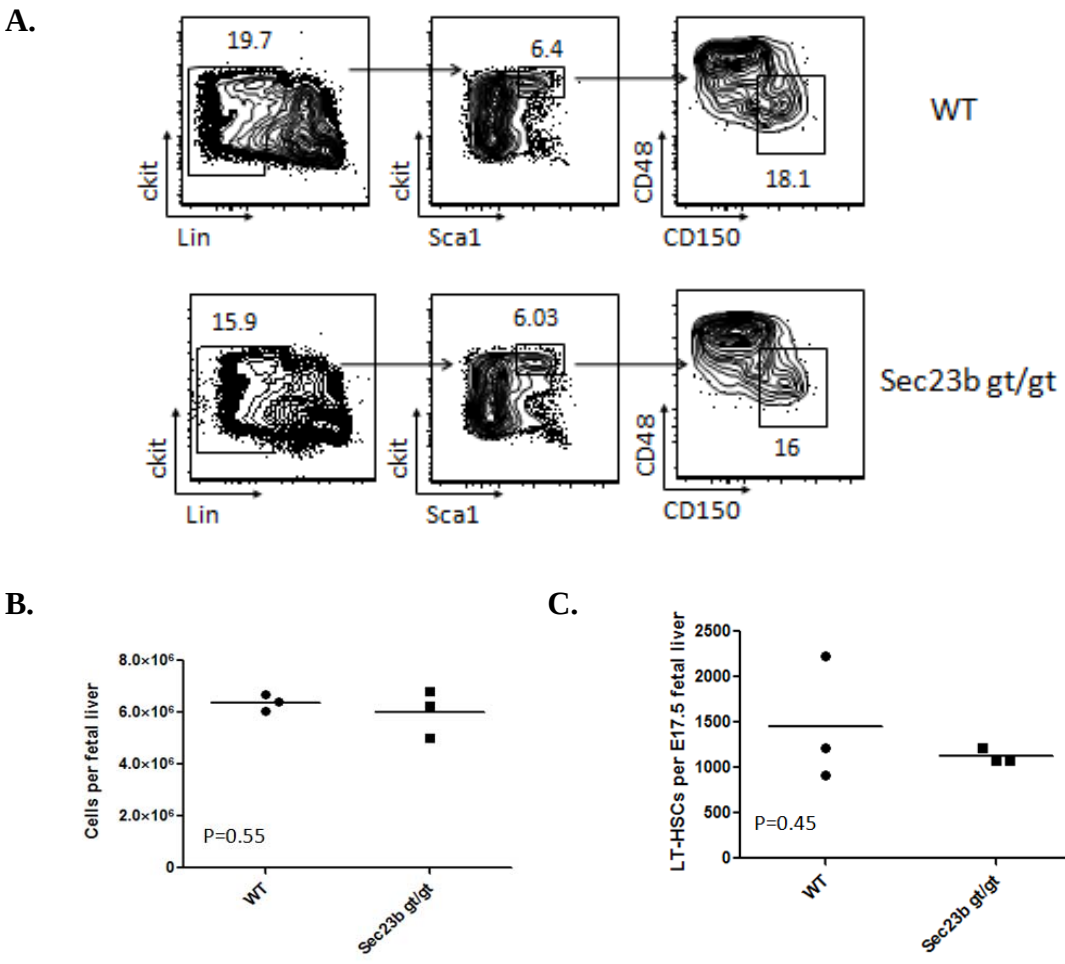

Figure 2- 8: Analysis of *Sec23b gt/gt* fetal liver cells shows indistinguishable cell counts from wild type for total fetal liver cells and long term hematopoietic stem cells.

ckit+Sca1+CD48-CD150+(lin-) LT-HSCs were analyzed from 3 WT and 3 *Sec23b gt/gt* fetal livers.

A) Gating strategy for analyzing LT-HSCs showing panels from one WT and one Sec23b gt/gt sample of the six total analyzed. No significant difference by T-test in B) total number of cells per fetal liver or C) LT-HSCs was observed between the two samples. Each point represents one fetal liver and lines indicate mean value for each group.

A.

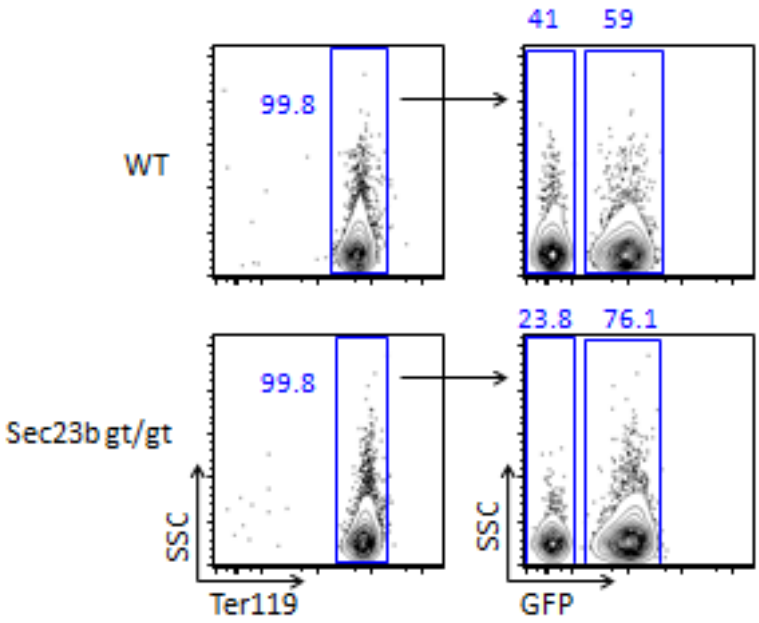

B.

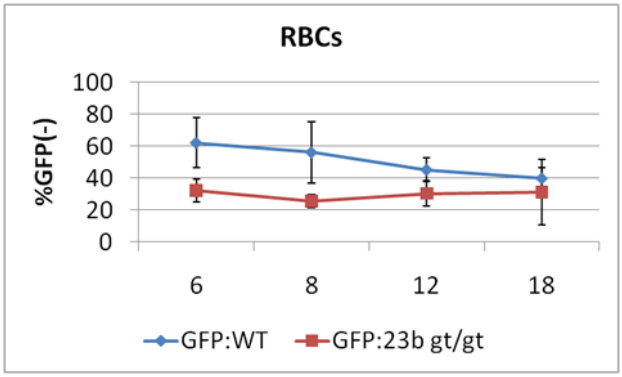

Figure 2- 9: RBC competitive fetal liver transplant shows long term persistence of GFP- cells in mice transplanted with wild type or *Sec23b gt/gt* fetal liver cells.

A) Gating strategy on Ter119+ red blood cells shows clear populations of GFP+ and GFP- RBCs. B) GFP- cells persisted over the 18 week course of the transplant for mice receiving WT or *Sec23b gt/gt* tester cells. A lower percentage GFP- RBCs was observed in mice receiving *Sec23b gt/gt* fetal liver cells. N=5-7 mice per group.

A.

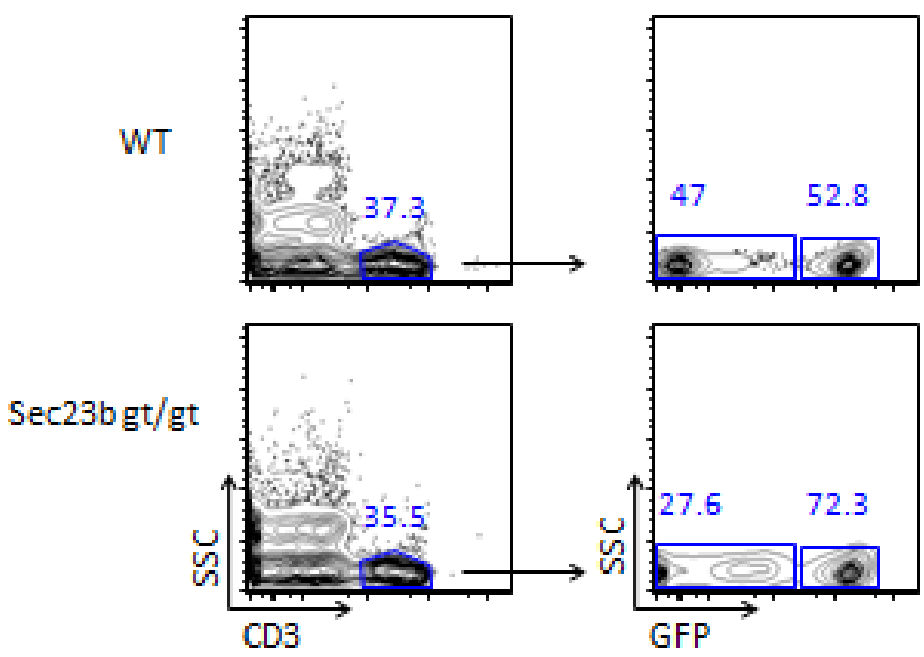
WT
37.3
47
52.8
Sec23b gt/gt
35.5
27.6
72.3
SSC
CD3
SSC
GFP

B.

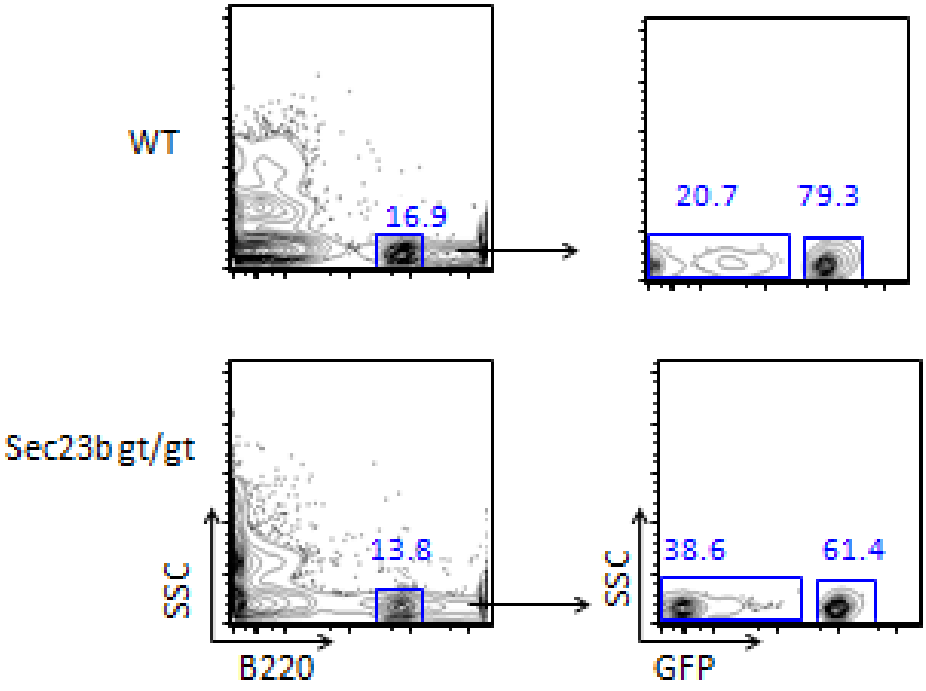
WT
16.9
20.7
79.3
Sec23b gt/gt
13.8
38.6
61.4
SSC
B220
SSC
GFP

C.

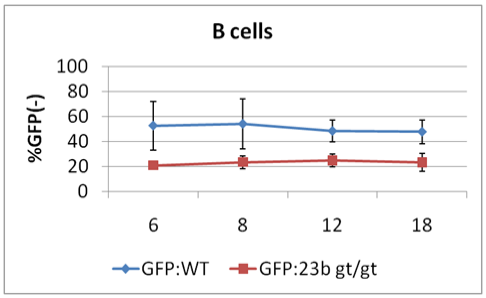

D.

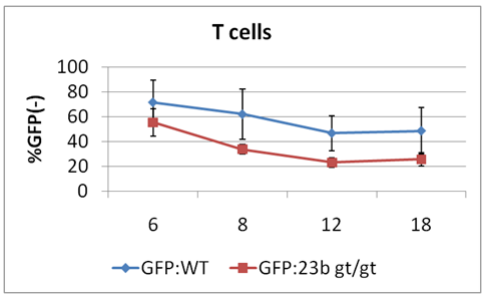

Figure 2- 10: Lymphocyte competitive fetal liver transplant shows long term persistence of GFP- cells in mice transplanted with wild type or Sec23b gt/gt fetal liver cells.

A) CD3+ T and B) B220+ B lymphocytes show clear populations of GFP+ and GFP- cells. B) to D) GFP- cells persisted over the 18 week course of the transplant for mice receiving WT or *Sec23b gt/gt* tester cells. Lower percentages of GFP- cells were observed in mice receiving *Sec23b gt/gt* fetal liver cells for both B and T cells. N=5-7 mice per group.

A.

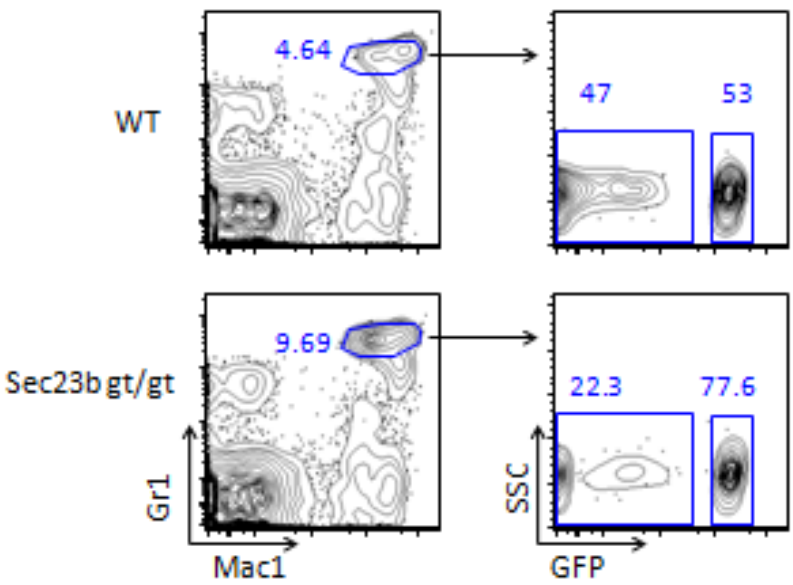

B.

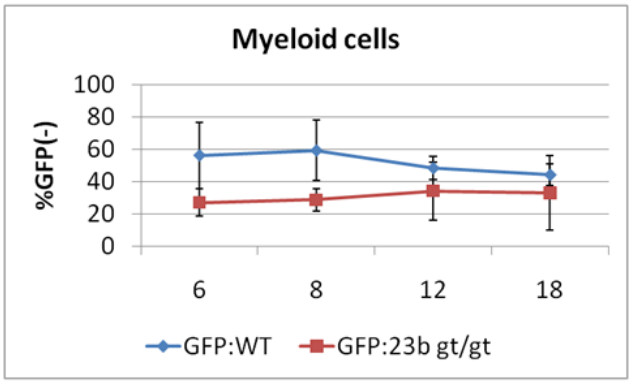

Figure 2- 11: Myeloid competitive fetal liver transplant shows long term persistence of GFP- cells in mice transplanted with wild type or *Sec23b gt/gt* fetal liver cells.

A) Gating strategy on Mac1+Gr1+ myeloid cells shows clear populations of GFP+ and GFP- cells. B) GFP- cells persisted over the 18 week course of the transplant for mice receiving WT or *Sec23b gt/gt* tester cells. A lower percentage GFP- Mac1+Gr1+ cells was observed in mice receiving *Sec23b gt/gt* fetal liver cells. N=5-7 mice per group.

A.

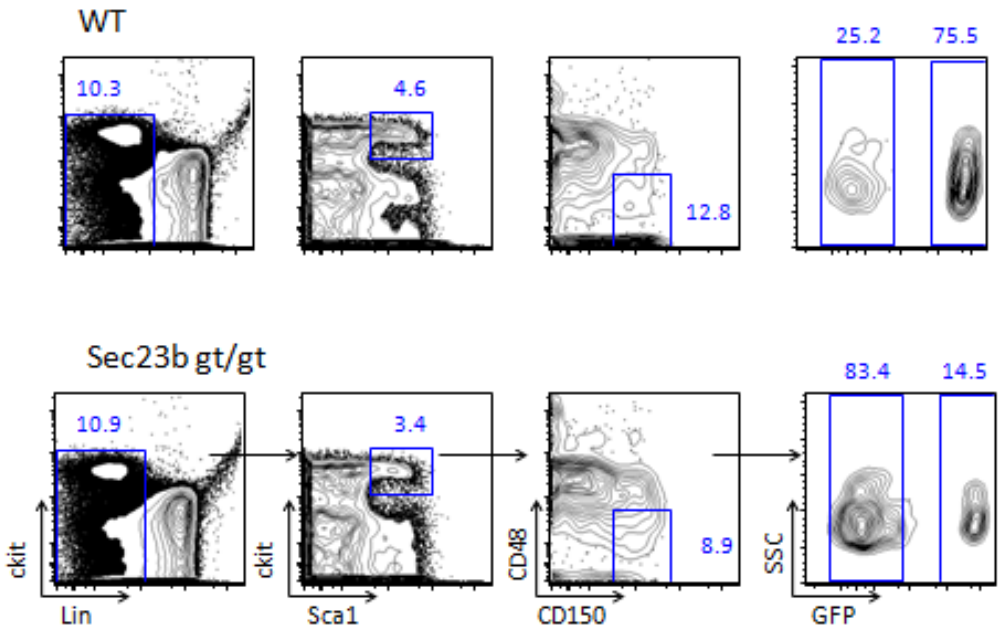

B.

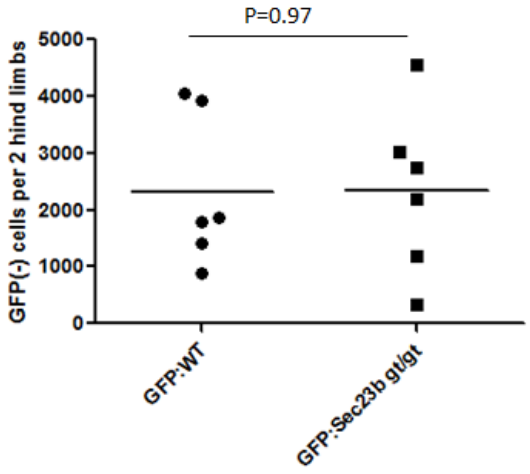

Figure 2- 12: Analysis of LT-HSCs in competitive transplant recipients shows indistinguishable numbers of GFP- LT-HSCs in mice receiving WT or *Sec23b gt/gt* fetal liver cells.

A) Gating strategy for determining GFP+ vs. GFP- LT-HSCs.

B) In mice receiving both WT and *Sec23b gt/gt* tester cells, persistence of GFP- cells was observed at 18 weeks post-transplant with no significant difference in the total number of cells between WT and *Sec23b gt/gt* groups. Each point represents one mouse.

A.

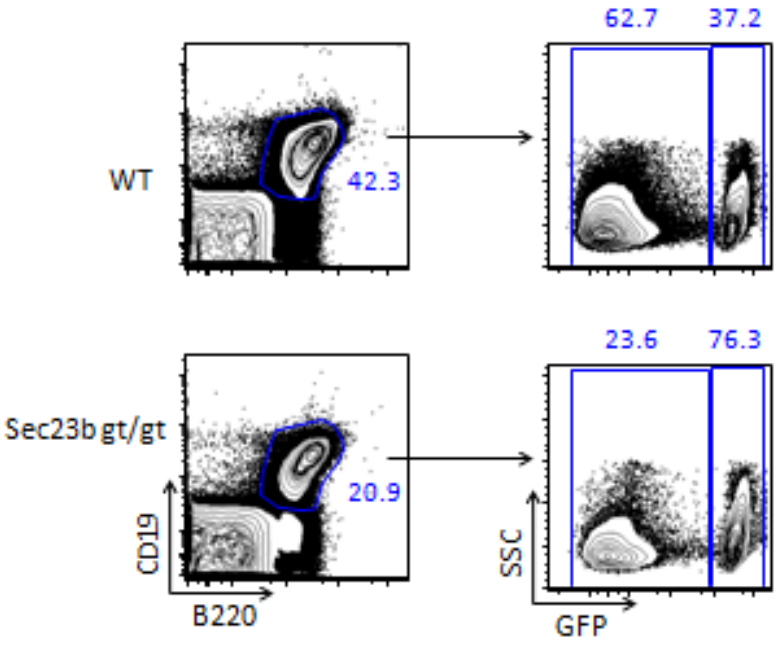

B.

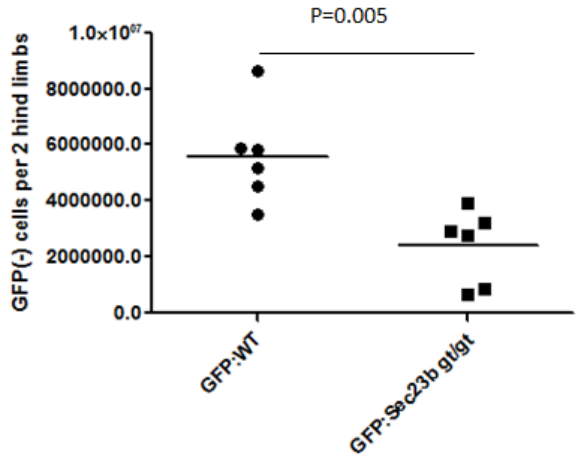

Figure 2- 13: GFP- bone marrow B cells are significantly decreased in *Sec23b gt/gt* fetal liver cell recipients.

A) Gating strategy for defining GFP+ and GFP- bone marrow B cells. B) A statistically significant decrease in *Sec23b gt/gt* GFP- bone marrow B cells was also observed at 18 weeks post-transplant. However, no significant difference was observed in the percent GFP- peripheral B cells in the secondary transplant as a more stringent assay for engraftment, so this finding was not investigated further.

A.

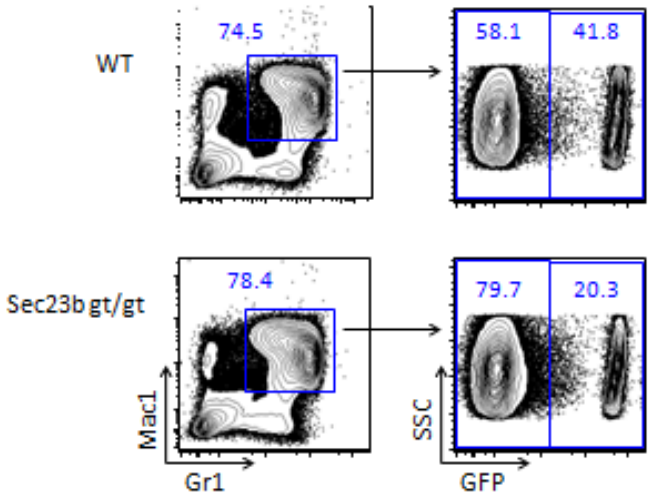

B.

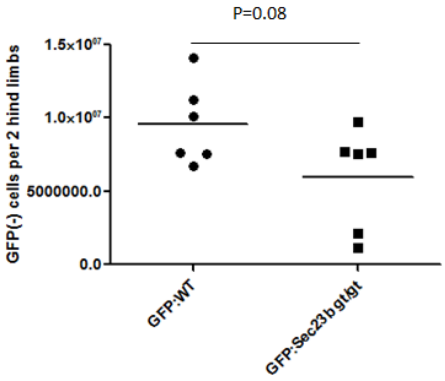

C.

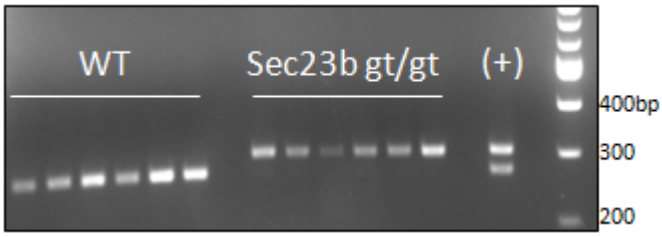

Figure 2- 14: GFP- myeloid cells show long term persistence from WT and *Sec23b gt/gt* recipients in a competitive transplant.

A) Gating strategy for defining GFP+ and GFP- mature myeloid cells. B) No statistically significant difference was observed in GFP- *Sec23b gt/gt* myeloid cells compared to wildtype controls at 18 weeks post-transplant. C) GFP- myeloid cells were sorted and PCR was carried out to demonstrate the genotype of the tester cells for each group of mice. (+) control is a PCR from a *Sec23b+/gt* tail snip.

A.

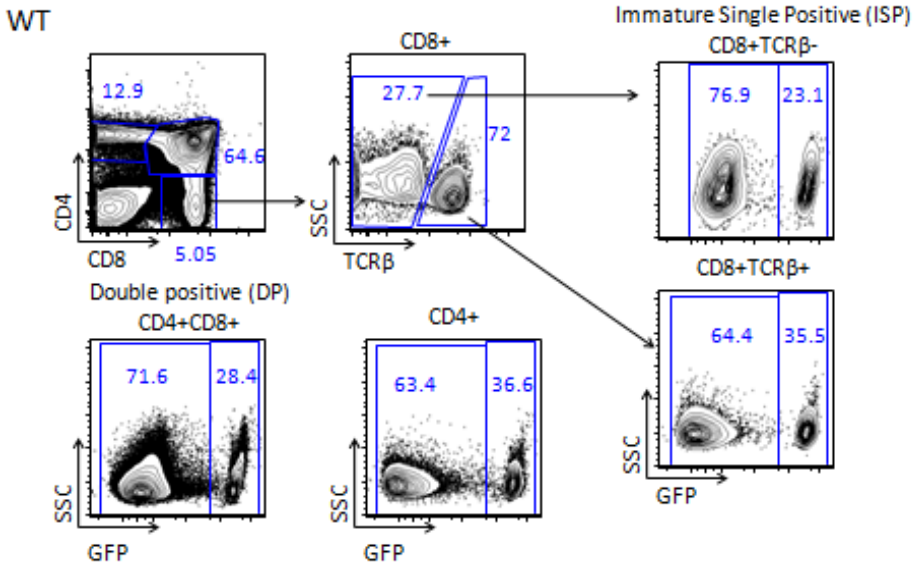
WT
12.9
64.6
CD4
CD8
5.05
CD8+
27.7
72
SSC
TCRβ
Immature Single Positive (ISP)
CD8+TCRβ-
76.9
23.1
CD8+TCRβ+
64.4
35.5
SSC
GFP
Double positive (DP)
CD4+CD8+
71.6
28.4
SSC
GFP
CD4+
63.4
36.6
SSC
GFP

B.

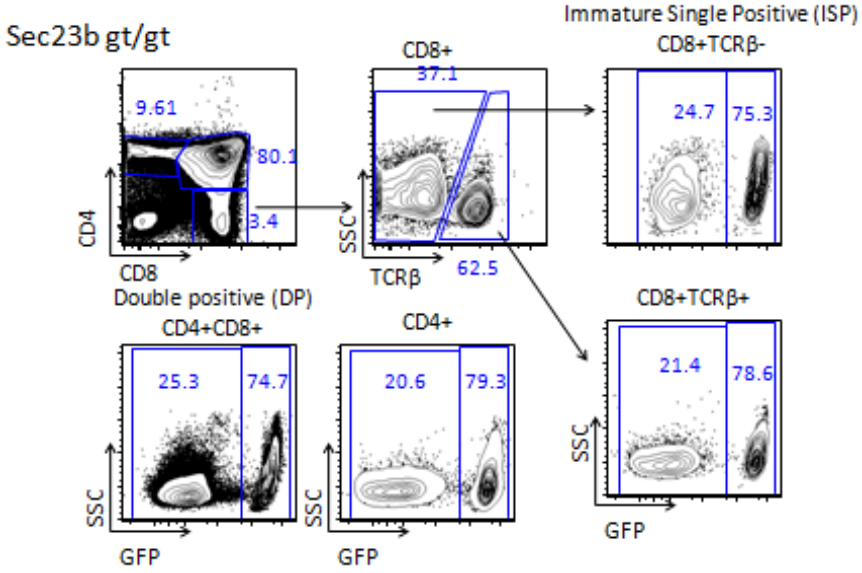
Sec23b gt/gt
9.61
80.1
3.4
CD4
CD8
CD8+
37.1
SSC
TCRβ
62.5
Immature Single Positive (ISP)
CD8+TCRβ-
24.7
75.3
Double positive (DP)
CD4+CD8+
25.3
74.7
SSC
GFP
CD4+
20.6
79.3
SSC
GFP
CD8+TCRβ+
21.4
78.6
SSC
GFP

C.

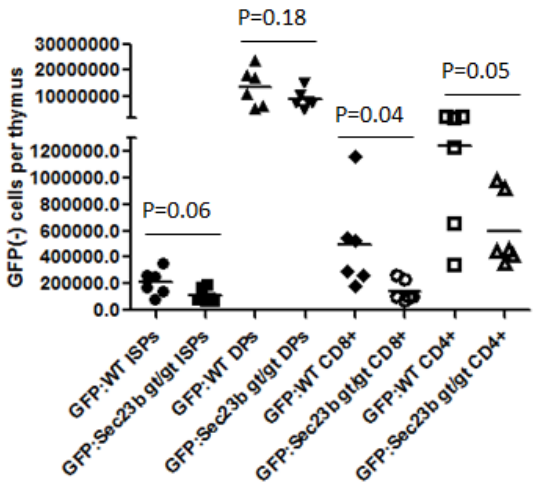

Figure 2- 15: Long term persistence of GFP- thymocytes for WT and *Sec23b gt/gt* recipients.

A) Gating strategy for competitive transplant mice receiving WT tester cells. T cell lineages analyzed are CD8+T cell receptor β (TCRβ)- immature single positives, CD4+CD8+ double positives, CD4+ and CD8+ cells. B) Gating strategy for mice receiving Sec23b gt/gt tester cells. C) Persistence of GFP- cells was observed at all points in T cell maturation.

A.

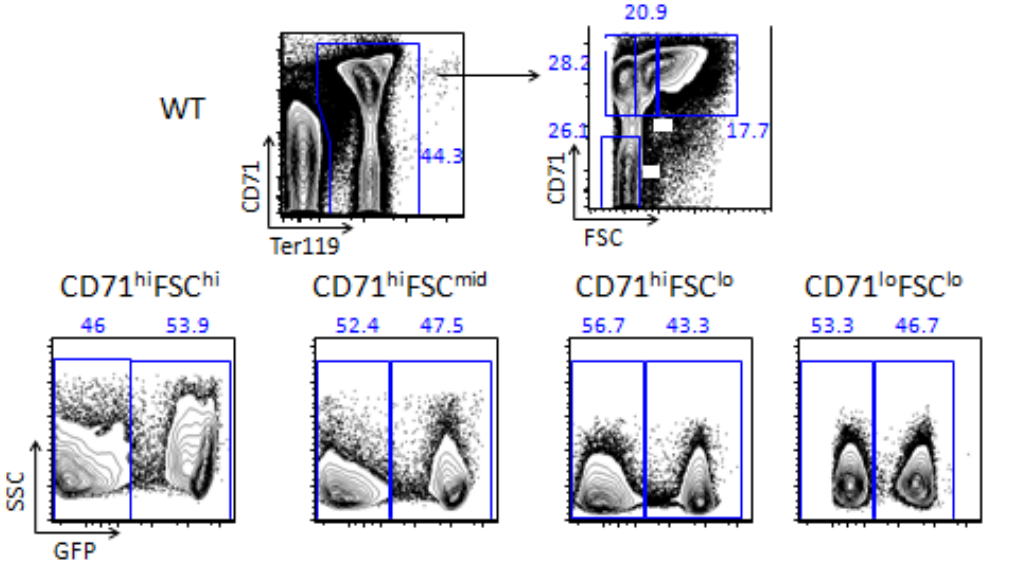
WT
CD71
Ter119
44.3
20.9
28.2
26.1
17.7
CD71
FSC
CD71hiFSChi
CD71hiFSCmid
CD71hiFSClo
CD71loFSClo
46
53.9
52.4
47.5
56.7
43.3
53.3
46.7
SSC
GFP

B.

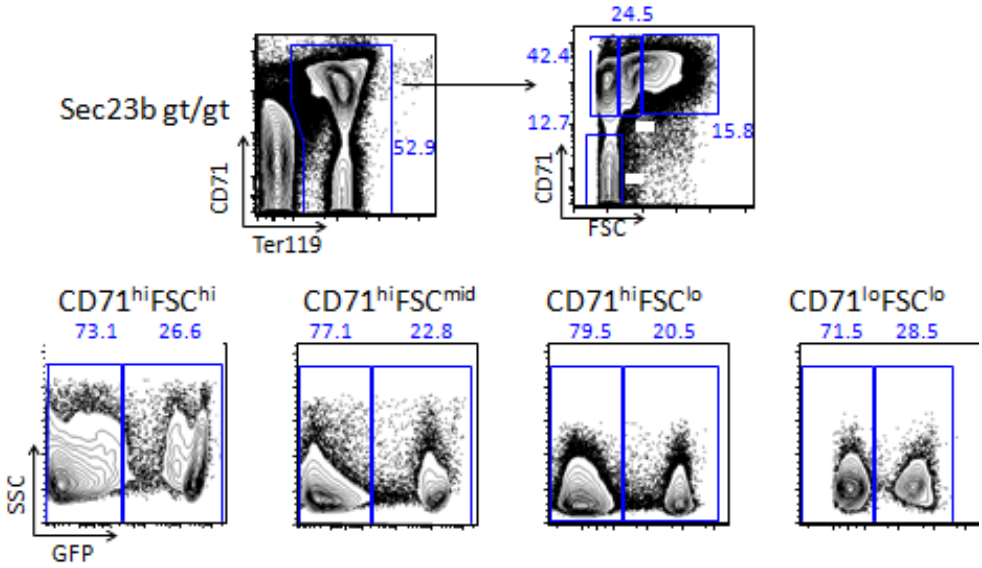
Sec23b gt/gt
CD71
Ter119
52.9
24.5
42.4
12.7
15.8
CD71
FSC
CD71hiFSChi
CD71hiFSCmid
CD71hiFSClo
CD71loFSClo
73.1
26.6
77.1
22.8
79.5
20.5
71.5
28.5
SSC
GFP

C.

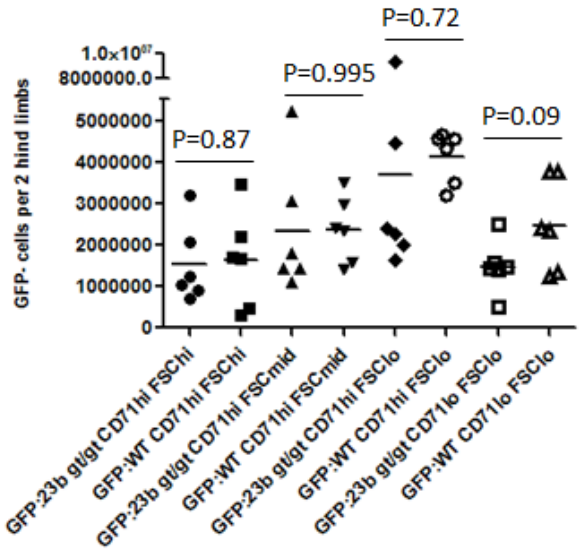

Figure 2- 16: Long term persistence of GFP- Ter119+ red blood cell precursors for WT and *Sec23b gt/gt* fetal liver cell recipients.

A) The gating strategy used for analyzing the erythroid lineage took all Ter119 positive cells as a marker of committed erythroid precursors. Erythroid cells were further gated by Forward scatter (FSC) as a measure of size and level of CD71 expression, as more primitive progenitors are larger and express higher levels of CD71 while more mature erythrocytes are smaller and decrease their expression of CD71. B) The second row of graphs shows the populations of GFP+ and GFP- for each of the Ter119+ populations above. C) Persistence of GFP- cells were seen in the erythroid lineage in all stages of differentiation analyzed. No significant difference was observed between GFP- cells in mice receiving WT or Sec23b gt/gt tester cells at any point in the erythroid differentiation analyzed.

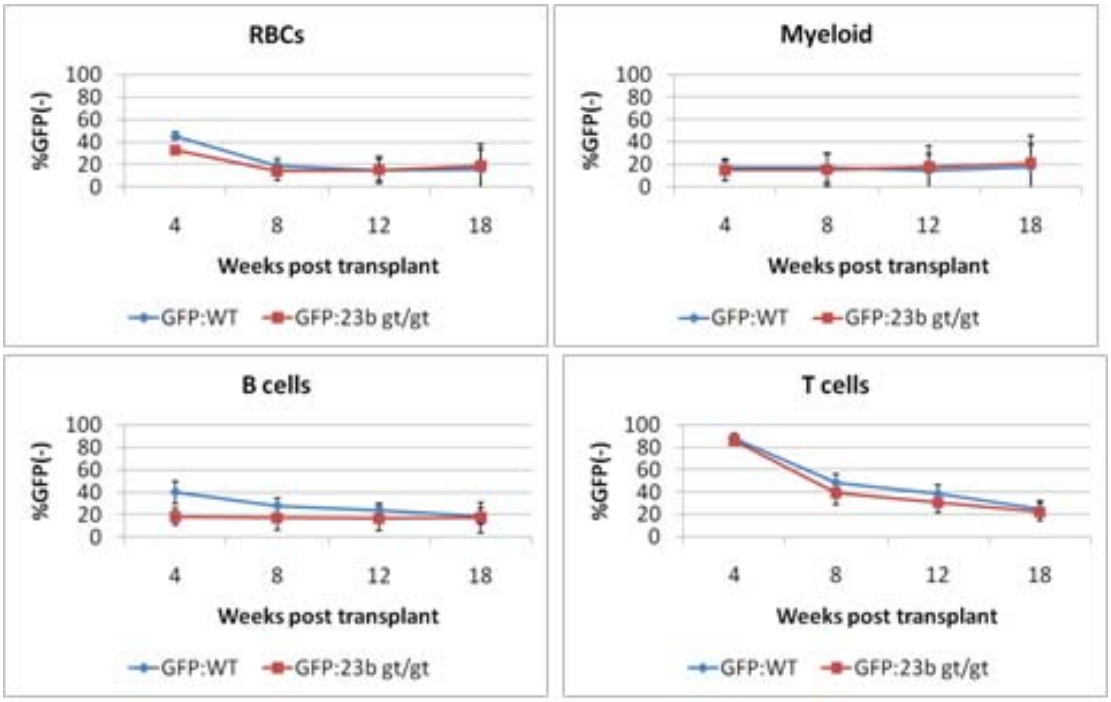

Figure 2- 17: Secondary bone marrow transplant peripheral blood analysis shows long term persistence of GFP- cells in mice receiving GFP:WT and GFP:*Sec23b gt/gt* bone marrow.

Persistence of GFP- cells was observed in mice receiving GFP:*Sec23b gt/gt* fetal liver cells in RBCs, T cells, B cells and myeloid cells. Gating strategies were the same as for the fetal liver transplant. N=13-15 mice per group.

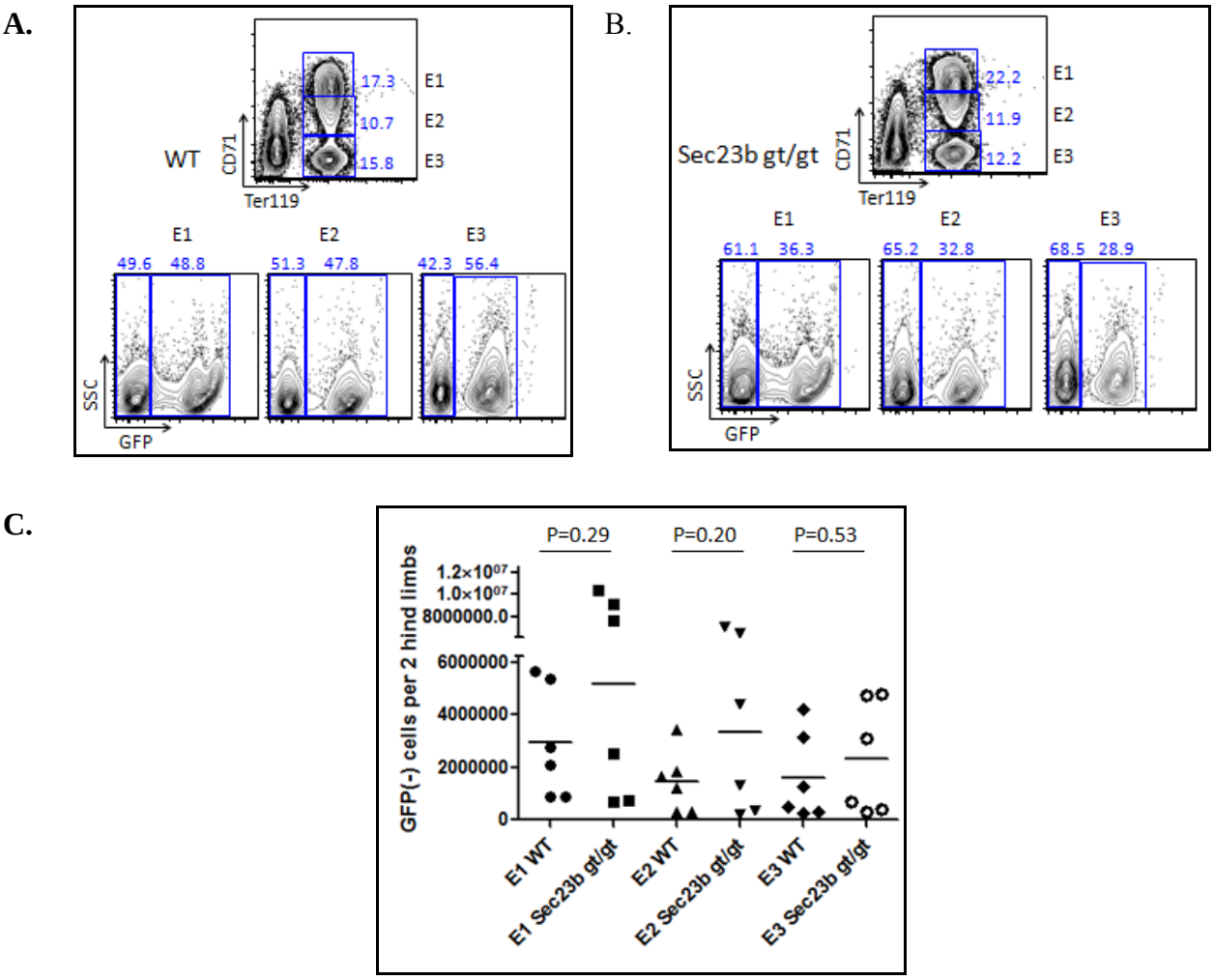

Figure 2- 18: Secondary transplant of GFP:WT and GFP:*Sec23b gt/gt* bone marrow shows long term persistence of GFP- cells in both groups of transplant recipients.

A subset of secondary transplant recipients was sacrificed for analysis of their bone marrow at 26 weeks post-transplant.

A) - B) Gating strategy for erythroid cells for secondary transplant. C) Persistence of GFP- cells was seen in mice receiving WT and Sec23b gt/gt tester cells in all stages of erythroid differentiation analyzed. No significant difference in number of GFP- cells was observed between mice receiving WT or Sec23b gt/gt tester cells at any point in erythroid differentiation. Each point represents one mouse.

A.

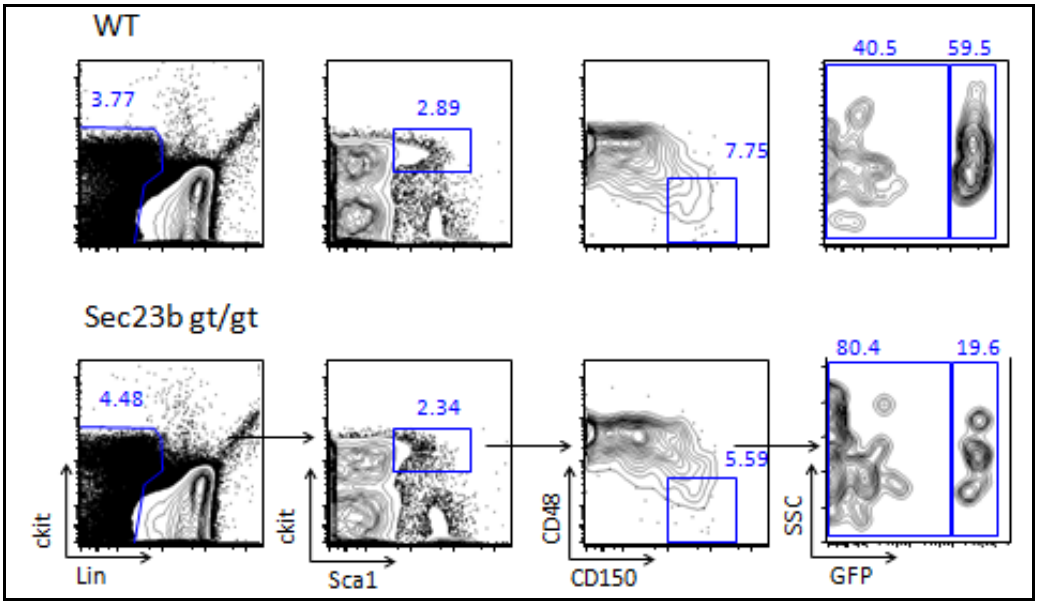

B.

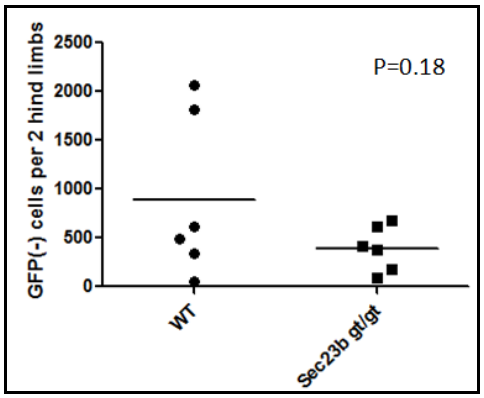

Figure 2- 19: Long term persistence of GFP- LT-HSCs in secondary transplant recipients.

A) Gating strategy for ckit+Sca1+CD150+CD48-(lin-) LT-HSCs. B) Persistence of GFP- LT-HSCs was seen in mice receiving WT and Sec23b gt/gt tester cells at 26 weeks post-transplant. No significant difference in number of GFP- cells was observed between mice receiving WT or Sec23b gt/gt tester cells.

A.

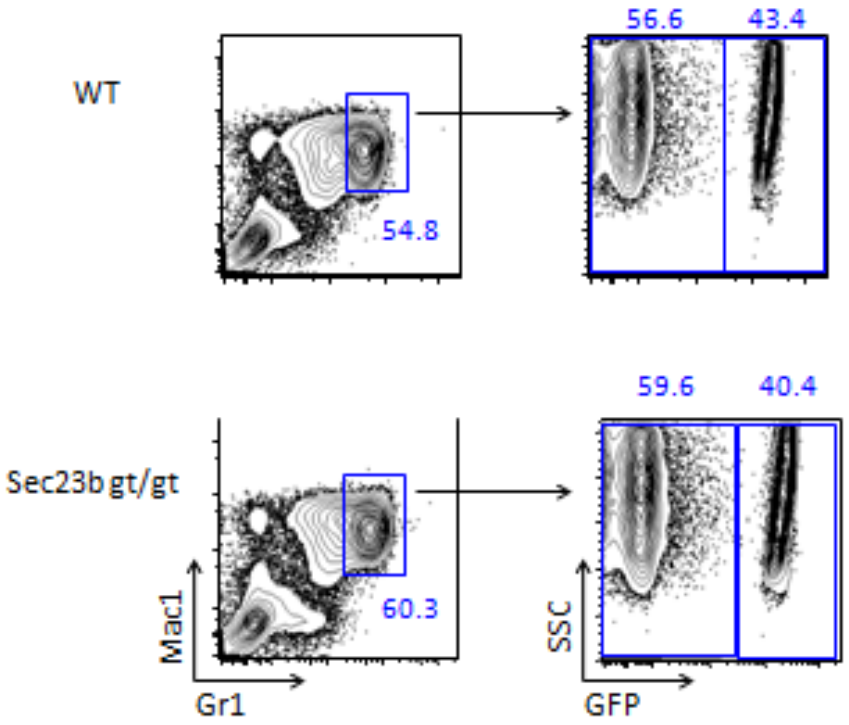
WT
56.6
43.4
54.8
Sec23b gt/gt
59.6
40.4
60.3
Mac1
Gr1
SSC
GFP

B.

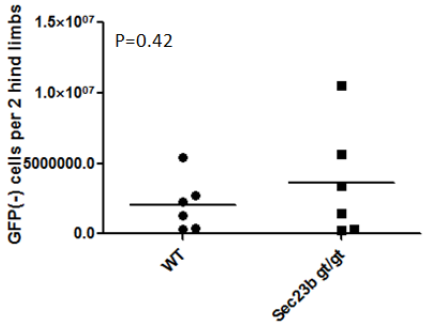
GFP(-) cells per 2 hind limbs
1.5×10^07
1.0×10^07
5000000.0
0.0
P=0.42
WT
Sec23b gt/gt

C.

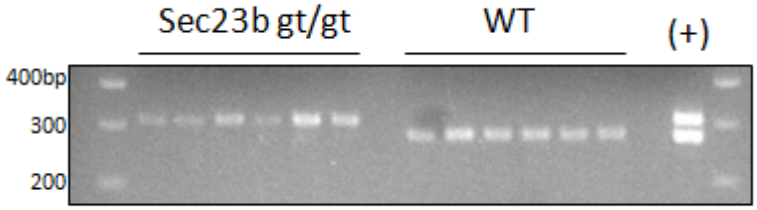

Figure 2- 20: Persistence of GFP- myeloid cells in secondary transplant recipients.

A) Gating strategy for Mac1+Gr1+ mature myeloid cells in the bone marrow. B) Persistence of GFP- myeloid cells in secondary transplants of mice receiving both WT and Sec23b gt/gt tester cells at 26 weeks post-transplant. No significant difference was observed between Sec23b gt/gt recipients and WT controls. C) In order to demonstrate the genotype of the tester cells, GFP- Mac1+Gr1+ myeloid cells were sorted from the bone marrow of the mice analyzed. The cells were lysed and PCR was carried out to determine the presence of the WT or Sec23b gt/gt allele. (+) control is a PCR from a Sec23b+/gt tail snip.

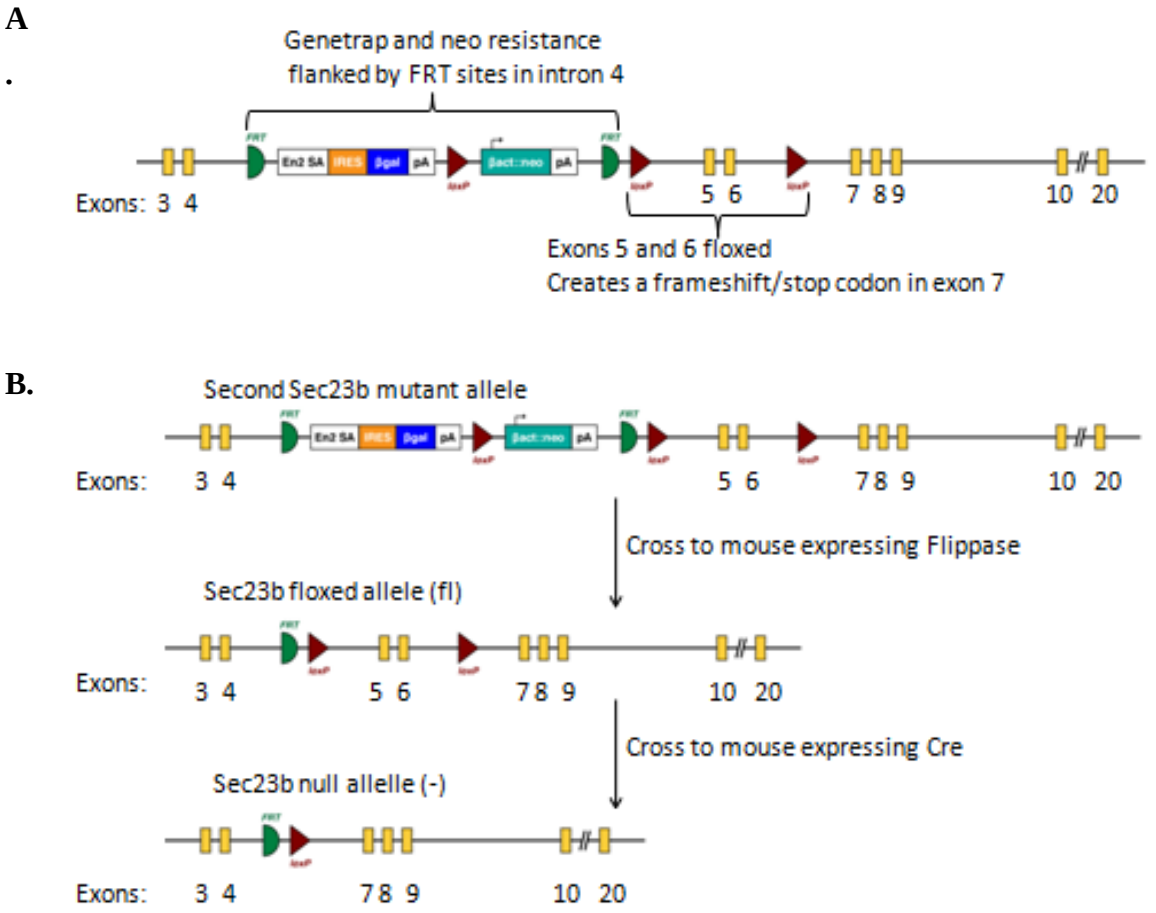

Figure 2- 21: Generation of a floxed Sec23b allele.

Mice heterozygous for a second *Sec23b* mutant allele were obtained as a gift from Bin Zhang.

A) This allele has a gene trap inserted in intron 4 of the gene flanked by FRT sites (green semicircle). Downstream of this, exons 5 and 6 are flanked by LoxP sites (red triangles) which create a frameshift and stop codon in exon 7. B) Schematic of breeding scheme to generate null allele. Mice heterozygous for the second Sec23b allele were crossed to mice expressing Flippase under the control of the human β-actin promoter. Mice heterozygous for the floxed allele were crossed to mice expressing cre recombinase under the control of the adenovirus EIIA promoter to generate Sec23b+/- mice.

A.

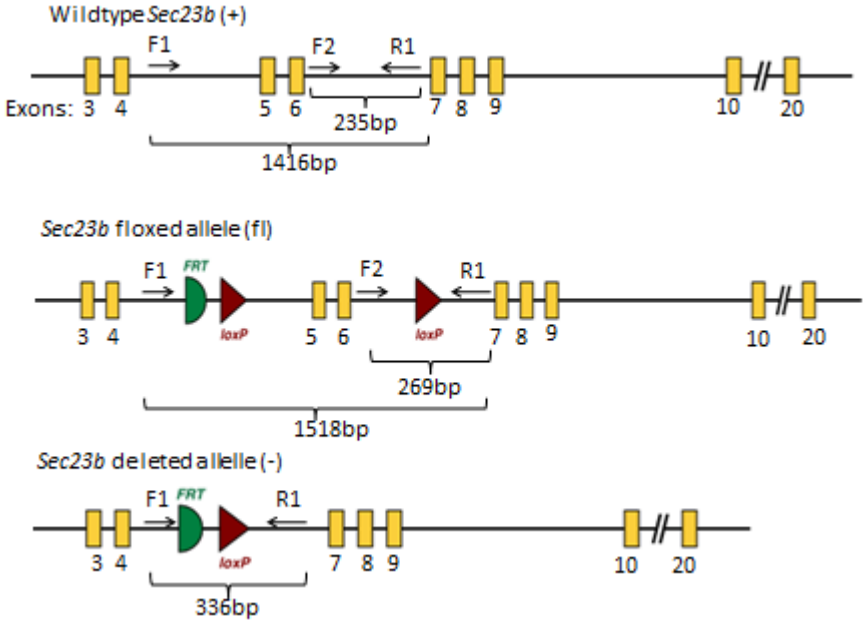

B.

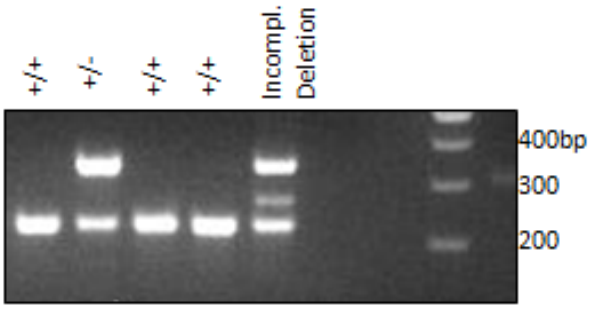

Figure 2- 22: Genotyping assay for second Sec23b allele.

A) Genotyping was performed using a 3 primer assay, with primers upstream of the floxed exons (F1) and two primers crossing one of the LoxP sites (F2 and R1). This reaction yields a 235 bp band for the WT allele and a 336 bp band for the deleted allele. The floxed allele yields a 269 bp band which is exactly 34 bp larger than the WT band since it includes the LoxP site. The elongation cycle of the PCR reaction was not long enough to amplify a product between F1 and R1 for the (+) and fl alleles. B) Genotypes of tail DNA showing +/+ and +/- genotypes. There is also one mouse that is chimeric for the WT, floxed and null alleles as a result of incomplete deletion of exons 5 and 6.

Note: Chapter 2 will be submitted as a manuscript titled, "Sec23b deficiency in mice results in pancreatic destruction but no apparent defect in erythropoiesis." By Matthew Vasievich, Rami Khoriaty, Bin Zhang, Jesse Rinehart, Morgan Jones, Ivan Maillard, and David Ginsburg.

Acknowledgements: Many thanks to Ivan Maillard MD PhD and Morgan Jones for their help and expertise in teaching me how to do flow cytometry and collection of data. Thanks also to Bin Zhang for the *Sec23b gt/gt* neonate CBCs, initial characterization of the pancreas phenotype and obtaining the second *Sec23b* mutant allele from EUCOMM.

CHAPTER III:

SILAC Labeling Of A Whole Mouse And Proteomic Analysis Of The Membrane Fraction Of Sec23b Gt/Gt Red Blood Cells

Abstract

Stable Isotope Labeling of Amino acids in Cells (SILAC) is a proteomics method that quantitatively determines relative amounts of specific proteins in a complex protein mixture. In this study we use the method first described by Kruger et al. to label an entire mouse with 13C lysine, an approach that can be used to study quantitative differences between proteins *in vivo*. Our results show efficient labeling with 13C lysine in kidney, liver and red blood cells. SILAC proteomic analysis of *Sec23b gt/gt* transplant recipients detected RBC membrane proteins, but no proteins from the unlabeled fraction were quantitatively decreased in our analysis.

Introduction

Stable Isotope Labeling of Amino acids in Cell culture (SILAC) is a proteomic technique used to quantify differences in the amount of a given protein between two samples [81,82]. SILAC analysis is conducted by incubating control cells in media containing lysine that has been synthesized using a heavy, non-radioactive isotope of carbon (13C). As a result, these lysines are exactly 6 atomic mass units heavier than lysines containing 12C. As the cells grow and normal protein turnover occurs over time, these heavy lysine residues will be incorporated into the proteins of the cells, eventually constituting nearly all of the lysine pool. Since lysine is an essential amino acid, all lysine incorporated into proteins will be derived from the media. An experimental group of cells is grown under the same conditions but in the absence of the heavy isotope. The samples can then be analyzed by lysing each group of cells and mixing the lysates in a

1:1 ratio by protein concentration. This 1:1 mixture is then digested with the endopeptidase LysC, which cleaves proteins after the amino acid lysine. After digestion, the mixture is fractionated by mass spectrometry which sorts peptides by their mass/charge ratio (m/z) resulting in a 3 Da shift of the labeled peptides since lysine has a charge of +2. In the resulting spectra, since the control cells were labeled with the heavy lysine, the peaks will be shifted separating the control spectra from the experimental spectra[81]. Comparing peak heights between identical peptides gives a quantitative analysis of the relative levels of a given protein between two samples in an unbiased fashion.

There have been several successful applications of SILAC *in* vitro to study various signaling pathways and cellular processes. For example, SILAC has been used to identify novel proteins in the insulin signaling pathway and determine the kinetics of their activation [83] and study sites of regulated phosphorylation on ion transporters [84]. SILAC proteomics have also been used to determine the effect of growth factors on the differentiation of mesenchymal stem cells and to define a fraction of the mouse brain proteome [85,86]. An enrichment step is important in proteomics analysis due to the wide dynamic range of protein concentrations that can be present in more complex protein preparations such as whole cell or tissue lysates or plasma. When analyzed by mass spectrometry, lower abundance proteins that may be of interest might be considered 'noise' by the instrument and not analyzed[81]. The above studies have used an immunoprecipitation approach to study finite numbers of proteins by mass spectrometry. Another approach to fractionate protein mixtures for analysis can be to study other sub-cellular compartments such as the mitochondria to generate less complex proteins populations that are able to be analyzed by mass spectrometry [87]. The membrane fraction of cells can also be analyzed by mass spectrometry. The human and mouse red blood cell membrane proteomes were recently characterized, [88,89] making the red blood cell a good target for proteomic studies in a whole animal. SILAC labeling has recently been used *in vivo* by modifying the diet of a mouse such that all lysine consumed by the mouse is labeled with 13C ref [90]. A high degree of protein labeling with heavy lysine (>96%) was achieved in liver, gut, heart and red blood cells.

Here we use whole mouse SILAC labeling to study mouse red blood cells derived from hematopoietic precursors deficient for SEC23B. Recently, it was shown that humans with mutations in *SEC23B* are affected with Congenital Dyserythropoietic Anemia type II (CDAII) [61,62]. SEC23B is part of the COPII coat that forms on the cytoplasmic side of the endoplasmic reticulum (ER) to traffic proteins from the ER lumen forward to the Golgi apparatus. There may be RBC membrane proteins that specifically traffic with SEC23B in human patients causing this disruption in red cell maturation and bi-nucleation in the late erythroblast phase. In this study, we use 13C lysine to label a whole mouse and study the effects of SEC23B deficiency on protein trafficking in erythropoiesis using SILAC proteomics.

Materials and Methods

SILAC labeling of a whole mouse. One kilogram of mouse chow containing 13C labeled lysine as the only lysine source (SILAC chow) was purchased from Cambridge Isotope Labs (Andover, Mass). The SILAC chow was stored at -20ºC. C57BL/6J mice were obtained from Jackson Laboratory (stock#000664). All mouse procedures were conducted in accordance with the policies of the University Committee for the Use and Care of Animals (UCUCA). Starting at four weeks of age, 2 C57BL/6J (F0) female mice housed in the same cage were fed SILAC chow at one pellet per mouse per day. When $\geq$1 pellet of chow remained, only one additional pellet was added to the cage for that day. At six weeks of age, each female was separated into an individual cage and exposed to a C57BL/6J male mouse overnight, and this process repeated until a copulation plug was observed the following morning. Near term, the two pregnant females were combined into a single cage. F1 pups were weaned at 3 weeks of age, with separation of male and female pups (Figure 3-1).

Pups were euthanized at 8 weeks of age with collection of whole blood via cardiac puncture into sodium citrate (Sigma) to a final dilution of 1:9. The following organs were harvested and snap frozen in liquid nitrogen and stored at -80ºC: heart, lungs, liver, spleen, stomach, pancreas, small intestine, large intestine, kidney, adrenals, salivary glands, skeletal muscle, brain, eye, skin, white fat, and testis.

RBC ghost preparation. RBCs were collected from whole blood by centrifugation at 2300g. The RBC pellet was washed twice in Phosphate Buffered Saline (PBS), pH 7.4, followed by lysis in ghost lysis buffer (5mM Na2PO4, 1.3 mM EDTA, pH=7.6) with protease inhibitors (Roche, stock#11873580001). Lysates were fractionated by centrifugation at 16,000g and the supernatant containing the RBC membrane fraction subsequently washed 4-6 times in ghost lysis buffer, followed by storage in lysis buffer at -80ºC.

Sec23b gt/gt fetal liver cell transplant. Fetal liver cell transplant was performed as previously described [40]. Briefly, timed matings were carried out overnight between heterozygous *Sec23b+/gt* mice and the following morning, females were checked for copulation plugs. Pregnant female mice were sacrificed at 17.5 days post coitus and fetal livers of pups were suspended in freezing medium consisting of 65% RPMI 1640 medium, 25% Fetal Bovine Serum (FBS) and 10% DMSO. Fetal liver cells were frozen at -80ºC overnight and transferred to liquid nitrogen storage the next day. DNA was prepared from fetal mouse tissue for genotyping. DNA was prepared by incubating the fetal mouse tissue with tail lysis buffer and proteinase K (Roche). PCR on the DNAs was carried out as described above. For transplant, 6-12 week C57BL/6J mice were ordered from the Jackson Laboratory (Bar Harbor, ME) and lethally irradiated in a Cesium Gammacell 40 Exactor irradiator with two doses of 675 rads spaced 3 hours apart. Frozen WT and *Sec23b gt/gt* fetal liver cells were thawed and cell suspensions were made to 3,333 cells/μL in 300 μL of RPMI 1640 medium with 2% FBS and injected into the retro-orbital venous sinus of irradiated recipient mice. Irradiated mice were kept on acidified tap water (pH=2.35) for 3 weeks post-transplant. Blood was drawn from *Sec23b gt/gt* transplant recipients at 8 weeks post-transplant and RBC ghosts were prepared as described above.

Mass Spectrometry. SILAC labeled RBC ghosts, kidney and liver samples were sent to Jesse Rinehart (Yale University) for polyacrylamide gel electrophoresis and mass spectrometry analysis on an n-UPLC LTQ OT Mass Spectrometer (Thermo Scientific). A kidney from an F2 SILAC labeled mouse was also obtained by Jesse Rinehart from Cambridge Isotope Labs (Andover, Mass). RBC ghosts were diluted in ghost lysis buffer

to a total protein concentration of 0.5 μg/μL. SILAC-labeled RBC ghosts were mixed 1:1 with unlabeled ghosts prepared from C57BL/6 mice, 129 mice or mice receiving *Sec23b gt/gt* fetal liver cells, and fractionated by electrophoresis on a 4-15% acrylamide gel. Similar analyses were performed on SILAC-labeled kidney and liver specimens mixed 1:1 with unlabeled tissue obtained from control C57BL/6J mice. Lanes from 4-15% acrylamide gels were separated into 32 individual slices for Mass spectroscopic (MS) analysis. For each protein identified, a SILAC ratio was calculated. This ratio is the ratio of the peak height for the unlabeled or light peptides for that protein to the labeled or heavy peptides for that protein. Variability in mixing the labeled and unlabeled samples is corrected by taking an overall SILAC ratio. The overall SILAC ratio is the median value of the SILAC ratios for all proteins identified.

Western blot. Western blot analysis was performed as previously described [37]. The transferrin receptor was detected with a monoclonal antibody (Invitrogen, cat. 13-6800).

Results

Efficiency of labeling

A 100 kDa band corresponding to Band 3 was analyzed by mass spectrometry. Analysis of the protein demonstrated >99% labeling of the F0 SILAC RBC ghost fraction. Mass spectrometry analysis of a 1:1 mixture with either C57BL/6J or 129 ghosts demonstrated approximately equal ratios of heavy:light peptide (Figure 3-2).

Liver lysates from the F1 SILAC labeled mouse and a C57BL/6J wildtype mouse were analyzed by PAGE and mass spectrometry. The peptide identified in the liver analysis was prolyl-4-hydroxylase (Figure 3-3). The SILAC labeled protein when run in the absence of the unlabeled protein was found to have approximately 0.5% unlabled protein; therefore the SILAC F1 liver was approximately 99.5% labeled with heavy lysine. Analysis of a peptide derived from kidney showed 100% SILAC labeling and no residual unlabeled peptide present. This peptide was also analyzed from a SILAC labeled

kidney from Cambridge Isotope Labs. The sample from Cambridge Isotope Labs from an F2 mouse was found to be only 96% labeled (Figure 3-4).

SILAC analysis of Sec23b gt/gt transplant recipients

A mouse receiving *Sec23b gt/gt* fetal liver cells was bled at eight weeks post-transplant. RBC ghost fractions were prepared, mixed 1:1 by volume with SILAC labeled RBC ghosts of equal protein concentration (Figure 3-5). The overall SILAC ratio was found to be 0.83. SILAC ratios were adjusted to account for variability in mixing by dividing the overall ratio by the median value. At least three of the top nine proteins with the highest SILAC (L:H) ratios are serum proteins including albumin, transferrin and alpha-1-antitrypsin. The RBC ghost protein with the highest SILAC ratio is the transferrin receptor with an adjusted SILAC ratio of 2.77 (Table 3-1, 1 of 9). The RBC membrane protein with the lowest SILAC ratio was the vinculin protein with an adjusted ratio of 0.59 (Table 3-1, 9 of 9). Western blot analysis for the transferrin receptor revealed no consistent difference in quantity or migration pattern between samples derived from WT or *Sec23b gt/gt* transplant recipients (Figure 3-6).

Discussion

In this study we show that we are able to successfully label red blood cell ghosts, kidney and liver in a mouse with heavy lysine after only one generation. We were able to attain a level of labeling close to 100%. In our initial analysis of the labeling of RBC ghosts in the F0 mice, it is likely that the RBCs are among the first cell types to become fully labeled because of their high turnover rate with an estimated lifespan of 50-60 days [91,92]. We attempted to use these highly labeled RBC ghosts to detect RBC membrane proteins that might be quantitatively decreased in *Sec23b gt/gt* RBCs. While our results did detect RBC membrane proteins, no quantitative decrease in any RBC membrane protein was detected. Serum proteins were found to be in greater abundance in the unlabeled sample. This is likely due to subtle differences in the purification method such that there was more serum contamination in the unlabeled compared to the labeled sample. A western blot was done on RBC ghost samples for the transferrin receptor which was shown to be the RBC ghost protein with the greatest change between the

SILAC labeled and unlabeled ghosts. This western analysis showed no consistent difference in expression between mice receiving WT fetal liver cells versus mice receiving *Sec23b gt/gt* fetal liver cells. In spite of these results, the use of SILAC proteomics and our labeled mice could be useful in defining cargo subsets in other mice with mutations in the secretory pathway. In the published literature, Vangl2 is a known cargo for *Sec24b* in mouse neuronal development[30]. Using SILAC proteomics to analyze sub-proteomes from mouse neurons could yield other cargoes for *Sec24b*. SILAC labeling in a mouse could also be used to investigate other cargoes of the LMAN1/MCFD2 complex in a mouse model of combined Factor V and Factor VIII deficiency (Bin Zhang, personal communication). Factor V is synthesized in mouse megakaryocytes and is reduced in mice deficient for *LMAN1*. Analysis of platelets from *LMAN1-/-* mice could yield insight into other *LMAN1* cargoes in thrombopoiesis.

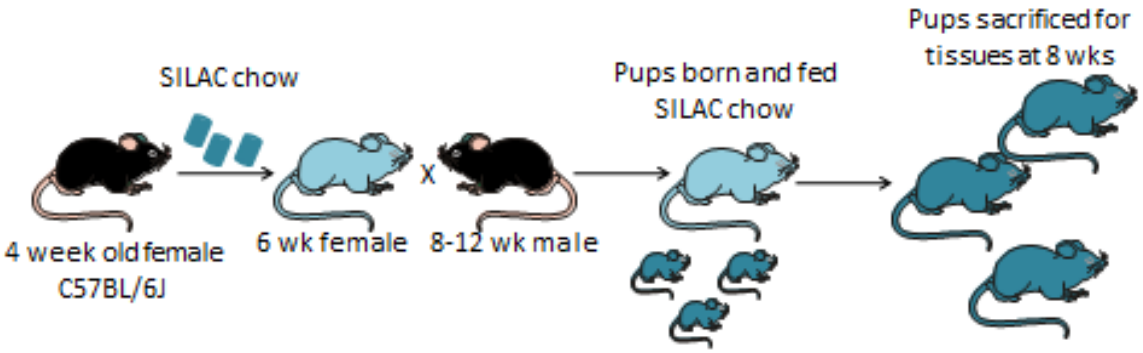

Figure 3- 1: Whole mouse in-vivo SILAC labeling.

Four week old female mice were maintained on chow containing ^{13}C lysine as the only lysine source (SILAC chow). At 6 weeks of age, females on SILAC chow (aqua mice) were mated with a C57BL/6 male. Progeny from this mating were maintained exclusively on SILAC chow (blue mice) until tissue harvest at eight weeks of age.

A.

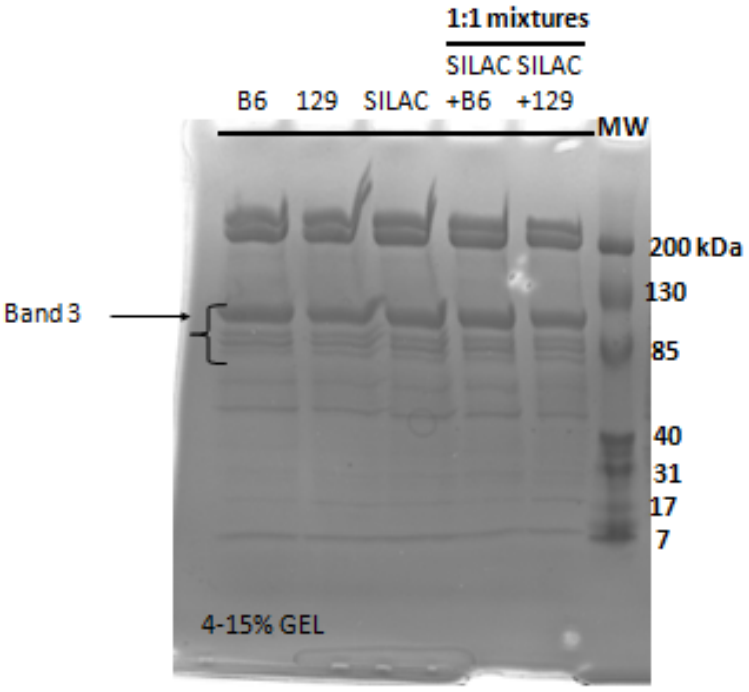
1:1 mixtures
SILAC SILAC
B6 129 SILAC +B6 +129
MW
200 kDa
130
85
40
31
17
7
Band 3
4-15% GEL

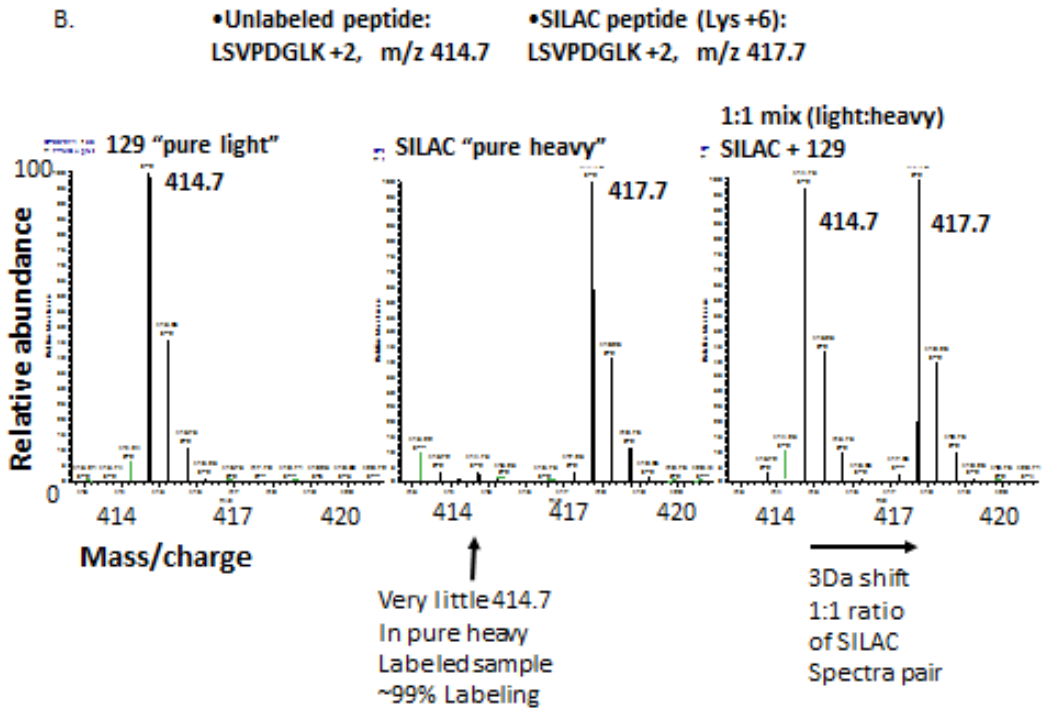

Figure 3- 2: MS analysis of RBC ghost Band 3 protein.

Blood was drawn from the F0 mice receiving SILAC chow after 12 weeks on a SILAC diet.

A) 4-15% acrylamide gel showing RBC ghosts from a C57BL/6 mouse, a 129 mouse and the labeled SILAC mouse as well as 1:1 mixtures of the B6:SILAC and 129:SILAC. The portion of the gel identified by the bracket was cut out and submitted for mass spectrometry analysis. B) Enlarged spectra from a peptide from the Band 3 protein from the SILAC ghosts, 129 ghosts and the mixtures of the two demonstrating the 3 Da shift and the absence of any residual light peptide in the SILAC alone (From Jesse Rinehart, Yale University).

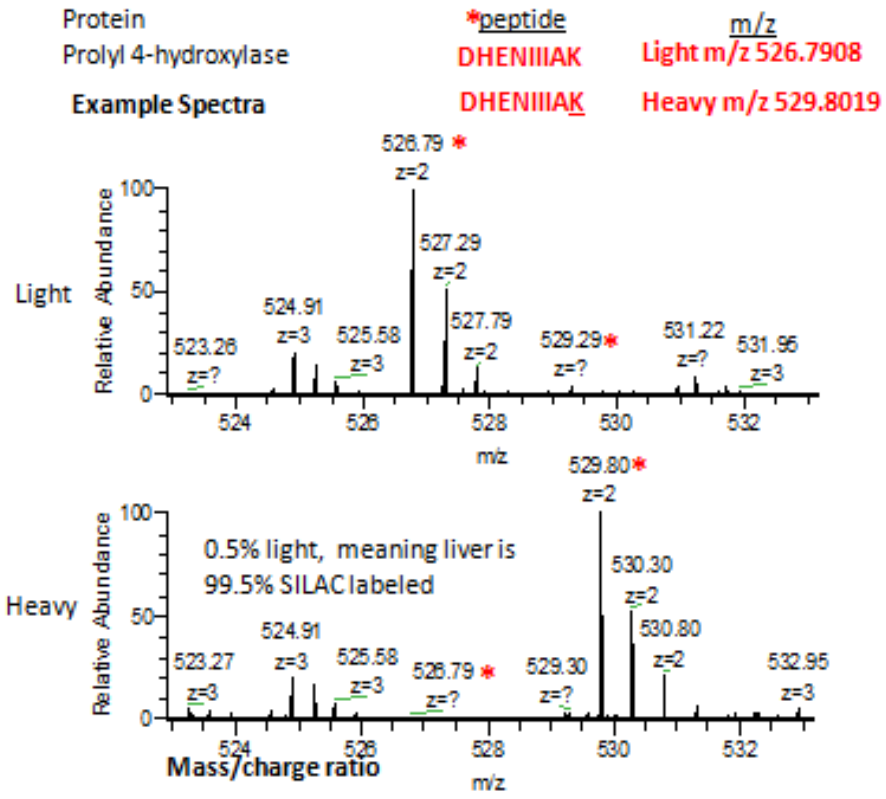

Figure 3- 3: MS analysis of liver from SILAC labeled mice.

Sample spectra from a peptide of prolyl-4-hydroxylase derived from liver. The 'light' panel indicates a peptide from the liver from a C57BL/6J unlabeled mouse and the 'heavy' panel shows a peptide from the F1 SILAC labeled mouse showing 99.5% heavy peptide in the SILAC alone sample indicating 99.5% labeling (From Jesse Rinehart, Yale University).

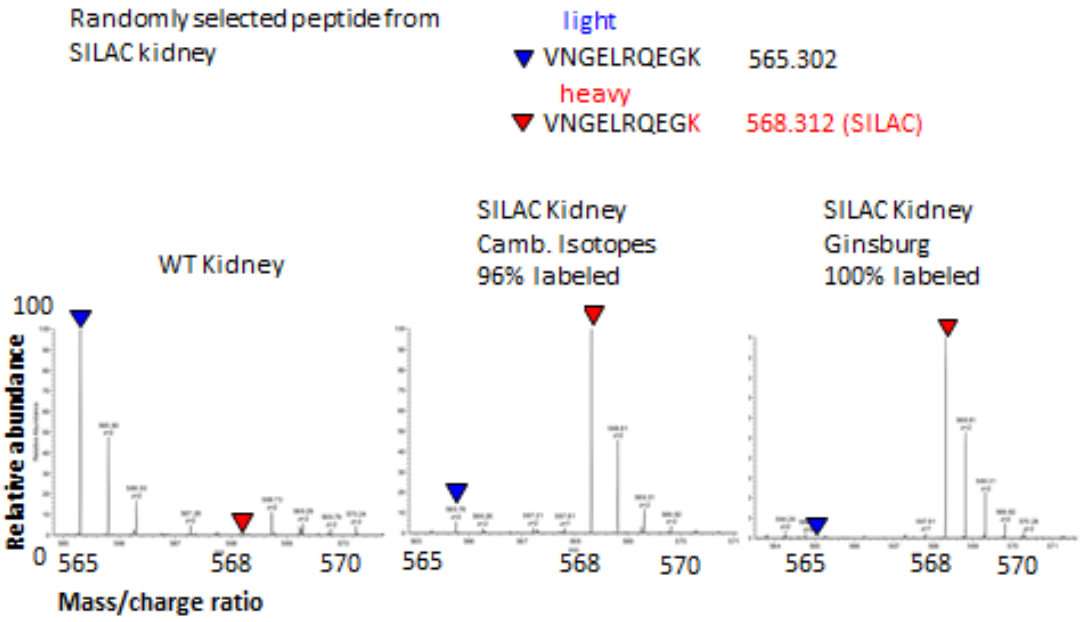

Figure 3- 4: MS analysis of kidney from SILAC labeled mice.

Example spectra of a randomly selected peptide from an F1 SILAC labeled kidney shows 100% labeling when compared with a WT or commercially labeled F2 SILAC labeled kidney from Cambridge Isotope Labs. The peptide corresponds to Fumarylacetoacetate hydrolase domain-containing protein 1 (From Jesse Rinehart, Yale University).

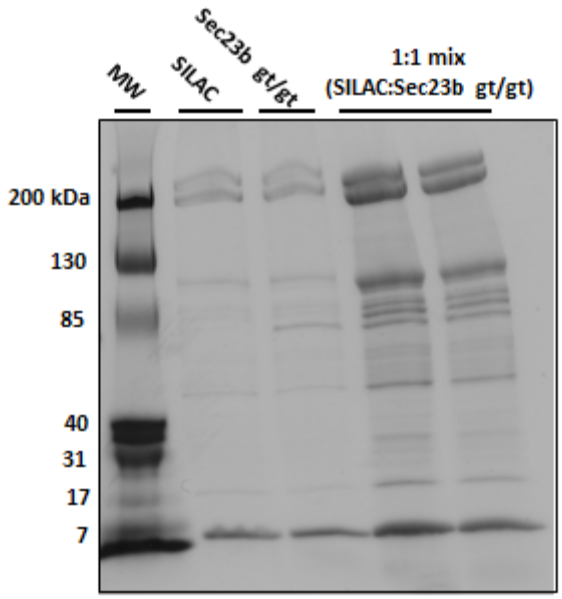

Figure 3- 5: SILAC mass spectrometry analysis of RBC ghosts from *Sec23b gt/gt* fetal liver cell recipients

A recipient mouse of *Sec23b gt/gt* fetal liver cells was bled eight weeks post transplant and RBC ghost preparations were made and mixed 1:1 with RBC ghosts from SILAC mice. Above depicts the acrylamide gel with the SILAC ghosts, the *Sec23b gt/gt* ghosts and a 1:1 mixture of the two. MW=molecular weight marker. (From Jesse Rinehart, Yale University).

Table 3- 1: Protein IDs and SILAC ratios from Sec23b gt/gt recipient (From Jesse Rinehart, Yale University).

Accession	SILAC ratio (L/H)	Adjusted SILAC ratio (L/H)	No. of peptides	Description
IPI00129225	139100.00	167590.36	3	Kng1 Isoform LMW of Kininogen-1
IPI00131695	80.94	97.52	3	Alb Serum albumin
IPI00129755	78.72	94.84	2	Serpina1b Alpha-1-antitrypsin 1-2
IPI00131695	75.2	90.60	19	Alb Serum albumin
IPI00954676	59.43	71.60	3	Serpina1a Serpina1a protein
IPI00475157	31.25	37.65	2	Serpina1b Serpina1b protein
IPI00877236	24.57	29.60	3	Apoa1 apolipoprotein A-I precursor
IPI00139788	17.63	21.24	11	Trf Serotransferrin
IPI00139788	15.57	18.76	4	Trf Serotransferrin
IPI00122312	2.595	3.13	2	Fgg Putative uncharacterized protein
IPI00124700	2.303	2.77	7	Tfrc Transferrin receptor protein 1
IPI00461249	2.18	2.63	2	Gm12141 similar to Heat shock protein 1
IPI00123181	2.141	2.58	4	Myh9 Myosin-9
IPI00132799	1.916	2.31	2	C1qbp complement component 1, q subcomponent binding protein
IPI00130280	1.746	2.10	2	Atp5a1 ATP synthase subunit alpha, mitochondrial
IPI00762198	1.723	2.08	3	Hbb-b1 Beta-globin
IPI00308885	1.667	2.01	2	Hspd1 Isoform 1 of 60 kDa heat shock protein, mitochondrial
IPI00230540	1.571	1.89	2	Vdac1 Isoform Mt-VDAC1 of Voltage-dependent anion-selective channel protei
IPI00316491	1.56	1.88	2	Hbb-b2 Hemoglobin subunit beta-2
IPI00228343	1.533	1.85	2	Fech Ferrochelatase
IPI00316491	1.493	1.80	2	Hbb-b2 Hemoglobin subunit beta-2
IPI00116302	1.486	1.79	2	Eif2s2 Eukaryotic translation initiation factor 2 subunit 2
IPI00831055	1.481	1.78	6	Hbb-b1 Beta-globin
IPI00762198	1.48	1.78	3	Hbb-b1 Beta-globin
IPI00110658	1.476	1.78	3	Hba-a2;Hba-a1 Putative uncharacterized protein

Accession	SILAC ratio (L/H)	Adjusted SILAC ratio (L/H)	No. of peptides	Description
IPI00110658	1.472	1.77	5	Hba-a2;Hba-a1 Putative uncharacterized protein
IPI00848802	1.463	1.76	2	LOC100045527 similar to Ac2-210 isoform 2
IPI00110658	1.431	1.72	3	Hba-a2;Hba-a1 Putative uncharacterized protein
IPI00831055	1.394	1.68	7	Hbb-b1 Beta-globin
IPI00474637	1.382	1.67	2	Gm13891;Rpl10;Gm10041;LOC100048223;LOC100048462 60S ribosomal protein L10
IPI00119305	1.366	1.65	3	Pa2g4 Proliferation-associated protein 2G4
IPI00110658	1.321	1.59	2	Hba-a2;Hba-a1 Putative uncharacterized protein
IPI00118384	1.314	1.58	4	Ywhae 14-3-3 protein epsilon
IPI00339916	1.286	1.55	3	Eprs Bifunctional aminoacyl-tRNA synthetase
IPI00117569	1.283	1.55	3	Rps11 Putative uncharacterized protein
IPI00762198	1.28	1.54	3	Hbb-b1 Beta-globin
IPI00110658	1.277	1.54	5	Hba-a2;Hba-a1 Putative uncharacterized protein
IPI00307837	1.261	1.52	9	Eef1a1 Elongation factor 1-alpha 1
IPI00831055	1.258	1.52	4	Hbb-b1 Beta-globin
IPI00110658	1.258	1.52	8	Hba-a2;Hba-a1 Putative uncharacterized protein
IPI00831055	1.254	1.51	9	Hbb-b1 Beta-globin
IPI00138716	1.254	1.51	2	Rap2b Ras-related protein Rap-2b
IPI00129526	1.251	1.51	4	Hsp90b1 Endoplasmin
IPI00831055	1.25	1.51	10	Hbb-b1 Beta-globin
IPI00331345	1.245	1.50	3	Rps3a 40S ribosomal protein S3a
IPI00110658	1.237	1.49	3	Hba-a2;Hba-a1 Putative uncharacterized protein
IPI00110658	1.237	1.49	2	Hba-a2;Hba-a1 Putative uncharacterized protein
IPI00652998	1.233	1.49	3	Hsp90b1 Putative uncharacterized protein
IPI00408892	1.233	1.49	5	Rab7 Ras-related protein Rab-7a
IPI00308706	1.222	1.47	2	Rpl5;Gm15500 60S ribosomal protein L5

Accession	SILAC ratio (L/H)	Adjusted SILAC ratio (L/H)	No. of peptides	Description
IPI00314950	1.201	1.45	2	Rplp0 60S acidic ribosomal protein P0
IPI00108454	1.188	1.43	2	- 29 kDa protein
IPI00126083	1.171	1.41	3	Ehd1 EH domain-containing protein 1
IPI00953783	1.153	1.39	5	Mthfd1 methylenetetrahydrofolate dehydrogenase 1
IPI00129526	1.153	1.39	4	Hsp90b1 Endoplasmin
IPI00408892	1.139	1.37	2	Rab7 Ras-related protein Rab-7a
IPI00110658	1.127	1.36	5	Hba-a2;Hba-a1 Putative uncharacterized protein
IPI00122862	1.125	1.36	11	Mthfd1 C-1-tetrahydrofolate synthase, cytoplasmic
IPI00116498	1.115	1.34	3	Ywhaz 14-3-3 protein zeta/delta
IPI00123199	1.114	1.34	2	Nap1l1 Nucleosome assembly protein 1-like 1
IPI00831055	1.114	1.34	8	Hbb-b1 Beta-globin
IPI00230416	1.104	1.33	3	Eif2s3y Eukaryotic translation initiation factor 2 subunit 3, Y-linked
IPI00110658	1.101	1.33	5	Hba-a2;Hba-a1 Putative uncharacterized protein
IPI00113845	1.101	1.33	2	Psmb1 Proteasome subunit beta type-1
IPI00119618	1.084	1.31	2	Canx Calnexin
IPI00224518	1.079	1.30	4	Rab5c Ras-related protein Rab-5C
IPI00266281	1.074	1.29	5	Txnl1 Thioredoxin-like protein 1
IPI00132410	1.072	1.29	2	Rab5a Ras-related protein Rab-5A
IPI00118676	1.071	1.29	2	Eif4a1 Eukaryotic initiation factor 4A-I
IPI00849045	1.07	1.29	2	Gm10293;Gapdh similar to Glyceraldehyde-3-phosphate dehydrogenase
IPI00317710	1.062	1.28	2	Hspa4l Isoform 1 of Heat shock 70 kDa protein 4L
IPI00116498	1.055	1.27	3	Ywhaz 14-3-3 protein zeta/delta
IPI00462072	1.051	1.27	8	Eno1;LOC100044223;Gm5506 Alpha-enolase
IPI00831055	1.051	1.27	10	Hbb-b1 Beta-globin
IPI00116281	1.048	1.26	2	Cct6a T-complex protein 1 subunit zeta

Accession	SILAC ratio (L/H)	Adjusted SILAC ratio (L/H)	No. of peptides	Description
IPI00123639	1.042	1.26	7	Calr Calreticulin
IPI00224518	1.037	1.25	4	Rab5c Ras-related protein Rab-5C
IPI00136483	1.02	1.23	4	Psmb7 Proteasome subunit beta type-7
IPI00113849	1.018	1.23	3	Cdc42 Isoform 2 of Cell division control protein 42 homolog
IPI00656325	1.016	1.22	5	Nsf Vesicle-fusing ATPase
IPI00319994	1.011	1.22	3	Ldha L-lactate dehydrogenase A chain
IPI00319992	1.008	1.21	12	Hspa5 78 kDa glucose-regulated protein
IPI00116277	1.006	1.21	4	Cct4 T-complex protein 1 subunit delta
IPI00122815	1.005	1.21	4	P4hb Putative uncharacterized protein
IPI00469114	1.005	1.21	11	Hba-a2;Hba-a1 Hemoglobin subunit alpha
IPI00221581	0.9974	1.20	5	Eif4b Eukaryotic translation initiation factor 4B
IPI00331214	0.9964	1.20	3	Cd36 Platelet glycoprotein 4
IPI00918032	0.9934	1.20	5	Hbb-b1 Beta-globin
IPI00467833	0.9903	1.19	3	Tpi1 triosephosphate isomerase 1
IPI00459570	0.9878	1.19	5	Tpm3 Putative uncharacterized protein
IPI00323357	0.9848	1.19	3	Hspa8 Heat shock cognate 71 kDa protein
IPI00553333	0.983	1.18	17	Hbb-b1 Hemoglobin subunit beta-1
IPI00762198	0.9828	1.18	19	Hbb-b1 Beta-globin
IPI00116281	0.9813	1.18	3	Cct6a T-complex protein 1 subunit zeta
IPI00110658	0.98	1.18	12	Hba-a2;Hba-a1 Putative uncharacterized protein
IPI00606473	0.9799	1.18	2	Fam55d Isoform 1 of Protein FAM55D
IPI00845802	0.9793	1.18	20	Hba-a2;Hba-a1 hemoglobin alpha, adult chain 2
IPI00831055	0.9764	1.18	20	Hbb-b1 Beta-globin
IPI00138406	0.9763	1.18	2	Rap1a Ras-related protein Rap-1A
IPI00831055	0.976	1.18	16	Hbb-b1 Beta-globin

Accession	SILAC ratio (L/H)	Adjusted SILAC ratio (L/H)	No. of peptides	Description
IPI00453803	0.9751	1.17	4	Ube2o Ubiquitin-conjugating enzyme E2 O
IPI00831055	0.973	1.17	15	Hbb-b1 Beta-globin
IPI00230642	0.9729	1.17	2	Cast Isoform 3 of Calpastatin
IPI00831055	0.9722	1.17	18	Hbb-b1 Beta-globin
IPI00831055	0.9712	1.17	15	Hbb-b1 Beta-globin
IPI00469114	0.9708	1.17	8	Hba-a2;Hba-a1 Hemoglobin subunit alpha
IPI00469114	0.9632	1.16	12	Hba-a2;Hba-a1 Hemoglobin subunit alpha
IPI00395157	0.9606	1.16	10	Epb4.1 Isoform 1 of Protein 4.1
IPI00330619	0.9591	1.16	2	Vac14 Protein VAC14 homolog
IPI00653918	0.9553	1.15	2	Epb4.2 Putative uncharacterized protein
IPI00457962	0.9537	1.15	2	Gypc Glycophorin-C
IPI00135686	0.9519	1.15	8	Ppib Peptidyl-prolyl cis-trans isomerase B
IPI00319965	0.9514	1.15	5	Psmd6 26S proteasome non-ATPase regulatory subunit 6
IPI00133977	0.9488	1.14	2	Nap1l4 Putative uncharacterized protein
IPI00323357	0.9487	1.14	30	Hspa8 Heat shock cognate 71 kDa protein
IPI00221402	0.9486	1.14	13	Aldoa Fructose-bisphosphate aldolase A
IPI00108895	0.9467	1.14	4	Psmc4 26S protease regulatory subunit 6B
IPI00225961	0.9454	1.14	4	Phgdh D-3-phosphoglycerate dehydrogenase
IPI00123639	0.9383	1.13	2	Calr Calreticulin
IPI00230642	0.9373	1.13	2	Cast Isoform 3 of Calpastatin
IPI00468691	0.9361	1.13	3	Abcg2 ATP-binding cassette sub-family G member 2
IPI00830704	0.9359	1.13	2	Tpm1 33 kDa protein
IPI00113869	0.9357	1.13	10	Bsg Isoform 2 of Basigin
IPI00851010	0.931	1.12	4	Gm13464 similar to Glyceraldehyde-3-phosphate dehydrogenase
IPI00471406	0.9308	1.12	2	Rnf123 Isoform 2 of E3 ubiquitin-protein ligase RNF123

Accession	SILAC ratio (L/H)	Adjusted SILAC ratio (L/H)	No. of peptides	Description
IPI00114560	0.9284	1.12	8	Rab1 Ras-related protein Rab-1A
IPI00135640	0.9282	1.12	4	Psmc5 26S protease regulatory subunit 8
IPI00267295	0.9274	1.12	4	Psmd1 26S proteasome non-ATPase regulatory subunit 1
IPI00331163	0.9265	1.12	3	Skp1a S-phase kinase-associated protein 1
IPI00323357	0.9261	1.12	4	Hspa8 Heat shock cognate 71 kDa protein
IPI00113845	0.924	1.11	7	Psmb1 Proteasome subunit beta type-1
IPI00668185	0.9212	1.11	3	LOC641192 similar to heat shock protein 70 cognate
IPI00135640	0.9211	1.11	4	Psmc5 26S protease regulatory subunit 8
IPI00283862	0.9203	1.11	9	Psma1 Proteasome subunit alpha type-1
IPI00831055	0.9197	1.11	12	Hbb-b1 Beta-globin
IPI00123176	0.9188	1.11	9	- 37 kDa protein
IPI00457962	0.9188	1.11	2	Gypc Glycophorin-C
IPI00131407	0.9168	1.10	3	Psma5 Proteasome subunit alpha type-5
IPI00457962	0.9165	1.10	2	Gypc Glycophorin-C
IPI00462008	0.9164	1.10	12	LOC100047352 similar to Glyceraldehyde-3-phosphate dehydrogenase
IPI00849046	0.9144	1.10	8	LOC100046806;Gm10327 similar to Glyceraldehyde-3-phosphate dehydrogenase (
IPI00309207	0.9142	1.10	2	Pafah1b1 Isoform 1 of Platelet-activating factor acetylhydrolase IB subuni
IPI00626909	0.9141	1.10	5	Capn1 Calpain-1 catalytic subunit
IPI00273646	0.914	1.10	15	Gm3272;Gm2574;LOC100042025; Gm10293;Gapdh;Gm10359;Gm120 33;Gm5138 Glyceralde
IPI00399459	0.9139	1.10	11	- 36 kDa protein
IPI00116563	0.9112	1.10	3	Rab5b Rab5B
IPI00850434	0.9099	1.10	11	Gm13292 similar to Glyceraldehyde-3-phosphate dehydrogenase (GAPDH) isofor

Accession	SILAC ratio (L/H)	Adjusted SILAC ratio (L/H)	No. of peptides	Description
IPI00663957	0.9099	1.10	11	- similar to Glyceraldehyde-3-phosphate dehydrogenase (GAPDH) isoform 1
IPI00420745	0.9094	1.10	6	Psma2 Proteasome subunit alpha type
IPI00230108	0.9088	1.09	15	Pdia3 Protein disulfide-isomerase A3
IPI00314439	0.9067	1.09	5	Psmd3 26S proteasome non-ATPase regulatory subunit 3
IPI00116277	0.9066	1.09	6	Cct4 T-complex protein 1 subunit delta
IPI00123354	0.9057	1.09	2	Ubac1 Ubiquitin-associated domain-containing protein 1
IPI00113214	0.9048	1.09	2	Usp5 Ubiquitin carboxyl-terminal hydrolase 5
IPI00133706	0.9034	1.09	8	Rab1b Ras-related protein Rab-1B
IPI00462605	0.9032	1.09	9	Gm16470 similar to Glyceraldehyde-3-phosphate dehydrogenase
IPI00323748	0.903	1.09	4	Stom Erythrocyte band 7 integral membrane protein
IPI00467833	0.9029	1.09	2	Tpi1 triosephosphate isomerase 1
IPI00277001	0.9016	1.09	4	Psma4 Proteasome subunit alpha type-4
IPI00403232	0.9011	1.09	2	Gm6498 Glyceraldehyde 3-phosphate dehydrogenase
IPI00471443	0.9007	1.09	9	Gm9781;Eif3j;LOC100044332 Eukaryotic translation initiation factor 3 subun
IPI00314467	0.9001	1.08	2	Psmb3 Proteasome subunit beta type-3
IPI00133066	0.8985	1.08	4	Psmd12 Putative uncharacterized protein
IPI00131406	0.8984	1.08	4	Psma7 Proteasome subunit alpha type-7
IPI00466919	0.8973	1.08	5	Pgd 6-phosphogluconate dehydrogenase, decarboxylating
IPI00123494	0.8961	1.08	5	Psmd2 26S proteasome non-ATPase regulatory subunit 2
IPI00320217	0.8955	1.08	3	Cct2 T-complex protein 1 subunit beta

Accession	SILAC ratio (L/H)	Adjusted SILAC ratio (L/H)	No. of peptides	Description
IPI00131845	0.8945	1.08	2	Psma6 Proteasome subunit alpha type-6
IPI00131406	0.8929	1.08	8	Psma7 Proteasome subunit alpha type-7
IPI00129512	0.8921	1.07	2	Psmb4 Proteasome subunit beta type-4
IPI00225322	0.8909	1.07	10	Add1 Isoform 2 of Alpha-adducin
IPI00187272	0.8897	1.07	7	5730469M10Rik Uncharacterized protein C10orf58 homolog
IPI00136483	0.8889	1.07	6	Psmb7 Proteasome subunit beta type-7
IPI00387232	0.8888	1.07	3	Nsfl1c Isoform 3 of NSFL1 cofactor p47
IPI00466919	0.887	1.07	3	Pgd 6-phosphogluconate dehydrogenase, decarboxylating
IPI00930878	0.8862	1.07	10	Psmc3 proteasome (prosome, macropain) 26S subunit, ATPase 3
IPI00752685	0.8858	1.07	4	Gm8055 similar to Glyceraldehyde-3-phosphate dehydrogenase
IPI00114560	0.8856	1.07	5	Rab1 Ras-related protein Rab-1A
IPI00312058	0.8839	1.06	10	Cat Catalase
IPI00659907	0.8838	1.06	3	EG545741 similar to glyceraldehyde-3-phosphate-dehydrogenase isoform 1
IPI00458393	0.8836	1.06	2	Atl3 Isoform 1 of Atlastin-3
IPI00776014	0.8829	1.06	2	Myo15 Isoform 2 of Myosin-XV
IPI00126042	0.8804	1.06	3	Rab14 Ras-related protein Rab-14
IPI00387494	0.8797	1.06	7	Hspa2 heat shock protein 2
IPI00649865	0.8776	1.06	4	Epb4.1 Erythrocyte protein band 4.1
IPI00131845	0.8768	1.06	6	Psma6 Proteasome subunit alpha type-6
IPI00110760	0.8744	1.05	3	Dnajb4 DnaJ homolog subfamily B member 4
IPI00116279	0.8732	1.05	9	Cct5 T-complex protein 1 subunit epsilon
IPI00869393	0.8722	1.05	17	Cat catalase
IPI00226234	0.8716	1.05	3	Plaa Phospholipase A-2-activating protein
IPI00130118	0.8716	1.05	7	Rab10 Ras-related protein Rab-10
IPI00136000	0.8712	1.05	3	Add1 Isoform 1 of Alpha-adducin

Accession	SILAC ratio (L/H)	Adjusted SILAC ratio (L/H)	No. of peptides	Description
IPI00323748	0.8705	1.05	2	Stom Erythrocyte band 7 integral membrane protein
IPI00474771	0.8704	1.05	34	Ank1 Isoform Er3 of Ankyrin-1
IPI00317902	0.8701	1.05	2	Psmb5 Proteasome subunit beta type-5
IPI00319994	0.8693	1.05	11	Ldha L-lactate dehydrogenase A chain
IPI00556827	0.8677	1.05	3	Atp2b1 plasma membrane calcium ATPase 1
IPI00463589	0.8664	1.04	6	Atp2b4 plasma membrane calcium ATPase 4 isoform x/b
IPI00649502	0.8659	1.04	5	Epb4.1 Erythrocyte protein band 4.1
IPI00277001	0.8657	1.04	4	Psma4 Proteasome subunit alpha type-4
IPI00886359	0.8656	1.04	2	Add1 Protein
IPI00467055	0.8656	1.04	3	Csnk1a1 Isoform 2 of Casein kinase I isoform alpha
IPI00751369	0.8644	1.04	16	Ldha lactate dehydrogenase A isoform 2
IPI00119871	0.8639	1.04	5	Ank1 Ank1 protein
IPI00331174	0.8639	1.04	2	Cct7 T-complex protein 1 subunit eta
IPI00331644	0.8611	1.04	2	Psma3 Proteasome subunit alpha type-3
IPI00227843	0.8607	1.04	2	Tpp2 Isoform Short of Tripeptidyl-peptidase 2
IPI00120761	0.8604	1.04	3	Slc4a1 Isoform Erythrocyte of Band 3 anion transport protein
IPI00464296	0.8593	1.04	2	Epb4.1l3 Isoform 8 of Band 4.1-like protein 3
IPI00473685	0.8579	1.03	10	Usp14 ubiquitin specific protease 14 isoform 2
IPI00469268	0.8574	1.03	3	Cct8 T-complex protein 1 subunit theta
IPI00111137	0.857	1.03	3	Kel Kell blood group glycoprotein homolog
IPI00120761	0.8549	1.03	2	Slc4a1 Isoform Erythrocyte of Band 3 anion transport protein
IPI00116279	0.8537	1.03	3	Cct5 T-complex protein 1 subunit epsilon

Accession	SILAC ratio (L/H)	Adjusted SILAC ratio (L/H)	No. of peptides	Description
IPI00136253	0.8532	1.03	2	Dnajb1 DnaJ homolog subfamily B member 1
IPI00648008	0.8525	1.03	2	Epb4.1 Erythrocyte protein band 4.1
IPI00411115	0.8519	1.03	5	Rab8b Ras-related protein Rab-8B
IPI00755019	0.8518	1.03	40	Ank1 Isoform Br4 of Ankyrin-1
IPI00474771	0.8515	1.03	41	Ank1 Isoform Er3 of Ankyrin-1
IPI00623506	0.8512	1.03	2	Ank3 Brain-specific ankyrin-G
IPI00173249	0.8512	1.03	2	Ank3 ankyrin 3, epithelial isoform h
IPI00227235	0.8512	1.03	2	Ank2 Isoform 2 of Ankyrin-2
IPI00131407	0.8496	1.02	4	Psma5 Proteasome subunit alpha type-5
IPI00114962	0.8494	1.02	5	Capn5 Calpain-5
IPI00187443	0.8493	1.02	2	Eif5;LOC100047658 Eukaryotic translation initiation factor 5
IPI00315463	0.8487	1.02	3	Reep5 receptor accessory protein 5
IPI00128945	0.8474	1.02	3	Psmb2 Proteasome subunit beta type-2
IPI00330804	0.8472	1.02	4	Hsp90aa1 Heat shock protein HSP 90-alpha
IPI00133605	0.846	1.02	3	Pklr Pyruvate kinase isozymes R/L
IPI00463589	0.8458	1.02	11	Atp2b4 plasma membrane calcium ATPase 4 isoform x/b
IPI00125880	0.8456	1.02	3	Pacsin2 Protein kinase C and casein kinase substrate in neurons protein 2
IPI00395157	0.8455	1.02	5	Epb4.1 Isoform 1 of Protein 4.1
IPI00113214	0.8455	1.02	4	Usp5 Ubiquitin carboxyl-terminal hydrolase 5
IPI00654038	0.8455	1.02	4	Epb4.1 Putative uncharacterized protein
IPI00130489	0.8445	1.02	5	Rab35 Ras-related protein Rab-35
IPI00556827	0.8434	1.02	4	Atp2b1 plasma membrane calcium ATPase 1
IPI00110588	0.8422	1.01	5	Msn Moesin
IPI00138406	0.8422	1.01	9	Rap1a Ras-related protein Rap-1A
IPI00130589	0.8391	1.01	3	Sod1 Superoxide dismutase [Cu-Zn]
IPI00471266	0.8389	1.01	3	Txnrd2 Isoform 2 of Thioredoxin reductase 2, mitochondrial
IPI00119618	0.8387	1.01	8	Canx Calnexin

Accession	SILAC ratio (L/H)	Adjusted SILAC ratio (L/H)	No. of peptides	Description
IPI00459570	0.8369	1.01	13	Tpm3 Putative uncharacterized protein
IPI00130118	0.8358	1.01	6	Rab10 Ras-related protein Rab-10
IPI00121534	0.8354	1.01	10	Car2 Carbonic anhydrase 2
IPI00323230	0.8346	1.01	16	Spna1 Spectrin alpha chain, erythrocyte
IPI00654038	0.8334	1.00	16	Epb4.1 Putative uncharacterized protein
IPI00395157	0.833	1.00	24	Epb4.1 Isoform 1 of Protein 4.1
IPI00411115	0.8325	1.00	8	Rab8b Ras-related protein Rab-8B
IPI00278611	0.8321	1.00	12	Tpm3 Isoform 1 of Tropomyosin alpha-3 chain
IPI00622235	0.8315	1.00	20	Vcp Transitional endoplasmic reticulum ATPase
IPI00676914	0.8307	1.00	19	LOC675857 similar to valosin isoform 1
IPI00395157	0.8307	1.00	5	Epb4.1 Isoform 1 of Protein 4.1
IPI00421223	0.8303	1.00	4	Tpm4 Tropomyosin alpha-4 chain
IPI00403266	0.8299	1.00	2	Flot2 Flotillin 2, isoform CRA_a
IPI00650000	0.8298	1.00	8	Epb4.1 Putative uncharacterized protein
IPI00187272	0.8294	1.00	6	5730469M10Rik Uncharacterized protein C10orf58 homolog
IPI00831330	0.8292	1.00	10	Tpm1 tropomyosin 1, alpha isoform 6
IPI00331644	0.8291	1.00	2	Psma3 Proteasome subunit alpha type-3
IPI00555069	0.8269	1.00	3	Pgk1 Phosphoglycerate kinase 1
IPI00121534	0.8266	1.00	7	Car2 Carbonic anhydrase 2
IPI00650000	0.8246	0.99	14	Epb4.1 Putative uncharacterized protein
IPI00320217	0.8246	0.99	2	Cct2 T-complex protein 1 subunit beta
IPI00123319	0.8241	0.99	5	Tpm2 Isoform 1 of Tropomyosin beta chain
IPI00831055	0.8235	0.99	13	Hbb-b1 Beta-globin
IPI00119871	0.8229	0.99	2	Ank1 Ank1 protein
IPI00336362	0.8228	0.99	6	Aldh1a7 Aldehyde dehydrogenase, cytosolic 1

Accession	SILAC ratio (L/H)	Adjusted SILAC ratio (L/H)	No. of peptides	Description
IPI00653918	0.8215	0.99	3	Epb4.2 Putative uncharacterized protein
IPI00169707	0.8212	0.99	14	Tpm3 Tropomyosin 3, gamma
IPI00323230	0.8208	0.99	22	Spna1 Spectrin alpha chain, erythrocyte
IPI00464296	0.8207	0.99	2	Epb4.1l3 Isoform 8 of Band 4.1-like protein 3
IPI00320204	0.8205	0.99	6	2210023G05Rik hypothetical protein LOC72361
IPI00653918	0.8205	0.99	4	Epb4.2 Putative uncharacterized protein
IPI00270326	0.8196	0.99	7	Psmc2 Putative uncharacterized protein
IPI00395157	0.8192	0.99	3	Epb4.1 Isoform 1 of Protein 4.1
IPI00131376	0.8184	0.99	5	Spnb1 spectrin beta 1
IPI00323230	0.818	0.99	10	Spna1 Spectrin alpha chain, erythrocyte
IPI00555059	0.8179	0.99	2	Prdx6 Peroxiredoxin-6
IPI00120761	0.8177	0.99	10	Slc4a1 Isoform Erythrocyte of Band 3 anion transport protein
IPI00407954	0.8171	0.98	7	Rap1b;LOC100048397 Ras-related protein Rap-1b
IPI00125328	0.817	0.98	7	Epb4.9 Dematin
IPI00323230	0.8162	0.98	15	Spna1 Spectrin alpha chain, erythrocyte
IPI00831626	0.8159	0.98	10	Tpm1 tropomyosin 1, alpha isoform 7
IPI00464296	0.8144	0.98	5	Epb4.1l3 Isoform 8 of Band 4.1-like protein 3
IPI00114925	0.8142	0.98	2	Nans Putative uncharacterized protein
IPI00649502	0.8122	0.98	25	Epb4.1 Erythrocyte protein band 4.1
IPI00420812	0.8116	0.98	2	Slc14a1 Solute carrier family 14 (Urea transporter), member 1, isoform CRA
IPI00131376	0.8113	0.98	105	Spnb1 spectrin beta 1
IPI00323748	0.8106	0.98	13	Stom Erythrocyte band 7 integral membrane protein
IPI00229294	0.8104	0.98	8	Epb4.1l3 Isoform 2 of Band 4.1-like protein 3

Accession	SILAC ratio (L/H)	Adjusted SILAC ratio (L/H)	No. of peptides	Description
IPI00120761	0.8103	0.98	5	Slc4a1 Isoform Erythrocyte of Band 3 anion transport protein
IPI00120761	0.8102	0.98	3	Slc4a1 Isoform Erythrocyte of Band 3 anion transport protein
IPI00679092	0.8089	0.97	20	LOC630963 similar to erythroid spectrin alpha
IPI00222386	0.8088	0.97	2	Chmp2b Charged multivesicular body protein 2b
IPI00319652	0.8087	0.97	6	Gpx1 Glutathione peroxidase 1
IPI00923082	0.8086	0.97	2	Gm1821 Putative uncharacterized protein
IPI00470152	0.8086	0.97	2	Gm6111;Rps27a;Ubb;Ubc ribosomal protein S27a
IPI00929768	0.8078	0.97	2	Pgk2 phosphoglycerate kinase 2
IPI00121534	0.8074	0.97	2	Car2 Carbonic anhydrase 2
IPI00622235	0.8073	0.97	6	Vcp Transitional endoplasmic reticulum ATPase
IPI00649753	0.8069	0.97	39	Epb4.1 erythrocyte membrane protein band 4.1 isoform 3
IPI00133428	0.8065	0.97	5	Psmc1 26S protease regulatory subunit 4
IPI00323230	0.805	0.97	144	Spna1 Spectrin alpha chain, erythrocyte
IPI00131376	0.8044	0.97	108	Spnb1 spectrin beta 1
IPI00653918	0.804	0.97	24	Epb4.2 Putative uncharacterized protein
IPI00655150	0.8039	0.97	7	Tmod1 tropomodulin 1
IPI00323748	0.8039	0.97	8	Stom Erythrocyte band 7 integral membrane protein
IPI00130304	0.8037	0.97	5	Bag2 BAG family molecular chaperone regulator 2
IPI00131376	0.8033	0.97	6	Spnb1 spectrin beta 1
IPI00131376	0.8033	0.97	21	Spnb1 spectrin beta 1
IPI00322312	0.803	0.97	4	Arhgdia Rho GDP-dissociation inhibitor 1
IPI00331128	0.8027	0.97	9	Rab8a Ras-related protein Rab-8A
IPI00120761	0.802	0.97	8	Slc4a1 Isoform Erythrocyte of Band 3 anion transport protein
IPI00463589	0.8019	0.97	4	Atp2b4 plasma membrane calcium ATPase 4 isoform x/b
IPI00119871	0.8015	0.97	3	Ank1 Ank1 protein

Accession	SILAC ratio (L/H)	Adjusted SILAC ratio (L/H)	No. of peptides	Description
IPI00169707	0.8015	0.97	6	Tpm3 Tropomyosin 3, gamma
IPI00830333	0.8015	0.97	4	Tpm1 29 kDa protein
IPI00323230	0.8013	0.97	67	Spna1 Spectrin alpha chain, erythrocyte
IPI00896727	0.8012	0.97	4	Cand1 Cullin-associated NEDD8-dissociated protein 1
IPI00117264	0.8006	0.96	3	Park7 Protein DJ-1
IPI00331556	0.7984	0.96	20	Hspa4 Heat shock 70 kDa protein 4
IPI00266875	0.7984	0.96	9	Actg2 Smooth muscle gamma-actin
IPI00120761	0.7982	0.96	3	Slc4a1 Isoform Erythrocyte of Band 3 anion transport protein
IPI00319652	0.7977	0.96	6	Gpx1 Glutathione peroxidase 1
IPI00125328	0.7973	0.96	8	Epb4.9 Dematin
IPI00395157	0.7972	0.96	8	Epb4.1 Isoform 1 of Protein 4.1
IPI00136000	0.7971	0.96	7	Add1 Isoform 1 of Alpha-adducin
IPI00896727	0.797	0.96	3	Cand1 Cullin-associated NEDD8-dissociated protein 1
IPI00109455	0.7965	0.96	2	Nudt16 U8 snoRNA-decapping enzyme
IPI00754071	0.7964	0.96	2	Prdx6 22 kDa protein
IPI00653918	0.7962	0.96	3	Epb4.2 Putative uncharacterized protein
IPI00120761	0.7954	0.96	5	Slc4a1 Isoform Erythrocyte of Band 3 anion transport protein
IPI00655150	0.7954	0.96	8	Tmod1 tropomodulin 1
IPI00753793	0.7952	0.96	2	Spna2 Isoform 2 of Spectrin alpha chain, brain
IPI00131376	0.7946	0.96	14	Spnb1 spectrin beta 1
IPI00114593	0.7945	0.96	15	Actc1 Actin, alpha cardiac muscle 1
IPI00120761	0.7943	0.96	4	Slc4a1 Isoform Erythrocyte of Band 3 anion transport protein
IPI00120761	0.7941	0.96	3	Slc4a1 Isoform Erythrocyte of Band 3 anion transport protein
IPI00323122	0.7934	0.96	15	Add2 Isoform 1 of Beta-adducin
IPI00470152	0.793	0.96	4	Gm6111;Rps27a;Ubb;Ubc ribosomal protein S27a
IPI00136000	0.7927	0.96	8	Add1 Isoform 1 of Alpha-adducin
IPI00885570	0.7927	0.96	6	Actb Beta-actin (Fragment)

Accession	SILAC ratio (L/H)	Adjusted SILAC ratio (L/H)	No. of peptides	Description
IPI00227835	0.7926	0.95	6	Tpm1 Isoform 2 of Tropomyosin alpha-1 chain
IPI00679092	0.7924	0.95	117	LOC630963 similar to erythroid spectrin alpha
IPI00323230	0.7919	0.95	127	Spna1 Spectrin alpha chain, erythrocyte
IPI00131299	0.7909	0.95	2	Pde6c Isoform 1 of Cone cGMP-specific 3',5'-cyclic phosphodiesterase subun
IPI00753815	0.7902	0.95	2	Spna2 Isoform 1 of Spectrin alpha chain, brain
IPI00464296	0.7893	0.95	3	Epb4.1l3 Isoform 8 of Band 4.1-like protein 3
IPI00323230	0.7891	0.95	13	Spna1 Spectrin alpha chain, erythrocyte
IPI00136929	0.7888	0.95	2	Actg1 Gamma actin-like protein
IPI00331556	0.7884	0.95	15	Hspa4 Heat shock 70 kDa protein 4
IPI00653918	0.7881	0.95	10	Epb4.2 Putative uncharacterized protein
IPI00653921	0.788	0.95	7	Rdx radixin isoform a
IPI00116558	0.7875	0.95	4	Rhog Rho-related GTP-binding protein RhoG
IPI00278611	0.787	0.95	6	Tpm3 Isoform 1 of Tropomyosin alpha-3 chain
IPI00153107	0.7869	0.95	4	Blmh Bleomycin hydrolase
IPI00121887	0.7864	0.95	2	Tcea1 Isoform 2 of Transcription elongation factor A protein 1
IPI00323122	0.7853	0.95	11	Add2 Isoform 1 of Beta-adducin
IPI00395157	0.7833	0.94	2	Epb4.1 Isoform 1 of Protein 4.1
IPI00626662	0.7831	0.94	5	Aldh1a1 Retinal dehydrogenase 1
IPI00626662	0.7827	0.94	17	Aldh1a1 Retinal dehydrogenase 1
IPI00131376	0.7823	0.94	10	Spnb1 spectrin beta 1
IPI00395157	0.7822	0.94	8	Epb4.1 Isoform 1 of Protein 4.1
IPI00653918	0.7813	0.94	2	Epb4.2 Putative uncharacterized protein
IPI00124497	0.7808	0.94	2	Flt1 Vascular endothelial growth factor receptor 1
IPI00222386	0.7805	0.94	2	Chmp2b Charged multivesicular body protein 2b
IPI00120761	0.7793	0.94	6	Slc4a1 Isoform Erythrocyte of Band 3 anion transport protein

Accession	SILAC ratio (L/H)	Adjusted SILAC ratio (L/H)	No. of peptides	Description
IPI00132206	0.7793	0.94	2	Dnajc5 DnaJ homolog subfamily C member 5
IPI00556827	0.7787	0.94	3	Atp2b1 plasma membrane calcium ATPase 1
IPI00120761	0.7786	0.94	10	Slc4a1 Isoform Erythrocyte of Band 3 anion transport protein
IPI00420812	0.7783	0.94	3	Slc14a1 Solute carrier family 14 (Urea transporter), member 1, isoform CRA
IPI00131376	0.7782	0.94	7	Spnb1 spectrin beta 1
IPI00111831	0.7781	0.94	3	Naca Nascent polypeptide-associated complex subunit alpha, muscle-specific
IPI00122858	0.778	0.94	3	Saps3 Isoform 1 of Serine/threonine-protein phosphatase 6 regulatory subun
IPI00474771	0.7776	0.94	6	Ank1 Isoform Er3 of Ankyrin-1
IPI00309481	0.7766	0.94	2	Epb4.1l2 Band 4.1-like protein 2
IPI00830884	0.7754	0.93	3	Tpm1 tropomyosin 1, alpha isoform 4
IPI00124830	0.7748	0.93	3	Cd47 Isoform 2 of Leukocyte surface antigen CD47
IPI00831110	0.7747	0.93	15	Mpp1 Membrane protein, palmitoylated
IPI00127163	0.7743	0.93	10	Ank1 Isoform Er1 of Ankyrin-1
IPI00136000	0.7733	0.93	2	Add1 Isoform 1 of Alpha-adducin
IPI00474771	0.7718	0.93	11	Ank1 Isoform Er3 of Ankyrin-1
IPI00653918	0.7713	0.93	5	Epb4.2 Putative uncharacterized protein
IPI00874482	0.771	0.93	14	Actg1 Actin, cytoplasmic 2
IPI00110827	0.7704	0.93	11	Acta1 Actin, alpha skeletal muscle
IPI00120761	0.7702	0.93	7	Slc4a1 Isoform Erythrocyte of Band 3 anion transport protein
IPI00831110	0.7683	0.93	10	Mpp1 Membrane protein, palmitoylated
IPI00753793	0.7679	0.93	2	Spna2 Isoform 2 of Spectrin alpha chain, brain
IPI00662681	0.7676	0.92	2	Slc43a1 Large neutral amino acids transporter small subunit 3
IPI00473320	0.7669	0.92	6	Actb Putative uncharacterized protein

Accession	SILAC ratio (L/H)	Adjusted SILAC ratio (L/H)	No. of peptides	Description
IPI00323122	0.7665	0.92	4	Add2 Isoform 1 of Beta-adducin
IPI00137706	0.7661	0.92	19	Mpp1 55 kDa erythrocyte membrane protein
IPI00403079	0.7659	0.92	2	Cd47 Isoform 1 of Leukocyte surface antigen CD47
IPI00120761	0.7657	0.92	9	Slc4a1 Isoform Erythrocyte of Band 3 anion transport protein
IPI00421166	0.7653	0.92	3	Epb4.2 Erythrocyte membrane protein band 4.2
IPI00331128	0.7647	0.92	2	Rab8a Ras-related protein Rab-8A
IPI00648008	0.7627	0.92	2	Epb4.1 Erythrocyte protein band 4.1
IPI00321978	0.7612	0.92	3	Ranbp1 Ran-specific GTPase-activating protein (Fragment)
IPI00230320	0.761	0.92	4	Car1 Carbonic anhydrase 1
IPI00111519	0.7604	0.92	2	Fn3k Fructosamine-3-kinase
IPI00323122	0.7598	0.92	4	Add2 Isoform 1 of Beta-adducin
IPI00131376	0.7578	0.91	14	Spnb1 spectrin beta 1
IPI00229294	0.7558	0.91	2	Epb4.1l3 Isoform 2 of Band 4.1-like protein 3
IPI00125328	0.7558	0.91	3	Epb4.9 Dematin
IPI00828796	0.7549	0.91	3	Ide insulin-degrading enzyme
IPI00137194	0.753	0.91	5	Slc16a1 Monocarboxylate transporter 1
IPI00123313	0.7525	0.91	4	Uba1 Ubiquitin-like modifier-activating enzyme 1
IPI00469268	0.7525	0.91	3	Cct8 T-complex protein 1 subunit theta
IPI00230320	0.7515	0.91	5	Car1 Carbonic anhydrase 1
IPI00123313	0.7502	0.90	8	Uba1 Ubiquitin-like modifier-activating enzyme 1
IPI00266875	0.7489	0.90	2	Actg2 Smooth muscle gamma-actin
IPI00221528	0.7487	0.90	7	Actbl2 Beta-actin-like protein 2
IPI00121788	0.7464	0.90	11	Prdx1 Peroxiredoxin-1
IPI00848536	0.7459	0.90	6	Gm7204 similar to MSP23 isoform 1
IPI00336324	0.7432	0.90	5	Mdh1 Malate dehydrogenase, cytoplasmic
IPI00421166	0.7431	0.90	2	Epb4.2 Erythrocyte membrane protein band 4.2
IPI00230320	0.7411	0.89	6	Car1 Carbonic anhydrase 1

Accession	SILAC ratio (L/H)	Adjusted SILAC ratio (L/H)	No. of peptides	Description
IPI00153098	0.7406	0.89	2	Osta Organic solute transporter subunit alpha
IPI00480406	0.7393	0.89	4	Actc1 Putative uncharacterized protein
IPI00474756	0.7384	0.89	7	- 29 kDa protein
IPI00135087	0.7371	0.89	3	Cops5 COP9 signalosome complex subunit 5
IPI00403079	0.7364	0.89	3	Cd47 Isoform 1 of Leukocyte surface antigen CD47
IPI00943373	0.7346	0.89	3	Fn3krp fructosamine 3 kinase related protein
IPI00120761	0.7332	0.88	4	Slc4a1 Isoform Erythrocyte of Band 3 anion transport protein
IPI00830159	0.7321	0.88	4	Rad23a Rad23a protein
IPI00124225	0.7299	0.88	5	Psme2 Proteasome activator complex subunit 2
IPI00648420	0.7292	0.88	2	Actg1 Actin, gamma, cytoplasmic 1
IPI00475248	0.7275	0.88	3	Eif2c2 Argonaute 2 protein (Fragment)
IPI00227843	0.7256	0.87	6	Tpp2 Isoform Short of Tripeptidyl-peptidase 2
IPI00125328	0.7251	0.87	4	Epb4.9 Dematin
IPI00307988	0.7238	0.87	2	Rad23a UV excision repair protein RAD23 homolog A
IPI00473320	0.722	0.87	3	Actb Putative uncharacterized protein
IPI00121788	0.7214	0.87	10	Prdx1 Peroxiredoxin-1
IPI00138892	0.7171	0.86	2	Gm11808;2810422J05Rik;Uba52 hypothetical protein LOC666586
IPI00113996	0.7153	0.86	2	Blvrb Flavin reductase
IPI00321734	0.7149	0.86	7	Glo1 Lactoylglutathione lyase
IPI00124225	0.7139	0.86	2	Psme2 Proteasome activator complex subunit 2
IPI00120761	0.7138	0.86	5	Slc4a1 Isoform Erythrocyte of Band 3 anion transport protein
IPI00230440	0.7134	0.86	3	Ahcy;Gm9826 Adenosylhomocysteinase
IPI00626994	0.712	0.86	6	Ipo5 Isoform 1 of Importin-5
IPI00224036	0.7104	0.86	4	Butr1 Putative uncharacterized protein

Accession	SILAC ratio (L/H)	Adjusted SILAC ratio (L/H)	No. of peptides	Description
IPI00654163	0.7102	0.86	2	Slc16a10 Isoform 1 of Monocarboxylate transporter 10
IPI00321978	0.7101	0.86	5	Ranbp1 Ran-specific GTPase-activating protein (Fragment)
IPI00124223	0.709	0.85	7	Psme1 Proteasome activator complex subunit 1
IPI00323881	0.7067	0.85	5	Kpnb1 Importin subunit beta-1
IPI00124223	0.7062	0.85	7	Psme1 Proteasome activator complex subunit 1
IPI00265471	0.7048	0.85	4	Adsl Putative uncharacterized protein
IPI00115157	0.7033	0.85	11	Snca Isoform 1 of Alpha-synuclein
IPI00330303	0.7028	0.85	10	Atic;LOC100046995 Bifunctional purine biosynthesis protein PURH
IPI00470981	0.6995	0.84	2	Rtn3 Isoform 1 of Reticulon-3
IPI00114329	0.6981	0.84	3	Gclm Glutamate--cysteine ligase regulatory subunit
IPI00117910	0.6974	0.84	4	Prdx2 Peroxiredoxin-2
IPI00127109	0.6968	0.84	5	1700009N14Rik RIKEN cDNA 1700009N14 gene
IPI00117910	0.6935	0.84	3	Prdx2 Peroxiredoxin-2
IPI00653918	0.6932	0.84	4	Epb4.2 Putative uncharacterized protein
IPI00120761	0.6927	0.83	4	Slc4a1 Isoform Erythrocyte of Band 3 anion transport protein
IPI00279218	0.6919	0.83	15	Apeh Isoform 2 of Acylamino-acid-releasing enzyme
IPI00117910	0.6919	0.83	3	Prdx2 Peroxiredoxin-2
IPI00753136	0.6909	0.83	4	Slc43a1 solute carrier family 43, member 1 isoform 1
IPI00221663	0.6893	0.83	10	Bpgm Bisphosphoglycerate mutase
IPI00127109	0.6878	0.83	5	1700009N14Rik RIKEN cDNA 1700009N14 gene
IPI00117910	0.6876	0.83	13	Prdx2 Peroxiredoxin-2
IPI00127163	0.6869	0.83	7	Ank1 Isoform Er1 of Ankyrin-1
IPI00113869	0.6845	0.82	8	Bsg Isoform 2 of Basigin
IPI00110588	0.6829	0.82	2	Msn Moesin
IPI00137194	0.6787	0.82	4	Slc16a1 Monocarboxylate transporter 1

Accession	SILAC ratio (L/H)	Adjusted SILAC ratio (L/H)	No. of peptides	Description
IPI00126861	0.6785	0.82	2	Tgm2 Protein-glutamine gamma-glutamyltransferase 2
IPI00117910	0.678	0.82	7	Prdx2 Peroxiredoxin-2
IPI00117910	0.674	0.81	3	Prdx2 Peroxiredoxin-2
IPI00117910	0.6729	0.81	5	Prdx2 Peroxiredoxin-2
IPI00421166	0.6719	0.81	3	Epb4.2 Erythrocyte membrane protein band 4.2
IPI00137194	0.6698	0.81	5	Slc16a1 Monocarboxylate transporter 1
IPI00331214	0.6692	0.81	6	Cd36 Platelet glycoprotein 4
IPI00121514	0.6672	0.80	8	Stip1 Stress-induced-phosphoprotein 1
IPI00127408	0.6669	0.80	5	Rac1 RAS-related C3 botulinum substrate 1, isoform CRA_a
IPI00157462	0.6669	0.80	5	Rac3 Ras-related C3 botulinum toxin substrate 3
IPI00121514	0.6641	0.80	9	Stip1 Stress-induced-phosphoprotein 1
IPI00137194	0.663	0.80	4	Slc16a1 Monocarboxylate transporter 1
IPI00121319	0.6629	0.80	2	Crip2 Cysteine-rich protein 2
IPI00113248	0.6536	0.79	2	Kras Isoform 2A of GTPase KRas
IPI00649647	0.6522	0.79	4	Rac3 RAS-related C3 botulinum substrate 3, isoform CRA_a
IPI00654163	0.6502	0.78	5	Slc16a10 Isoform 1 of Monocarboxylate transporter 10
IPI00408495	0.6473	0.78	5	Bsg Isoform 1 of Basigin
IPI00224036	0.6446	0.78	5	Butr1 Putative uncharacterized protein
IPI00138061	0.6419	0.77	2	Cr1l Isoform 1 of Complement regulatory protein Crry
IPI00153463	0.6416	0.77	2	Dhrs11 Dehydrogenase/reductase SDR family member 11
IPI00119871	0.6405	0.77	3	Ank1 Ank1 protein
IPI00221663	0.6403	0.77	11	Bpgm Bisphosphoglycerate mutase
IPI00387362	0.6397	0.77	2	Rhag Ammonium transporter Rh type A
IPI00467841	0.6373	0.77	2	Calm1;Calm3;Calm2 Putative uncharacterized protein
IPI00125658	0.6349	0.76	2	Gclc Glutamate--cysteine ligase catalytic subunit

Accession	SILAC ratio (L/H)	Adjusted SILAC ratio (L/H)	No. of peptides	Description
IPI00469987	0.6312	0.76	8	Gda Guanine deaminase
IPI00323971	0.6274	0.76	3	Impdh2 Inosine-5'-monophosphate dehydrogenase 2
IPI00469987	0.6256	0.75	8	Gda Guanine deaminase
IPI00127989	0.6236	0.75	6	LOC100048119;Ptges3;Gm9769 Prostaglandin E synthase 3
IPI00132475	0.6151	0.74	3	Lman1 Putative uncharacterized protein
IPI00153463	0.615	0.74	2	Dhrs11 Dehydrogenase/reductase SDR family member 11
IPI00468039	0.6054	0.73	2	Pnp2 Putative uncharacterized protein
IPI00310091	0.6035	0.73	3	Ppp2r1a Serine/threonine-protein phosphatase 2A 65 kDa regulatory subunit
IPI00127989	0.6024	0.73	3	LOC100048119;Ptges3;Gm9769 Prostaglandin E synthase 3
IPI00115157	0.6002	0.72	2	Snca Isoform 1 of Alpha-synuclein
IPI00117910	0.5911	0.71	2	Prdx2 Peroxiredoxin-2
IPI00676841	0.5867	0.71	6	Gm5081 hypothetical protein LOC328099
IPI00420812	0.5843	0.70	2	Slc14a1 Solute carrier family 14 (Urea transporter), member 1, isoform CRA
IPI00330862	0.5715	0.69	9	Ezr;LOC100044177 Ezrin
IPI00127163	0.5697	0.69	24	Ank1 Isoform Er1 of Ankyrin-1
IPI00310091	0.5647	0.68	4	Ppp2r1a Serine/threonine-protein phosphatase 2A 65 kDa regulatory subunit
IPI00113408	0.5572	0.67	3	Rpia Ribose-5-phosphate isomerase
IPI00607023	0.555	0.67	2	Pnp1 nucleoside phosphorylase
IPI00649502	0.5371	0.65	2	Epb4.1 Erythrocyte protein band 4.1
IPI00607023	0.5249	0.63	3	Pnp1 nucleoside phosphorylase
IPI00405227	0.4903	0.59	3	Vcl Vinculin

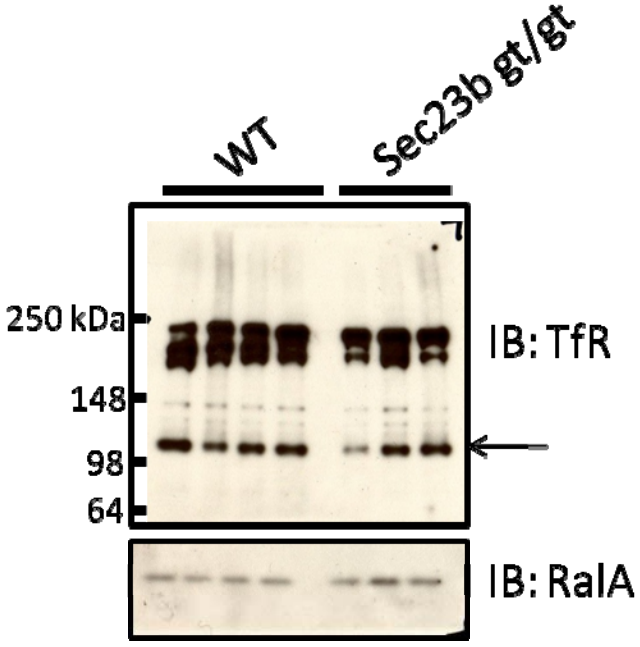

Figure 3- 6: Western blot of RBC ghosts for transferrin receptor.

Western blot for this protein (100 kDa band) did not show any consistent difference between mice receiving WT and *Sec23b gt/gt* fetal liver cells. The RBC membrane protein RalA was used as a loading control.

Acknowledgements: Many thanks to Jesse Rinehart, Yale University for his help and expertise in collection of mass spectrometry data.

CHAPTER IV:

Phenotypic Characterization of Sec23a gt/gt Mice and Study of the Interaction Between Sec23a and Sec23b

Abstract

Missense mutations in *SEC23A* lead to the human disorder Cranio-Lenticulo-Sutural Dysplasia (CLSD). In this study, we describe mice with a gene trap insertion in the *Sec23a* gene (*Sec23a gt*). Mice homozygous for the gene trap insertion die during mid-embryogenesis (E10.5 and E11.5). *Sec23a gt/gt* embryos demonstrate an open midbrain beginning at E11.5. In contrast to the previous description of skin fibroblasts from SEC23A deficient patients, Murine Embryonic Fibroblasts (MEFs) derived from *Sec23a gt/gt* mice do not show dilation of the endoplasmic reticulum. Consistent with the overlap in function of SEC23A and SEC23B, plasmid DNA constructs coding for fluorescently tagged SEC23A and SEC23B in transfected fibroblasts showed co-localization on confocal microscopy. While *Sec23a+/gt Sec23b+/gt* mice survive to weaning in expected numbers with no apparent phenotype, *Sec23a gt/gt Sec23b+/gt* mice are lost at an earlier time point during embryogenesis (loss of embryos begins at E9.5) than *Sec23a gt/gt Sec23b+/+* mice. These data suggest a partial overlap in function between SEC23A and SEC23B.

Introduction

Sec23p is a yeast protein that constitutes part of the COPII coat complex [93]. The COPII coat is responsible for transport of proteins from the endoplasmic reticulum to the Golgi apparatus [1,2]. Sec23p is responsible for binding the other components of the COPII coat and serves as a GTPase Activating Protein (GAP) for the small GTPase Sar1p, which helps budding and fission of the final COPII vesicle [94]. The formation of COPII

vesicles as a mode of cargo protein transport from the ER to the Golgi is a conserved pathway from yeast to mammals. However, mammals have two forms of Sec23 encoded by paralogous genes – *Sec23a* and *Sec23b.*

Homozygosity for a missense mutation in, F382L in *SEC23A* was identified in affected individuals with Cranio-Lenticulo Sutual Dysplasia (CLSD) [31] in a consanguineous Saudi family. CLSD is characterized by mild mental retardation, late closure of the cranial fontanelles, and Y-shaped cataracts. Subsequent studies showed that SEC23A with an F382L mutation fails to effectively act as a GAP in the presence of SEC13 and SEC31 [32]. Further, the failure of the SEC23A GAP activity only occurs when SEC23A is bound to SAR1B but not when bound to SAR1A. A second missense mutation (M702V) in SEC23A has also been identified in a patient with CLSD[95]. While this and the F382L mutation in SEC23A cause relatively mild disease in humans, perhaps more severe deficiency may be lethal.

Mutations in *SEC23A* have also been described in other animal model systems. For example, an L402X mutation termed *crusher* was described in the zebrafish orthologue of *SEC23A* in a chemical screen for craniofacial mutants. *Crusher* also appears to be due to a defect in collagen secretion [33].

In this chapter we describe the phenotype of mice with a gene trap insertion in the *Sec23a* gene. These mice were generated from embryonic stem cells with a gene trap insertion in the second intron of the *Sec23a* gene. Initial characterization of *Sec23a gt/gt* mice shows that they begin to die between E10.5 and E11.5 in development with no mutant embryos left after E12.5 (Bin Zhang, personal communication). Our focus here will be on characterization of *Sec23a gt/gt* murine embryonic fibroblasts and the interactions between Sec23a and Sec23b in mice.

Materials and Methods

Mice. The *Sec23a* ESC gene trap line RRE297 was obtained from the Bay Genomics gene trap consortium (http://www.genetrap.org/index.html) and injected into C57BL/6J blastocysts in the University of Michigan Transgenic Animal Core yielding

129P2/C57BL/6J chimeras. Germline transmission was achieved and mice heterozygous for the gene trap *Sec23a* allele were subsequently backcrossed 10 generations onto a C57BL/6J background (Generation of mice and 5 generations of backcrossing was carried out by Bin Zhang). Mice were housed at the University of Michigan and treated in accordance with the regulations of the University Animal Care and Use Committee (UCUCA).

PCR and genotyping. In order to genotype *Sec23a*+/*gt* mice, a three primer genotyping assay was used with one primer in intron two of *Sec23a* upstream of the gene trap insertion (5'-TTGGTCATAATTGAGTTGGTGTG-3'), one primer within the gene trap vector (5'-GACCTGGCTCCTATGGGATA-3') and one primer downstream of the gene trap insertion (5'-CAACCACAGGAAAAGGTTGC-3'). DNA was prepared from a tail biopsy of the mice and genotyping was done by PCR analysis. The gene trap allele give a 375 bp band when the PCR product was analyzed by gel electrophoresis and the wild type allele gives a 450 bp band (Figure 4-1) Mouse genotyping data was stored in the Jackson Labs Colony Management System for reference for future breeding and experiments.

Cloning. Plasmid constructs were obtained for mouse *Sec23a* and *Sec23b* from Open Biosystems, (stock #5364796 – Sec23a and #3591420, 4024353 – Sec23b) in the pCMV-SPORT6 expression vector. The entire cDNAs for *Sec23a* and *Sec23b* were subsequently amplified by PCR. The 5' primer for Sec23a (5'-CCGCTCGAGATACAACCTATTTGGAATTTATC-3') and Sec23b (5'-CCGTGATCATTAAGAGGCACTAGACACAGCCAG-3') had an additional 5' sequence for XhoI and the 3' primer for Sec23a (5'-CCGGGATCCTCAAGCAGCACTCGACACTGCAAG-3') had a 5' sequence for *BamHI* and Sec23b (5'-CCGTGATCATTAAGAGGCACTAGACACAGCCAG-3') had a 5' sequence for *BclI*. The Sec23a PCR product with attached restriction sites was cloned into the polylinker site of the pEGFP-C1 vector (Clontech) such that the GFP will be an N-terminal tag for Sec23a (GFP-SEC23A). The Sec23b PCR product was cloned into a variant of the pEGFP-C1 vector where GFP has been replaced with a monomeric form of RFP[96] (RFP-SEC23B).

Confocal microscopy. At 12.5 dpc, pregnant females from a *Sec23a+/gt* intercross were sacrificed and embryos were harvested to generate primary murine embryonic fibroblast (MEF) cells. Embryos were disrupted using 0.05% trypsin and grown in Dulbecco's Modified Eagle Medium (DMEM) supplemented with 10% FBS and 1x penicillin/streptomycin. A portion of the cells were taken for genotyping using the protocol described above. MEF cells were frozen in Freezing Medium (Gibco) at -80ºC overnight and then transferred to vapor phase liquid nitrogen storage (-186ºC). Cells were subsequently thawed for immunofluorescence studies and grown in the DMEM medium described above. MEF cells were grown to approximately 80% confluence and then fixed in methanol. Cells were subsequently incubated with antibodies against PDI (Assay Designs, stock# SPA-890D), ERGIC-53 (Sigma, stock# E1031), and Giantin (Covance Research Products, stock# PRB-114C) at a concentration of 1:500. Alexa fluor 488 goat anti-rabbit secondary antibodies (Molecular probes, A-11034) and mitotracker and lysotracker dyes (Molecular Probes) were used at a concentration of 1:1000. For transfection experiments, COS-1 cells were grown in DMEM medium as described above and transfected with GFP-SEC23A, RFP-SEC23B and a dominant negative form of Sar1a that contains an H79G mutation that prevents GTP hydrolysis and COPII budding. [97] FuGene transfection reagent was used (Roche, stock# 11815091001) and imaging was with an Olympus IX70 confocal microscope.

Electron microscopy. Mouse embryos were submitted to the University of Michigan Microscopy and Imaging Laboratory for processing and subsequently imaged on an Amray 1910 Field Emmission Scanning Electron Microscope. WT, *Sec23a+/gt*, and *Sec23a gt/gt* MEFs were plated out in a 6 well plate, submitted to the University of Michigan Microscopy and Imaging Laboratory for processing and imaged on a Philips CM-100 Transmission Electron microscope. Two observers blinded to genotype of the cells each scored the degree of ER dilation from 0 to 4+ in 24 cells each from a WT, *Sec23a+/gt* and a *Sec23a gt/gt* embryo.

CBC. Approximately 20 μL of peripheral blood was drawn from the retro-orbital plexus of mice and diluted 1:10 in 5% Bovine Serum Albumin (BSA) in PBS pH 7.4

(Gibco). Complete blood counts were obtained using an Advia120 blood analyzer (Bayer).

Results

ER dilation in Sec23a gt/gt MEFs

MEFs were stained with lysotracker and mitotracker dyes to identify mitochondria and lysosomes. PDI is a resident ER protein and staining in MEFs will mark the ER, ERGIC-53 marks the ER-Golgi intermediate compartment and Giantin is a Golgi marker. No consistent difference was observed in the intensity or morphology of staining for PDI, ERGIC-53, Giantin or the mitotracker or lysotracker dyes for E12.5 *Sec23a +/gt or Sec23a gt/gt* MEFs compared to wildtype (Figure 4-2 to 4-4). WT, *Sec23a+/gt*, and *Sec23a gt/gt* MEFs were also examined by transmission electron microscopy (TEM). Although a statistically significant increase in ER dilation was observed between WT and *Sec23a+/gt* cells, there was no difference between WT and *Sec23a gt/gt* cells (Figure 4-5).

Open midbrain in Sec23a gt/gt embryos

E11.5-12.5 *Sec23a gt/gt*, embryos were observed to have an open midbrain (Sue O'Shea, personal communication). This phenotype was observed in every E12.5 embryo studied. However, at least one E11.5 embryo was observed without the phenotype (Bin Zhang, personal communication). Scanning electron micrographs of this phenotype are shown in Figure 4-6.

Colocalization of Sec23 isoforms in COS cells

In order to determine if SEC23A and SEC23B co-localize in cells, we cloned SEC23A and SEC23B cDNAs into mammalian expression constructs that would express fusion proteins with GFP on the N-terminus of SEC23A (GFP-SEC23A) and RFP on the N-terminus of SEC23B (RFP-SEC23B) and transfected them into COS-1 cells. We also co-transfected a dominant negative form of Sar1a (H79G) which is locked in the GTP

bound state and will not allow COPII vesicles to bud from the endoplasmic reticulum membrane. In the absence of the dominant negative form of Sar1a, diffuse staining was observed throughout the cell with co-localization of both GFP-SEC23A and RFP-SEC23B. In the presence of the dominant negative form of Sar1a, we observed co-localization of red and green puncta which likely represent these proteins being recruited to the surface of the ER but unable to complete transport process (Figure 4-7).

Sec23a+/gt Sec23b+/gt mice are viable and fertile

Sec23a+/gt mice were crossed to *Sec23b+/gt* mice to generate *Sec23a+/gt Sec23b+/gt* double heterozygous mice and backcrossed to C57BL/6J mice. A total of 1090 offspring were generated over 13 generations from N5 to N18 backcrossed onto C57BL/6J and the expected Mendelian numbers of mice were observed for all 1090 mice genotyped (Table 4-1). CBCs from 3 WT and 6 *Sec23a+/gt Sec23b+/gt* mice showed no significant decrease in any of the 13 blood parameters measured (Table 4-2).

Synthetic lethality from interaction of mouse Sec23 paralogs

In order to further test overlap in function between SEC23A and SEC23B, *Sec23a+/gt Sec23b+/gt* were crossed to *Sec23a+/gt Sec23b+/+* mice. Chi square analysis comparing the proportion of all other genotypes to *Sec23a gt/gt Sec23b+/gt* embryos and comparing *Sec23a gt/gt Sec23b+/+* to *Sec23a gt/gt Sec23b+/gt* indicates that these embryos are underrepresented at E9.5 and suggests a significant genetic interaction between *Sec23a* and *Sec23b* (Table 4-3).

Discussion

In this chapter we studied mutant mice with a gene trap insertion in the *Sec23a* gene; these mice have an embryonic lethal phenotype between days E10.5 and E11.5 with no *Sec23a gt/gt* homozygotes present after E12.5. People with an F382L mutation in *SEC23A* are affected with CLSD. These patients exhibit defects in development of the eyes, cranial bones and central nervous system. We hypothesized that since there seemed to be a dramatic phenotype of dilated ER in the skin fibroblasts isolated from the patients,

that MEFs isolated from *Sec23a gt/gt* mice may also have a dilated ER. *Sec23a* is expressed in MEFs and no SEC23A protein is seen on western blot in *Sec23a gt/gt* MEFs (Bin Zhang, personal communication). In our experiments to show this both by confocal microscopy and transmission electron microscopy, we are unable to detect any differences in dilation of the ER or other post-ER structures in the cell between WT and *Sec23a gt/gt* MEFs. The increase in ER dilation between WT and *Sec23a+/gt* could simply be due to clonal variation between MEF lines. In spite of this lack of phenotype in the MEFs, there remains the open midbrain phenotype in at least one of the E11.5 embryos and all of the E12.5 embryos observed. This is not likely to be analogous to the human phenotype since there is no cartilage or bones at this point in development in the mouse. Also it is not clear if this phenotype is a specific effect of *Sec23a* deficiency or secondary to the cause of death. The COPII coat protein *Sec24b* has been reported to play a role in mouse nervous system development[30]. The open midbrain phenotype seen in these mice is not inconsistent with a role for *Sec23a* in the developing nervous system, possibly via an interaction with *Sec24b*. Further evidence for overlap in function of SEC23A and SEC23B are the data from the confocal experiments in which fluorescently tagged constructs for mouse *Sec23a* and *Sec23b* are transfected into COS cells along with a dominant negative form of Sar1a. Our data show that the fluorescently tagged Sec23 proteins overlap in punctae and all of the fluorescent protein is recruited to very intense punctae in cells that have also taken up the dominant negative form of Sar1. Although these studies do show overlap of the fluorescently tagged proteins, confocal microscopy does not resolve individual COPII vesicles. In studying the overlap of *Sec23a* and *Sec23b in vivo*, *Sec23a+/gt Sec23b+/gt* mice proved viable and fertile with no apparent phenotype. However, *Sec23a gt/gt Sec23b+/gt* mice appear to die at an earlier time point than *Sec23a gt/gt* mice suggesting a genetic interaction between these two proteins. Further, *Sec23a+/gt Sec23b gt/gt* also have a markedly more severe phenotype than *Sec23b gt/gt* alone with no *Sec23a+/gt Sec23b gt/gt* mice seen at E9.5 out of 70 embryos (Bin Zhang, personal communication).

The genetic interaction between *Sec23a* and *Sec23b* presents strong evidence for overlap in function between these two proteins. Perhaps SEC23A and SEC23B exist in

the same cells and are involved in transport of overlapping subsets of COPII cargo. It is particularly interesting that *Sec23a+/gt Sec23b gt/gt* die nine days earlier in development than *Sec23b gt/gt* mutants that survive to term. These data could imply that if SEC23A and SEC23B are both expressed in the same cells, SEC23A could be the dominant SEC23 isoform and SEC23B could be responsible for transporting a smaller subset of cargo. Alternatively, *Sec23a* and *Sec23b* could be expressed in different cell types and each could transport cargoes that interact such as receptor-ligand pairs which also could explain the genetic interaction between these two genes. There could be preferential interactions between SEC23A and SEC23B and the other COPII isoforms such that the expression profiles of the other members of the COPII coat and their relative affinities for SEC23A or SEC23B could also have an effect on the severity of the phenotypes in mutant mice.

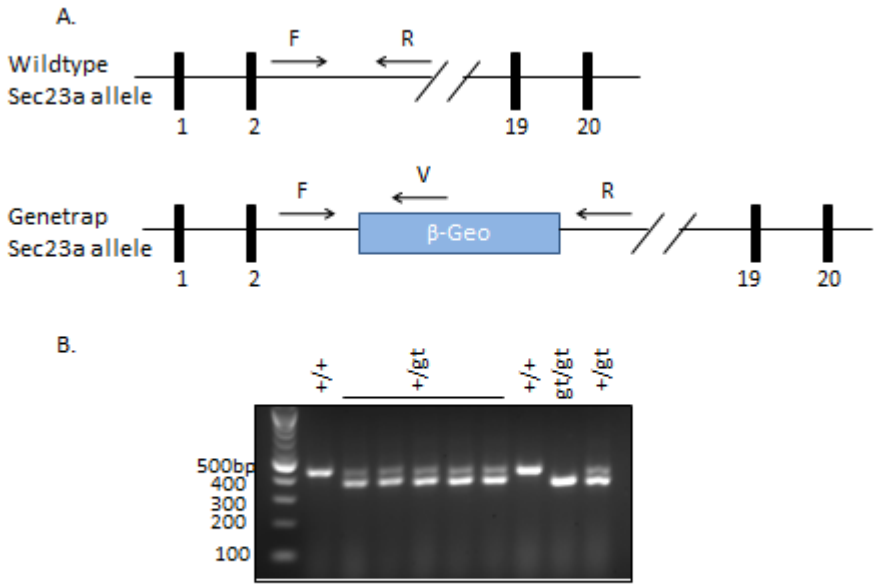

Figure 4- 1: Schematic of *Sec23a* gene trap allele and genotyping assay.

The *Sec23a* gene trap allele consists of a gene trap inserted into the second intron of the *Sec23a* gene. A) The genotyping assay employs 3 primers, one upstream and one downstream of the gene trap, with a third within the gene trap itself. PCR yields a 450 bp band from the WT allele and a 375 bp band for the gene trap allele. B) Sample genotypes of DNA prepared from fetal mice from a Sc23agt/+ intercross.

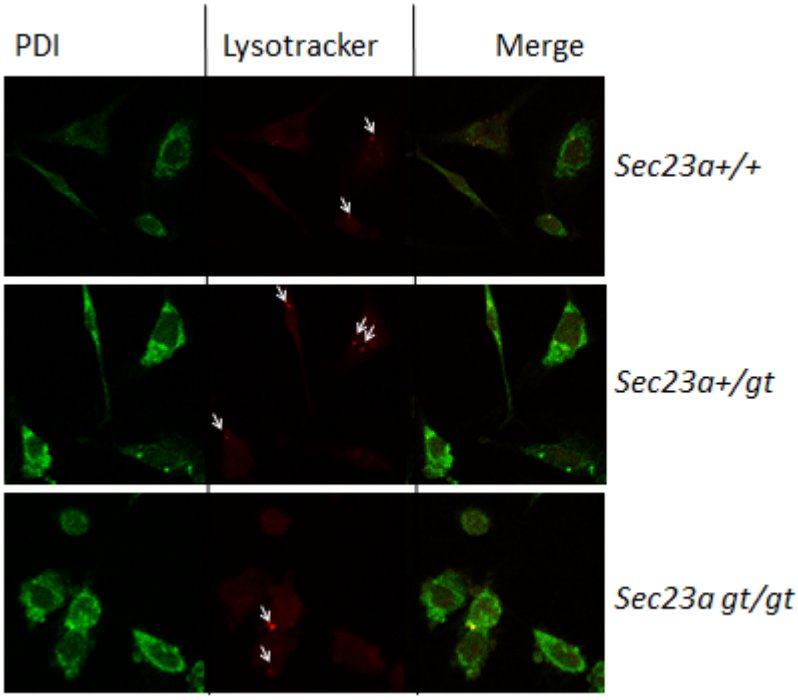

Figure 4- 2: Staining of MEFs for PDI and Lysotracker.

WT, *Sec23a +/gt* and *Sec23a gt/gt* MEFs were stained for the ER marker PDI (green), and a commercial lysotracker dye that stains lysosomes (red) (white arrows). No consistent difference was observed in intensity of ER or lysosome staining between WT and *Sec23a +/gt* or *Sec23a gt/gt* MEFs.

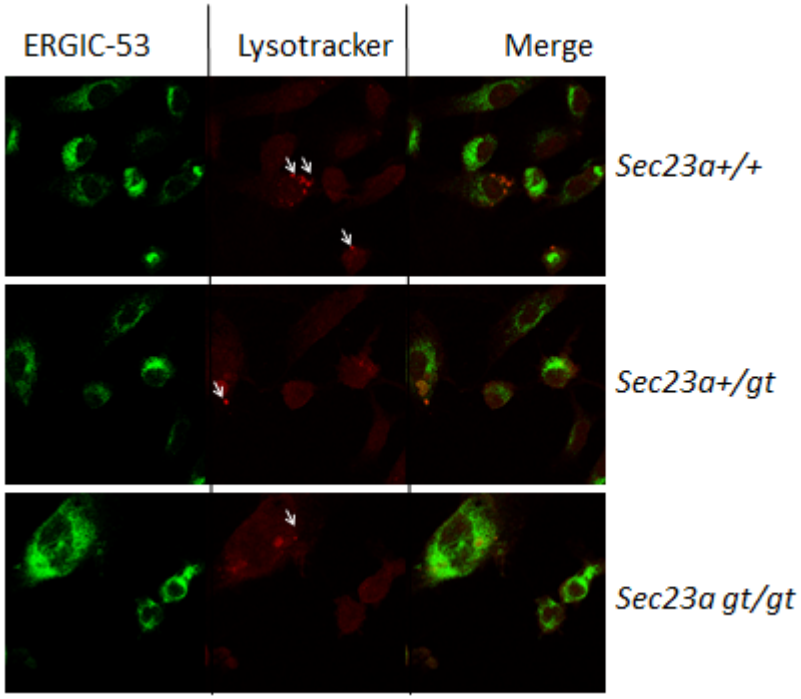

Figure 4- 3: Staining of MEFs for ERGIC-53 and Lysotracker.

WT, *Sec23a+/gt* and *Sec23a gt/gt* MEFs were stained for the ER-Golgi intermediate complex marker ERGIC-53 (green), and a commercial lysotracker dye (red) that stains lysosomes (white arrows). No apparent difference was observed in intensity of the ERGIC or lysosome staining between WT and *Sec23a +/gt* or *Sec23a gt/gt* MEFs.

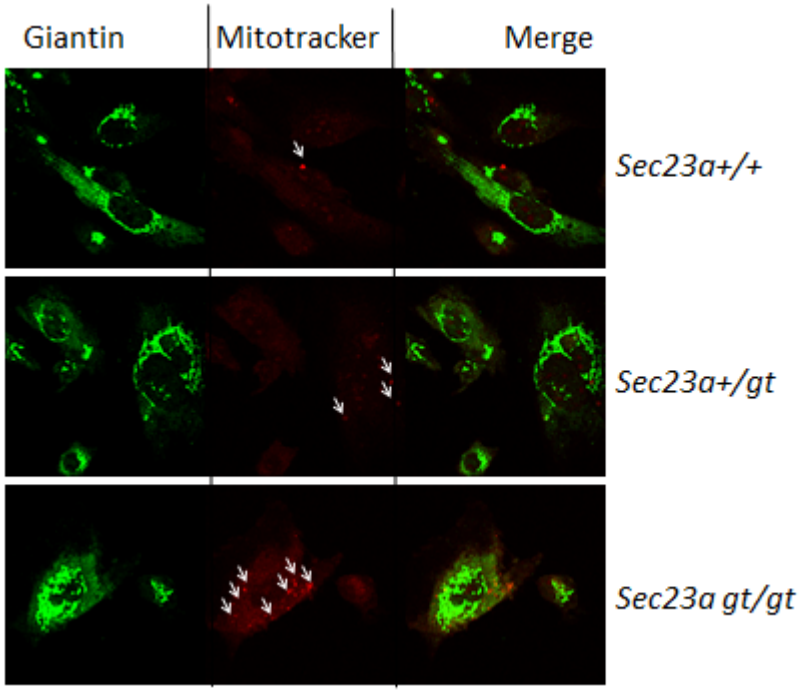

Figure 4- 4: Staining of MEFs for Giantin and mitotracker.

WT, *Sec23a +/gt* and *Sec23a gt/gt* MEFs were stained for the Golgi marker giantin (green), and a commercial mitotracker dye (red) that stains mitochondria (white arrows). No apparent difference was observed in intensity of the Golgi or mitochondria staining between WT and *Sec23a +/gt* or *Sec23a gt/gt* MEFs.

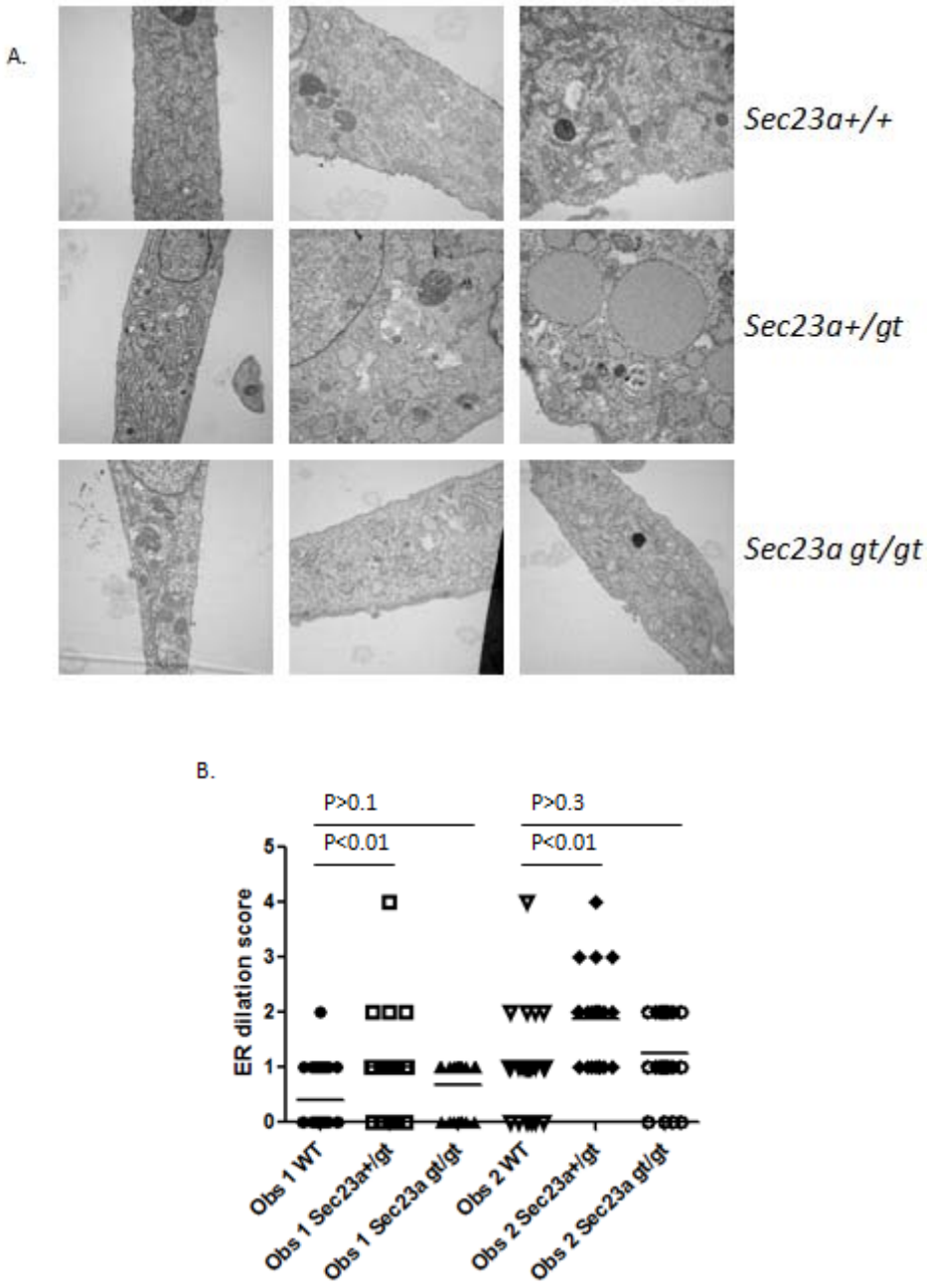

Figure 4- 5: Transmission Electron Micrograph analysis of *Sec23a gt/gt* MEFs.

A) Electron micrograph pictures taken at the same magnification for each MEF genotype. Images were taken by observers blinded to genotype. B) ER dilation score of each genotype by two observers blinded to genotype.

A. E11.5 embryos

Sec23a+/+

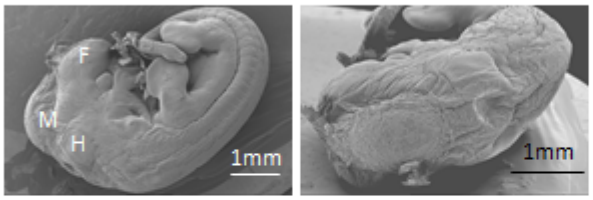

Sec23a gt/gt

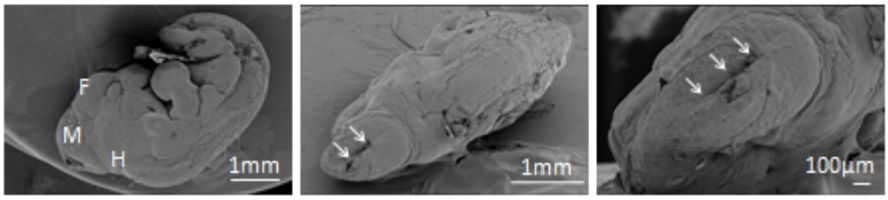

Sec23a gt/gt

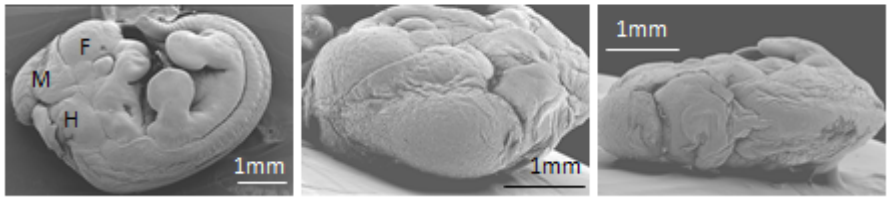

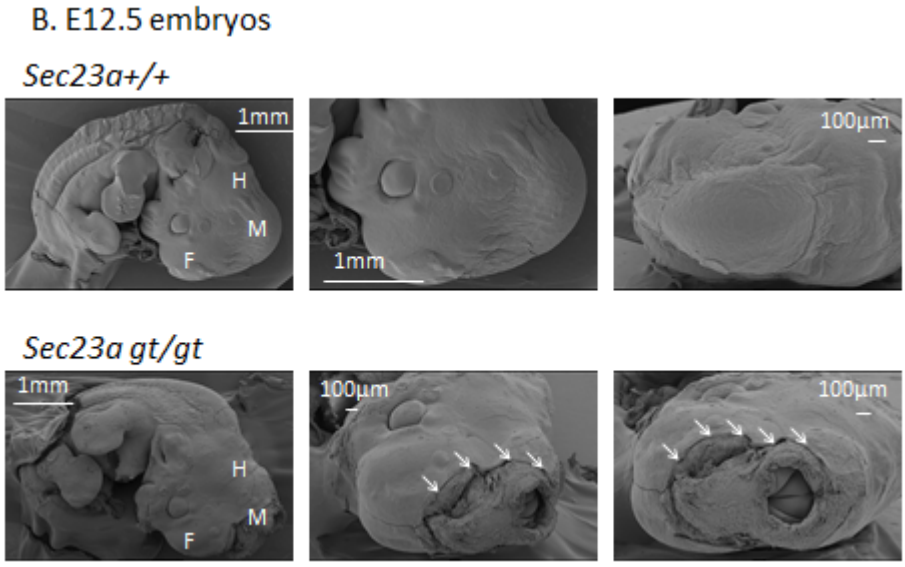

Figure 4- 6: SEM of head defect in *Sec23a gt/gt* embryos.

A) E11.5 WT and Sec23a gt/gt embryos with the open midbrain defect. The bottom row in panel A shows a Sec23a gt/gt mouse without the defect. B) E12.5 WT and Sec23a gt/gt embryo with open midbrain phenotype. The defect in panels A and B is illustrated by the white arrows. F=forebrain, M=midbrain, H=hindbrain.

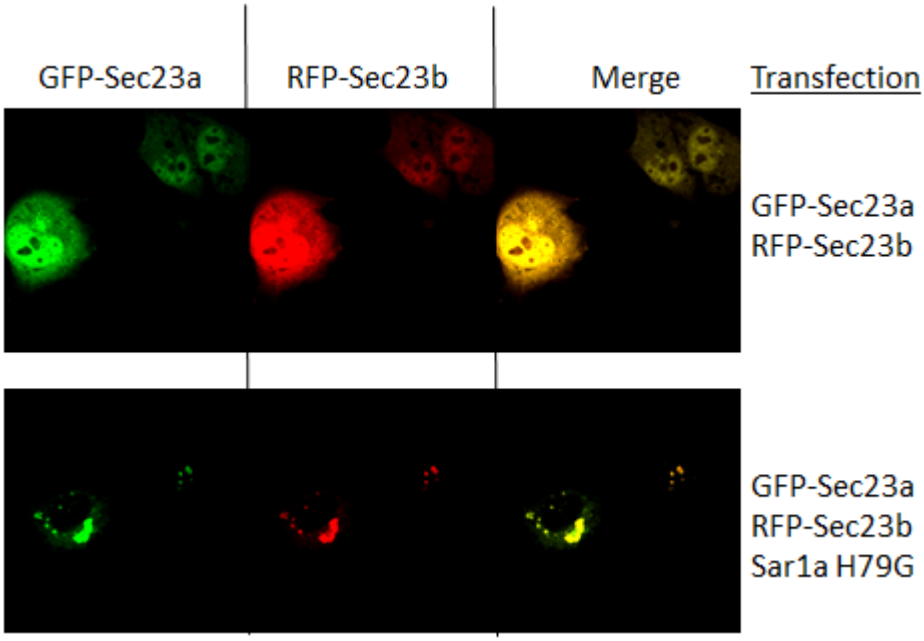

Figure 4- 7: Co-localization of fluorescently tagged Sec23a and Sec23b in COS cells.

GFP tagged Sec23a and RFP tagged Sec23b were transfected into COS cells along with a dominant negative form of Sar1. Co-localization of GFP and RFP was observed in the cells both in the presence or absence of the dominant negative Sar1.

Table 4- 1: Mendelian distribution of genotypes from *Sec23a+/gt Sec23b+/gt* mice backcrossed to C57BL/6J mice.

	Observed	**Expected**
23a+/+ 23b+/+	243	272.5
23a+/gt 23b+/+	288	272.5
23a+/+ 23b+/gt	279	272.5
23a+/gt 23b+/gt	280	272.5
Total	1090	1090
P value	0.218	

Sec23a+/gt Sec23b+/gt mice were backcrossed to C57BL/6J mice for 13 generations. The expected Mendelian ratios of genotypes were observed for the 1090 mice genotyped.

Table 4- 2: CBCs for WT and *Sec23a+/gt Sec23b+/gt* mice.

Sample	Genotype	Sex	WBC x10^3 cells/ uL	RBC x10^6 cells/ uL	HGB g/dL	HCT %	MCV fL	MCH pg	MCHC g/dL
12793	23a+/+b+/+	M	5.7	8	10	42	52.1	12.8	24.5
12817	23a+/+b+/+	F	4.8	9.5	12	50	52.1	12.5	23.9
12805	23a+/+b+/+	F	5	8.3	11	44	52.6	12.8	24.4
	Average		5.167	8.600	11.000	45.333	52.267	12.700	24.267
12785	23a+/-b+/-	F	8.7	9.7	12	50	51.7	12.6	24.4
12820	23a+/-b+/-	M	6.2	8.2	11	43	52.8	13.1	24.8
12810	23a+/-b+/-	M	8	9.9	13	52	52.5	13.3	25.4
12815	23a+/-b+/-	F	15.4	10.6	14	57	53.6	13.5	25.2
12814	23a+/-b+/-	M	5.5	8.9	12	47	53.3	13.8	26
12818	23a+/-b+/-	F	5.7	8.3	11	44	52.7	13.2	25
	Average		8.250	9.267	12.167	48.833	52.767	13.250	25.133
	P value		0.211	0.336	0.185	0.353	0.263	0.064	0.042

Sample	Genotype	Sex	CHCM g/dL	CH pg	RDW %	HDW g/dL	PLT x10^3 cells/uL	MPV fL
12793	23a+/+b+/+	M	26.2	13.6	12.8	1.59	330	4.6
12817	23a+/+b+/+	F	26.4	13.7	12.8	1.6	960	4.9
12805	23a+/+b+/+	F	26.5	13.9	12.6	1.58	440	4.5
	Average		26.367	13.733	12.733	1.590	576.667	4.667
12785	23a+/-b+/-	F	26.4	13.6	12.7	1.57	1200	5
12820	23a+/-b+/-	M	26.2	13.8	13	1.75	420	4.8
12810	23a+/-b+/-	M	26	13.6	12.1	1.57	610	4.6
12815	23a+/-b+/-	F	25.9	13.8	13	1.64	1010	5
12814	23a+/-b+/-	M	26.2	13.9	12.5	1.73	500	4.4
12818	23a+/-b+/-	F	26.6	14	12.33	1.58	1150	4.7
	Average		26.217	13.783	12.605	1.640	815.000	4.750
	P value		0.390	0.668	0.581	0.343	0.358	0.620

No significant decrease in any of the blood parameters analyzed was observed in 10-12 week old *Sec23a+/gt Sec23b+/gt* mice backcrossed to N7 onto a C57BL/6J background when compared to wildtype controls.

Table 4-3: Genetic interaction between *Sec23a* and *Sec23b*

Genotype	Expected fraction	Actual	Expected
Sec23a gt/gt 23b+/+	1/8	12	8
Sec23a gt/gt 23b gt/+	1/8	4	8
P value	0.046		
All other genotypes	7/8	87	79.625
Sec23a gt/gt 23b+/gt	1/8	4	11.375
P value	0.019		

Sec23a gt/gt Sec23b+/gt embryos were significantly decreased at E9.5 when compared against all other genotypes. (Data collected in collaboration with Bin Zhang).

Acknowledgements: Thanks to Bin Zhang for initial characterization of the *Sec23a gt/gt* mice and for help in collection of data for Table 4-3.

CHAPTER V:
Conclusions

ER to Golgi transport via COPII coated vesicles is a system that was first described in yeast and is a fundamental process important in all eukaryotic cells. However, human mutations in these coat proteins have been shown to cause remarkably tissue specific phenotypes, given the ubiquitous nature of this system. Our studies of mice with mutations in the COPII coat have yielded disparate phenotypes from humans, but also some degree of tissue specific phenotypes as seen in the pancreas of *Sec23b gt/gt* mice and CDAII and CLSD in humans.

Failure of a Sec23b gene trap allele to recapitulate CDAII

Recent reports have shown that people homozygous for mutations in the COPII coat protein *Sec23b* are affected with CDAII [61,62]. In chapter 2, we study the phenotype of mice with a gene trap insertion in the last intron of *Sec23b*. These mice die perinatally with severe degeneration of their exocrine pancreas and hypoglycemia. CBCs done on these mice showed no significant decrease in hemoglobin levels. Lethally irradiated mice receiving *Sec23b gt/gt* fetal liver cells showed no signs of anemia. The *Sec23b gt/gt* transplant recipients also did not show any of the typical biochemical or cellular signs of CDAII, including increased Myeloid:Erythroid ratio, high percentage of bi-nucleate erythroblasts in the bone marrow or the characteristic shift of Band 3 on SDS-PAGE analysis. In order to determine if a more subtle defect existed in *Sec23b gt/gt* hematopoietic cells, we undertook a competitive transplant approach using fetal liver cells from transgenic mice expressing GFP in hematopoietic cells as competitors. After primary competitive fetal liver transplants and secondary competitive bone marrow transplants, *Sec23b gt/gt* cells continue to persist in all blood lineages.

One caveat that is important to note in these experiments is the nature of the Sec23b gene trap allele. This gene trap interrupts splicing to the last exon of *Sec23b*, resulting in a fusion protein with the upstream exons fused to the β-galactosidase reporter encoded in the gene trap (Figure 2-1). One CDAII patient has been reported with a mutation in the last exon of *SEC23B*, as a compound heterozygote for another mutation elsewhere in the gene,[60] indicating that mutations in the last exon of the human gene can still cause CDAII. To examine potential residual function of the SEC23B gene trap fusion protein, an immunoprecipitation experiment was perfomed with an antibody against SEC24A, one of the binding partners of SEC23B (Chapter 2). These experiments detected a higher molecular weight protein consistent with the predicted size of the fusion co-precipitating with SEC24A in cell lysates from cells expressing the gene trap allele, but not from WT cells which suggests that the gene trap allele studied here could retain some residual function.

In order to determine the effect of total *Sec23b* deficiency in a mouse, we have obtained what should be a null allele from the European Conditional Mouse Mutagenesis Program (EUCOMM). This allele has exons 5 and 6 flanked with LoxP sites, is expected to cause a frameshift and premature stop codon in exon 7 after excision of the exons by cre recombinase. Characterization of this new allele will need to ensure that correct targeting has been achieved by Southern blot and also qRT-PCR studies to quantify the presence of any truncated *Sec23b* mRNA after the floxed exons have been deleted.

There are several possible outcomes with regard to the phenotype in these mice and comparing the results we have obtained with the first *Sec23b* gene trap allele and the new floxed allele. First, it could be that humans and mice simply have disparate phenotypes regarding *Sec23b* deficiency. In humans, the phenotype is CDAII, whereas in mice the phenotype is severe pancreatic insufficiency. One hypothesis to explain this difference might be the relative importance of the COPII isoforms in the different tissues in human and mouse. While both *Sec23a* and *Sec23b* may be expressed in a given tissue or cell type, one isoform may be preferentially used. Not only may *Sec23a* or *Sec23b* be more highly utilized in different tissues, but the other paralogs of the COPII coat may preferentially bind to either *Sec23a* or *Sec23b* and have an effect on which tissues are

most affected by mutations in the *Sec23* genes. Differences between humans and mice in preferential use of paralogous genes with overlapping function can also be seen in platelet biology. Activation of platelets by thrombin is mediated through protease-activated-receptors in humans and mice which exist as four paralogous genes in both species. However, which paralog is utilized on the surface of the platelet differs between the two species[98]. The shifting of paralog use for genes with overlapping function may be an important mechanism in evolution and speciation.

The second possibility is that the gene trap allele could provide sufficient residual function to rescue any blood phenotype that might exist in the mouse but not the pancreas. Once the experiments are carried out with a null allele, the pancreas phenotype may still exist, but upon setting up a transplant, the mice will recapitulate CDAII. In addition to these possibilities, a true null allele may have yet a different phenotype not yet described. Either result will be interesting and important in showing the effects of mutating the COPII pathway *in vivo.*

One experiment that would be instructive in determining *Sec23b* function in the mouse would be to rescue the pancreas phenotype with a *Sec23b* transgene expressed under the control of an exocrine or total pancreas promoter. Such tissue and pancreatic cell specific genes exist and we could use an elastase promoter to rescue only the exocrine pancreas [99] or Pancreatic and Duodenal Homeobox 1 (PDX1) to express *Sec23b* in both the exocrine and endocrine pancreas [100]. By rescuing the pancreatic phenotype we would be able to determine what other tissues might be affected by *Sec23b* deficiency. If the mice survived and no other toxicity was detected in other tissues this would also be instructive in showing that *Sec23b* deficiency only affects the pancreas when mutated in the whole animal.

SILAC proteomics

In chapter 3 we show that we are able to highly label mice by feeding them chow in which the lysine in the chow has every carbon replaced with 13C. In the original report of this technique, mice were fed the chow labeled with heavy lysine and bred for two generations to yield over 96% labeling efficiency [90]. The experiments we carried out

here showed that we have achieved 99% labeling in red blood cell ghost fractions, liver and kidney. These results provided us with a useful reagent in the tissues from these mice for further SILAC experiments.

We attempted to use red blood cell ghosts from the labeled mice to analyze red blood cells from mice that had been transplanted with fetal liver cells from *Sec23b gt/gt* mice. In our analysis we did identify red blood cell proteins. However, no proteins were significantly underrepresented in the unlabeled sample.

Although there were no RBC membrane proteins that were quantitatively reduced in the *Sec23b gt/gt* recipients, there were several identifications for serum proteins and other RBC cytoplasmic proteins such as hemoglobin. One piece of information that would be useful in future analyses of these types of mass spec data is the degree of enrichment for known RBC membrane proteins and to what extent the sample is contaminated with serum or RBC cytoplasmic proteins. As mentioned in chapter 3, a fractionation step is necessary in any proteomics analysis. Previous reports of the RBC membrane proteome [88,89] have shown the total number of proteins on the RBC membrane to be in the hundreds which could make it a good cellular sub-fraction for study.

Analysis of Sec23a gt/gt mice

In chapter 4 we analyze mice with a gene trap insertion in the second intron of the *Sec23a* gene. As mentioned previously, humans with an F382L mutation in *Sec23a* are affected with CLSD which is characterized by late closure of their cranial sutures, Y-shaped cataracts in the eyes and mild mental retardation [31]. In contrast, *Sec23a gt/gt* mice die during mid-embryogenesis. It is not clear if this is due to differences in the severity of the mutation beween mice and humans or a difference in biology between the two species.

Our results from immunofluorescence studies staining the MEF ER, ERGIC and Golgi apparatus did not indicate any striking difference in these cellular compartments between WT and *Sec23a gt/gt* MEFs. In order to detect a more subtle defect that might not be readily visible by light microscopy, we examined transmission electron

micrographs of MEF ER for dilation but were unable to detect any difference between wildtype and *Sec23b gt/gt* MEFs. This phenotype is in contrast to the human phenotype in which skin fibroblasts from the patients have dilated ER. However, no skin phenotype has been reported in these patients, indicating that the hypomorphic *SEC23A* allele described in these patients or SEC23B could provide sufficient residual function in skin fibroblasts. Study of whole *Sec23a gt/gt* embryos by scanning electron micrograph showed an open midbrain at E11.5; however, at least one embryo was identified that did not have the defect at E11.5. Further data are needed to more thoroughly characterize the open midbrain phenotype in the *Sec23a gt/gt* embryos such as the proportion of embryos at each developmental stage with the defect and perhaps if the defect is due to lack of proliferation in cells or a result of cell death of the cells already there. In order to determine the extent of overlap in function between SEC23A and SEC23B, we fluorescently tagged each protein and showed co-localization in COS cells. Further, we intercrossed *Sec23a+/gt* and *Sec23b+/gt* mice to generate double heterozygous mice. These mice proved to be viable and fertile with no hematologic phenotype by CBC. However, *Sec23a gt/gt Sec23b+/gt* mice die earlier than *Sec23a gt/gt* mice with reduced numbers at E9.5. These data suggest a genetic interaction between *Sec23a* and *Sec23b*. These data are consistent with the hypothesis that *Sec23a* and *Sec23b* transport overlapping sets of cargo.

One caveat is to ensure that the phenotypic effect seen both in the pancreatic degeneration in the *Sec23b gt/gt* mice and the embryonic lethality in the *Sec23a gt/gt* mice is specific to mutagenesis of the respective *Sec23* genes and not an effect of the gene trap on a nearby gene. To address this, we have generatd a second *Sec23b* mutant allele containing a gene trap in intron 4 and exons 5 and 6 are flanked by LoxP sites. When exons 5 and 6 are deleted, this creates a frameshift and premature stop codon in exon 7. The fact that mice homozygous for the intron 4 gene trap insertion recapitulate the pancreas phenotype suggests that our data characterizing the intron 19 gene trap are correct.

Other fundamental questions also remain in determining the roles of *Sec23a* and *Sec23b in vivo*. The first is to determine specifically which cells within a given tissue

express *Sec23a* and *Sec23b*. Immunohistochemistry and FACS sorting technology could be used in quantitating the relative protein levels in the different cells in the blood or bone marrow. Specific cell types such as B or T cells can be sorted and lysed for protein and the relative *Sec23a* and *Sec23b* expression levels can be determined by western. If *Sec23a* and *Sec23b* were expressed in the same cells, it would support the hypothesis of functional overlap.

In order to determine if *Sec23a* and *Sec23b* can substitute for one another is a rescue of the lethal phenotypes described above using a BAC recombineering approach. In these experiments, BAC transgenes containing the *Sec23a* or *Sec23b* gene and flanking genomic sequence would have a cDNA minigene for the opposite isofom recombineered into the locus to generate a *Sec23a* minigene in the context of the *Sec23b* genomic expression sequence and vice versa. Thus if the *Sec23a* cDNA in the genomic context of *Sec23b*, is able to rescue *Sec23b gt/gt* mice, this would show that the different phenotypes observed between these two mice is a result of differing gene expression programs rather than unique functional characteristics of each protein.

As a follow up to our previous data showing the co-localization of fluorescently tagged *Sec23a* and *Sec23b* in COS cells, immunogold staining of transmission electron micrographs of COPII vesicles could yield insight into whether or not SEC23A and SEC23B exist on the same vesicle. In this experiment different size gold particles would need to be used on antibodies for each of the different isoforms. COPII vesicles can be resolved by electron micrograph and if the gold beads appeared on the same vesicles, this would be evidence for the two proteins being carried on the same COPII vesicle and suggest whether all COPII vesicles carry similar subsets of cargo or if different classes of vesicles exist based on the cargoes or COPII coat isoforms.

Another important question is the expression patterns of the other COPII isoforms. Indeed crystal structures have shown Sec23 to interact with other members of the COPII coat [101]. There could be preferential interaction between *Sec23a* or *Sec23b* and the Sar1, Sec24 or Sec31 isoforms. This was shown to be the case in CLSD where the mutant form of SEC23A interacted more readily with SAR1A but not SAR1B [32].

Conclusion

In this thesis we describe the phenotypes for deficiency of *Sec23a* and *Sec23b* in the mouse. *Sec23a gt/gt* mice die during mid-embryogenesis while *Sec23b gt/gt* mice die near birth with degeneration of their exocrine pancreas. Humans with mutations in the orthologous *SEC23A* and *SEC23B* genes have tissue specific phenotypes in the bones of the skull and erythroblast respectively. While the human phenotypes are different from those seen in the mouse the diseases in both are manifested in specific tissues. However, the data to date do not support that these tissue specific phenotypes are a result of the genes only being expressed in those cell types. The studies presented here contribue to the understanding of COPII trafficking *in vivo* and how defects in this pathway are manifest in multi-cellular organisms.

REFERENCES

1. Baines AC, Zhang B. Receptor-mediated protein transport in the early secretory pathway. Trends Biochem Sci. 2007;32(8):381-388.
2. Bonifacino JS, Glick BS. The mechanisms of vesicle budding and fusion. Cell. 2004;116(2):153-166.
3. Supek F, Madden DT, Hamamoto S, Orci L, Schekman R. Sec16p potentiates the action of COPII proteins to bud transport vesicles. J Cell Biol. 2002;158(6):1029-1038.
4. Watson P, Townley AK, Koka P, Palmer KJ, Stephens DJ. Sec16 defines endoplasmic reticulum exit sites and is required for secretory cargo export in mammalian cells. Traffic. 2006;7(12):1678-1687.
5. Palmer KJ, Watson P, Stephens DJ. The role of microtubules in transport between the endoplasmic reticulum and Golgi apparatus in mammalian cells. Biochem Soc Symp. 2005(72):1-
6. Zhang B, Cunningham MA, Nichols WC, et al. Bleeding due to disruption of a cargo-specific ER-to-Golgi transport complex. Nat Genet. 2003;34(2):220-225.
7. Nichols WC, Seligsohn U, Zivelin A, et al. Mutations in the ER-Golgi intermediate compartment protein ERGIC-53 cause combined deficiency of coagulation factors V and VIII. Cell. 1998;93(1):61-70.
8. Kanapin A, Batalov S, Davis MJ, et al. Mouse proteome analysis. Genome Res. 2003;13(6B):1335-1344.
9. Novick P, Field C, Schekman R. Identification of 23 complementation groups required for post-translational events in the yeast secretory pathway. Cell. 1980;21(1):205-215.
10. Barlowe C, Orci L, Yeung T, et al. COPII: a membrane coat formed by Sec proteins that drive vesicle budding from the endoplasmic reticulum. Cell. 1994;77(6):895-907.
11. Bednarek SY, Ravazzola M, Hosobuchi M, et al. COPI- and COPII-coated vesicles bud directly from the endoplasmic reticulum in yeast. Cell. 1995;83(7):1183-1196.
12. Jensen D, Schekman R. COPII-mediated vesicle formation at a glance. J Cell Sci. 2011;124(Pt 1):1-4.

13. Fromme JC, Orci L, Schekman R. Coordination of COPII vesicle trafficking by Sec23. Trends Cell Biol. 2008;18(7):330-336.

14. Bhattacharyya D, Glick BS. Two mammalian Sec16 homologues have nonredundant functions in endoplasmic reticulum (ER) export and transitional ER organization. Mol Biol Cell. 2007;18(3):839-849.

15. Watson P, Forster R, Palmer KJ, Pepperkok R, Stephens DJ. Coupling of ER exit to microtubules through direct interaction of COPII with dynactin. Nat Cell Biol. 2005;7(1):48-55.

16. Miller EA, Beilharz TH, Malkus PN, et al. Multiple cargo binding sites on the COPII subunit Sec24p ensure capture of diverse membrane proteins into transport vesicles. Cell. 2003;114(4):497-509.

17. Shimoni Y, Kurihara T, Ravazzola M, Amherdt M, Orci L, Schekman R. Lst1p and Sec24p cooperate in sorting of the plasma membrane ATPase into COPII vesicles in Saccharomyces cerevisiae. J Cell Biol. 2000;151(5):973-984.

18. Kurihara T, Hamamoto S, Gimeno RE, Kaiser CA, Schekman R, Yoshihisa T. Sec24p and Iss1p function interchangeably in transport vesicle formation from the endoplasmic reticulum in Saccharomyces cerevisiae. Mol Biol Cell. 2000;11(3):983-998.

19. Mossessova E, Bickford LC, Goldberg J. SNARE selectivity of the COPII coat. Cell. 2003;114(4):483-495.

20. Martinez-Menarguez JA, Geuze HJ, Slot JW, Klumperman J. Vesicular tubular clusters between the ER and Golgi mediate concentration of soluble secretory proteins by exclusion from COPI-coated vesicles. Cell. 1999;98(1):81-90.

21. Oprins A, Rabouille C, Posthuma G, Klumperman J, Geuze HJ, Slot JW. The ER to Golgi interface is the major concentration site of secretory proteins in the exocrine pancreatic cell. Traffic. 2001;2(11):831-838.

22. Miller E, Antonny B, Hamamoto S, Schekman R. Cargo selection into COPII vesicles is driven by the Sec24p subunit. EMBO J. 2002;21(22):6105-6113.

23. Aridor M, Fish KN, Bannykh S, et al. The Sar1 GTPase coordinates biosynthetic cargo selection with endoplasmic reticulum export site assembly. J Cell Biol. 2001;152(1):213-229.

24. Kuehn MJ, Herrmann JM, Schekman R. COPII-cargo interactions direct protein sorting into ER-derived transport vesicles. Nature. 1998;391(6663):187-190.

25. Belden WJ, Barlowe C. Role of Erv29p in collecting soluble secretory proteins into ER-derived transport vesicles. Science. 2001;294(5546):1528-1531.

26. Nyfeler B, Reiterer V, Wendeler MW, et al. Identification of ERGIC-53 as an intracellular transport receptor of alpha1-antitrypsin. J Cell Biol. 2008;180(4):705-712.

27. Vollenweider F, Kappeler F, Itin C, Hauri HP. Mistargeting of the lectin ERGIC-53 to the endoplasmic reticulum of HeLa cells impairs the secretion of a lysosomal enzyme. J Cell Biol. 1998;142(2):377-389.

28. Appenzeller C, Andersson H, Kappeler F, Hauri HP. The lectin ERGIC-53 is a cargo transport receptor for glycoproteins. Nat Cell Biol. 1999;1(6):330-334.

29. Jones B, Jones EL, Bonney SA, et al. Mutations in a Sar1 GTPase of COPII vesicles are associated with lipid absorption disorders. Nat Genet. 2003;34(1):29-31.

30. Merte J, Jensen D, Wright K, et al. Sec24b selectively sorts Vangl2 to regulate planar cell polarity during neural tube closure. Nat Cell Biol. 2010;12(1):41-46; sup pp 41-48.

31. Boyadjiev SA, Fromme JC, Ben J, et al. Cranio-lenticulo-sutural dysplasia is caused by a SEC23A mutation leading to abnormal endoplasmic-reticulum-to-Golgi trafficking. Nat Genet. 2006;38(10):1192-1197.

32. Fromme JC, Ravazzola M, Hamamoto S, et al. The genetic basis of a craniofacial disease provides insight into COPII coat assembly. Dev Cell. 2007;13(5):623-634.

33. Lang MR, Lapierre LA, Frotscher M, Goldenring JR, Knapik EW. Secretory COPII coat component Sec23a is essential for craniofacial chondrocyte maturation. Nat Genet. 2006;38(10):1198-1203.

34. Schindler R, Itin C, Zerial M, Lottspeich F, Hauri HP. ERGIC-53, a membrane protein of the ER-Golgi intermediate compartment, carries an ER retention motif. Eur J Cell Biol. 1993;61(1):1-9.

35. Schweizer A, Fransen JA, Bachi T, Ginsel L, Hauri HP. Identification, by a monoclonal antibody, of a 53-kD protein associated with a tubulo-vesicular compartment at the cis-side of the Golgi apparatus. J Cell Biol. 1988;107(5):1643-1653.

36. Hauri HP, Kappeler F, Andersson H, Appenzeller C. ERGIC-53 and traffic in the secretory pathway. J Cell Sci. 2000;113 (Pt 4):587-596.

37. Zhang B, Kaufman RJ, Ginsburg D. LMAN1 and MCFD2 form a cargo receptor complex and interact with coagulation factor VIII in the early secretory pathway. J Biol Chem. 2005;280(27):25881-25886.

38. Jenny RJ, Pittman DD, Toole JJ, et al. Complete cDNA and derived amino acid sequence of human factor V. Proc Natl Acad Sci U S A. 1987;84(14):4846-4850.

39. Camire RM, Pollak ES, Kaushansky K, Tracy PB. Secretable human platelet-derived factor V originates from the plasma pool. Blood. 1998;92(9):3035-3041.

40. Yang TL, Pipe SW, Yang A, Ginsburg D. Biosynthetic origin and functional significance of murine platelet factor V. Blood. 2003;102(8):2851-2855.

41. Do H, Healey JF, Waller EK, Lollar P. Expression of factor VIII by murine liver sinusoidal endothelial cells. J Biol Chem. 1999;274(28):19587-19592.

42. Kumaran V, Benten D, Follenzi A, Joseph B, Sarkar R, Gupta S. Transplantation of endothelial cells corrects the phenotype in hemophilia A mice. J Thromb Haemost. 2005;3(9):2022-2031.

43. Zheng C, Liu HH, Yuan S, Zhou J, Zhang B. Molecular basis of LMAN1 in coordinating LMAN1-MCFD2 cargo receptor formation and ER-to-Golgi transport of FV/FVIII. Blood. 2010;116(25):5698-5706.

44. Neve EP, Lahtinen U, Pettersson RF. Oligomerization and interacellular localization of the glycoprotein receptor ERGIC-53 is independent of disulfide bonds. J Mol Biol. 2005;354(3):556-568.

45. Kappeler F, Klopfenstein DR, Foguet M, Paccaud JP, Hauri HP. The recycling of ERGIC-53 in the early secretory pathway. ERGIC-53 carries a cytosolic endoplasmic reticulum-exit determinant interacting with COPII. J Biol Chem. 1997;272(50):31801-31808.

46. Guy JE, Wigren E, Svard M, Hard T, Lindqvist Y. New insights into multiple coagulation factor deficiency from the solution structure of human MCFD2. J Mol Biol. 2008;381(4):941-955.

47. Zheng C, Liu HH, Zhou J, Zhang B. EF-hand domains of MCFD2 mediate interactions with both LMAN1 and coagulation factor V or VIII. Blood. 2010;115(5):1081-1087.

48. Nishio M, Kamiya Y, Mizushima T, et al. Structural basis for the cooperative interplay between the two causative gene products of combined factor V and factor VIII deficiency. Proc Natl Acad Sci U S A. 2010;107(9):4034-4039.

49. Wigren E, Bourhis JM, Kursula I, Guy JE, Lindqvist Y. Crystal structure of the LMAN1-CRD/MCFD2 transport receptor complex provides insight into combined deficiency of factor V and factor VIII. FEBS Lett. 2010;584(5):878-882.

50. Zhang B, Spreafico M, Zheng C, et al. Genotype-phenotype correlation in combined deficiency of factor V and factor VIII. Blood. 2008;111(12):5592-5600.

51. Heimpel H, Anselstetter V, Chrobak L, et al. Congenital dyserythropoietic anemia type II: epidemiology, clinical appearance, and prognosis based on long-term observation. Blood. 2003;102(13):4576-4581.

52. Denecke J, Kranz C, Nimtz M, et al. Characterization of the N-glycosylation phenotype of erythrocyte membrane proteins in congenital dyserythropoietic anemia type II (CDA II/HEMPAS). Glycoconj J. 2008;25(4):375-382.

53. Alloisio N, Texier P, Denoroy L, et al. The cisternae decorating the red blood cell membrane in congenital dyserythropoietic anemia (type II) originate from the endoplasmic reticulum. Blood. 1996;87(10):4433-4439.

54. Crookston JH, Crookston MC, Burnie KL, et al. Hereditary erythroblastic multinuclearity associated with a positive acidified-serum test: a type of congenital dyserythropoietic anaemia. Br J Haematol. 1969;17(1):11-26.

55. Denecke J, Marquardt T. Congenital dyserythropoietic anemia type II (CDAII/HEMPAS): where are we now? Biochim Biophys Acta. 2009;1792(9):915-920.

56. Heimpel H, Kellermann K, Neuschwander N, Hogel J, Schwarz K. The morphological diagnosis of congenital dyserythropoietic anemia: results of a quantitative analysis of peripheral blood and bone marrow cells. Haematologica. 2010;95(6):1034-1036.

57. Fermo E, Bianchi P, Notarangelo LD, et al. CDAII presenting as hydrops foetalis: molecular characterization of two cases. Blood Cells Mol Dis. 2010;45(1):20-22.

58. Iolascon A, Sabato V, de Mattia D, Locatelli F. Bone marrow transplantation in a case of severe, type II congenital dyserythropoietic anaemia (CDA II). Bone Marrow Transplant. 2001;27(2):213-215.

59. Remacha AF, Badell I, Pujol-Moix N, et al. Hydrops fetalis-associated congenital dyserythropoietic anemia treated with intrauterine transfusions and bone marrow transplantation. Blood. 2002;100(1):356-358. 60. Russo R, Esposito MR, Asci R, et al. Mutational spectrum in congenital dyserythropoietic anemia type II: identification of 19 novel variants in SEC23B gene. Am J Hematol. 2010;85(12):915-920.

61. Bianchi P, Fermo E, Vercellati C, et al. Congenital dyserythropoietic anemia type II (CDAII) is caused by mutations in the SEC23B gene. Hum Mutat. 2009;30(9):1292-1298.

62. Schwarz K, Iolascon A, Verissimo F, et al. Mutations affecting the secretory COPII coat component SEC23B cause congenital dyserythropoietic anemia type II. Nat Genet. 2009;41(8):936-940.

63. Iolascon A, Russo R, Esposito MR, et al. Molecular analysis of 42 patients with congenital dyserythropoietic anemia type II: new mutations in the SEC23B gene and a search for a genotype-phenotype relationship. Haematologica. 2010;95(5):708-715.

64. Chui D, Oh-Eda M, Liao YF, et al. Alpha-mannosidase-II deficiency results in dyserythropoiesis and unveils an alternate pathway in oligosaccharide biosynthesis. Cell. 1997;90(1):157-167.

65. Paw BH, Davidson AJ, Zhou Y, et al. Cell-specific mitotic defect and dyserythropoiesis associated with erythroid band 3 deficiency. Nat Genet. 2003;34(1):59-64.

66. Draptchinskaia N, Gustavsson P, Andersson B, et al. The gene encoding ribosomal protein S19 is mutated in Diamond-Blackfan anaemia. Nat Genet. 1999;21(2):169-175.

67. Gazda HT, Grabowska A, Merida-Long LB, et al. Ribosomal protein S24 gene is mutated in Diamond-Blackfan anemia. Am J Hum Genet. 2006;79(6):1110-1118.

68. Heimpel H, Wendt F. Congenital dyserythropoietic anemia with karyorrhexis and multinuclearity of erythroblasts. Helv Med Acta. 1968;34(2):103-115.

69. Iolascon A, Delaunay J, Wickramasinghe SN, Perrotta S, Gigante M, Camaschella C. Natural history of congenital dyserythropoietic anemia type II. Blood. 2001;98(4):1258-1260.

70. Wickramasinghe SN. Congenital dyserythropoietic anaemias: clinical features, haematological morphology and new biochemical data. Blood Rev. 1998;12(3):178-200.

71. Fukuda MN, Klier G, Scartezzini P. Congenital dyserythropoietic anaemia type II (HEMPAS): characterization of aberrant intracellular organelles by immunogold electron microscopy. Br J Haematol. 1987;67(1):95-101.

72. Vainchenker W, Guichard J, Breton-Gorius J. Morphological Abnormalities in cultured erythroid colonies (BFU-E) from the blood of two patients with HEMPAS. Br J Haematol. 1979;42(3):363-369.

73. Baines AJ, Banga JP, Gratzer WB, Linch DC, Huehns ER. Red cell membrane protein anomalies in congenital dyserythropoietic anaemia, type II (HEMP AS). Br J Haematol. 1982;50(4):563-574.

74. Anselstetter V, Horstmann HJ, Heimpel H. Congenital dyserythropoietic anaemia, types I and II: aberrant pattern of erythrocyte membrane proteins in CDA II, as revealed by two-dimensional polyacrylamide gel electrophoresis. Br J Haematol. 1977;35(2):209-215.

75. Wonke B. Clinical management of beta-thalassemia major. Semin Hematol. 2001;38(4):350-359.

76. Motto DG, Chauhan AK, Zhu G, et al. Shigatoxin triggers thrombotic thrombocytopenic purpura in genetically susceptible ADAMTS13-deficient mice. J Clin Invest. 2005;115(10):2752-2761.

77. Cui J, O'Shea KS, Purkayastha A, Saunders TL, Ginsburg D. Fatal haemorrhage and incomplete block to embryogenesis in mice lacking coagulation factor V. Nature. 1996;384(6604):66-68.

78. Schaefer BC, Schaefer ML, Kappler JW, Marrack P, Kedl RM. Observation of antigen-dependent CD8+ T-cell/ dendritic cell interactions in vivo. Cell Immunol. 2001;214(2):110-122.

79. Fermo E, Bianchi P, Notarangelo LD, et al. CDAII presenting as hydrops foetalis: molecular characterization of two cases. Blood Cells Mol Dis;45(1):20-22.

80. Sankaran VG, Xu J, Ragoczy T, et al. Developmental and species-divergent globin switching are driven by BCL11A. Nature. 2009;460(7259):1093-1097.

81. Mann M. Functional and quantitative proteomics using SILAC. Nat Rev Mol Cell Biol. 2006;7(12):952-958.

82. Ong SE, Mann M. A practical recipe for stable isotope labeling by amino acids in cell culture (SILAC). Nat Protoc. 2006;1(6):2650-2660.

83. Kruger M, Kratchmarova I, Blagoev B, Tseng YH, Kahn CR, Mann M. Dissection of the insulin signaling pathway via quantitative phosphoproteomics. Proc Natl Acad Sci U S A. 2008;105(7):2451-2456.

84. Rinehart J, Maksimova YD, Tanis JE, et al. Sites of regulated phosphorylation that control K-Cl cotransporter activity. Cell. 2009;138(3):525-536.

85. Kratchmarova I, Blagoev B, Haack-Sorensen M, Kassem M, Mann M. Mechanism of divergent growth factor effects in mesenchymal stem cell differentiation. Science. 2005;308(5727):1472-1477.

86. Ishihama Y, Sato T, Tabata T, et al. Quantitative mouse brain proteomics using culture-derived isotope tags as internal standards. Nat Biotechnol. 2005;23(5):617-621.

87. Pagliarini DJ, Calvo SE, Chang B, et al. A mitochondrial protein compendium elucidates complex I disease biology. Cell. 2008;134(1):112-123.

88. Pasini EM, Kirkegaard M, Mortensen P, Lutz HU, Thomas AW, Mann M. In-depth analysis of the membrane and cytosolic proteome of red blood cells. Blood. 2006;108(3):791-801.

89. Pasini EM, Kirkegaard M, Salerno D, Mortensen P, Mann M, Thomas AW. Deep coverage mouse red blood cell proteome: a first comparison with the human red blood cell. Mol Cell Proteomics. 2008;7(7):1317-1330.

90. Kruger M, Moser M, Ussar S, et al. SILAC mouse for quantitative proteomics uncovers kindlin-3 as an essential factor for red blood cell function. Cell. 2008;134(2):353-364.

91. Goodman JW, Smith LH. Erythrocyte life span in normal mice and in radiation bone marrow chimeras. Am J Physiol. 1961;200:764-770.

92. Berlin NI, Waldmann TA, Weissman SM. Life span of red blood cell. Physiol Rev. 1959;39(3):577-616.

93. Hicke L, Schekman R. Yeast Sec23p acts in the cytoplasm to promote protein transport from the endoplasmic reticulum to the Golgi complex in vivo and in vitro. EMBO J. 1989;8(6):1677-1684.

94. Antonny B, Madden D, Hamamoto S, Orci L, Schekman R. Dynamics of the COPII coat with GTP and stable analogues. Nat Cell Biol. 2001;3(6):531-537.

95. Boyadjiev S, Kim SD, Hata A, et al. Cranio-lenticulo-sutural dysplasia associated with defects in collagen secretion. Clin Genet. 2010.

96. Campbell RE, Tour O, Palmer AE, et al. A monomeric red fluorescent protein. Proc Natl Acad Sci U S A. 2002;99(12):7877-7882.

97. Ward TH, Polishchuk RS, Caplan S, Hirschberg K, Lippincott-Schwartz J. Maintenance of Golgi structure and function depends on the integrity of ER export. J Cell Biol. 2001;155(4):557-570.

98. Coughlin SR. How the protease thrombin talks to cells. Proc Natl Acad Sci U S A. 1999;96(20):11023-11027.

99. Li B, Wang X, Liu JL. Pancreatic acinar-specific overexpression of Reg2 gene offered no protection against either experimental diabetes or pancreatitis in mice. Am J Physiol Gastrointest Liver Physiol. 2010;299(2):G413-421.

100. Feldmann G, Collins K, Dal Molin M, et al. Inactivation of Brca2 cooperates with Trp53R172H to induce invasive pancreatic ductal adenocarcinomas in mice: A mouse model of familial pancreatic cancer. Cancer Biol Ther. 2011;11(11).

101. Bi X, Mancias JD, Goldberg J. Insights into COPII coat nucleation from the structure of Sec23.Sar1 complexed with the active fragment of Sec31. Dev Cell. 2007;13(5):635-645.